ADVANCED ARTIFICIAL DIELECTRIC MATERIALS

FOR MILLIMETER WAVELENGTH APPLICATIONS

Final Technical Report, Part A

Contract No. N00014-83-C-0447

AD-A220 221

ISRAEL S. JACOBS

General Electric Company
Corporate Research and Development
P.O. Box 8
Schenectady, New York 12301

Report Period 1 Aug 1983 – 30 Jun 1987

Prepared for

90-SRD-001

90 04 02 106

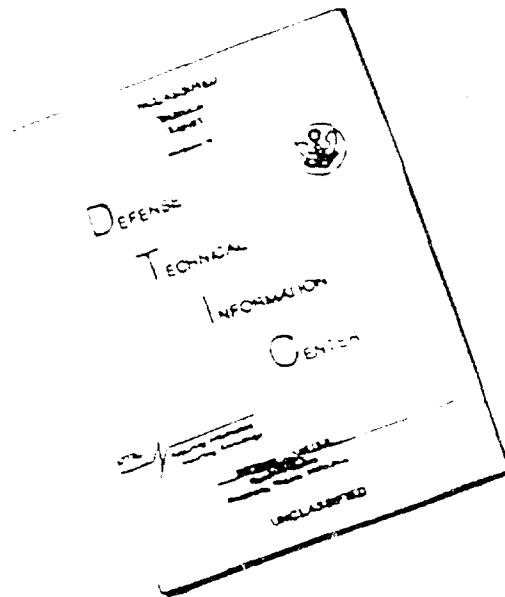# DISCLAIMER NOTICE

THIS DOCUMENT IS BEST
QUALITY AVAILABLE. THE COPY
FURNISHED TO DTIC CONTAINED
A SIGNIFICANT NUMBER OF
PAGES WHICH DO NOT
REPRODUCE LEGIBLY.

REPORT DOCUMENTATION PAGE

1a. REPORT SECURITY CLASSIFICATION	1b. RESTRICTIVE MARKINGS
Unclassified	

2a. SECURITY CLASSIFICATION AUTHORITY	3. DISTRIBUTION/AVAILABILITY OF REPORT
2b. DECLASSIFICATION/DOWNGRADING SCHEDULE	Reproduction in whole or in part is permitted for any purposes by the United States Government

4. PERFORMING ORGANIZATION REPORT NUMBER(S)	5. MONITORING ORGANIZATION REPORT NUMBER(S)
90-SRD-001	

6a. NAME OF PERFORMING ORGANIZATION	6b. OFFICE SYMBOL (If applicable)	7a. NAME OF MONITORING ORGANIZATION
General Electric Company Corporate Research and Development		Office of Naval Research – Code 1131

6c. ADDRESS (City, State and ZIP Code)	7b. ADDRESS (City, State and ZIP Code)
P.O. Box 8 Schenectady, NY 12301	800 N. Quincy Street Arlington, VA 22217

8a. NAME OF FUNDING/SPONSORING ORGANIZATION	8b. OFFICE SYMBOL (If applicable)	9. PROCUREMENT INSTRUMENT IDENTIFICATION NUMBER
Office of Naval Research	Code 1131	N 00014-83-C-0447

8c. ADDRESS (City, State and ZIP Code)	10. SOURCE OF FUNDING NOS.			
	PROGRAM ELEMENT NO.	PROJECT NO.	TASK NO.	WORK UNIT NO.
800 N. Quincy Street Arlington, VA 22217	61153N	RR02202	OC	

11. TITLE (Include Security Classification)
Advanced Artificial Dielectric Materials (U)

12. PERSONAL AUTHOR(S) Jacobs, Israel S.

13a. TYPE OF REPORT	13b. TIME COVERED	14. DATE OF REPORT (Yr., Mo., Day)	15. PAGE COUNT
Final Technical Report	FROM 83 Aug 01 TO 87 Jun 30	89 Nov 30	123

16. SUPPLEMENTARY NOTATION
Full Title of Contract:
Advanced Artificial Dielectric Materials for Millimeter Wavelength Applications

17.	COSATI CODES		18. SUBJECT TERMS (Continue on reverse if necessary and identify by block number)
FIELD	GROUP	SUB. GR.	artificial dielectrics, heterogeneous media, induced magnetic permeability, permittivity, random arrays, binder effects

19. ABSTRACT (Continue on reverse if necessary and identify by block number)

This is Part A of a two-part Final Technical Report and is restricted to essentially non-magnetic composite dielectrics. Part B, which contains classified material, treats magneto-dielectric composites. We study the electromagnetic properties (permeability and permittivity) of artificial dielectrics with metal particles (1 μm to 37 μm) randomly loaded into both polymeric and inorganic binders. The alloy powder particles are oxide-coated for isolation (non-percolating) and ferromagnetic only below room temperature for volume loading determination, p. Samples with p from 0.1 to 0.4 for various size fractions, were examined from about 1 GHz to 20 GHz, and for selected samples at 35 GHz and 90 GHz. The complex permeability results are in very good agreement with calculations of induced magnetic dipole effects as functions of frequency and particle diameter. Permittivity results (real part) are independent of particle diameter and essentially constant with frequency. Their dependence on loading is compared to the Clausius-Mossotti dipolar calculation, to the lattice array models with higher-order multipole interactions pioneered by Rayleigh, as well as to a pair-interaction model developed in this study; and also to an empirical curve obtained from several remarkably ideal experiments. The latter two comparisons are rather successful when the particles are closely spherical. We conclude that the microwave electromagnetic behavior of such non-percolating artificial dielectrics is well understood.

20. DISTRIBUTION/AVAILABILITY OF ABSTRACT	21. ABSTRACT SECURITY CLASSIFICATION
UNCLASSIFIED/UNLIMITED ☐ SAME AS RPT. ☒ DTIC USERS ☐	Unclassified

22a. NAME OF RESPONSIBLE INDIVIDUAL	22b. TELEPHONE NUMBER (Include Area Code)	22c. OFFICE SYMBOL
Dr. D.E. Polk (ONR)	(202) 696-4401	Code 1131 M

DD FORM 1473, 83 APR EDITION OF 1 JAN 73 IS OBSOLETE.

PREFACE

This Final Technical Report was prepared by General Electric Corporate Research and Development under ONR Contract No. 00014-83-C-0447. The Principal Investigator was Dr. Israel S. Jacobs of GE Corporate Research and Development, Applied Physics Laboratory, Materials Research Program. There were a number of major collaborators in this effort and they are identified in the Introduction.

The program was originally administered for its first two years under the direction of CDR William R. Schmidt, USN, Code 430B, and subsequently under the direction of Dr. Donald E. Polk, Code 1131M, of the Materials Division of the Office of Naval Research, Arlington, VA, 22217.

STATEMENT "A" per Wallace Smith
ONR/Code 1131F
TELECON   4/9/90   VG

Accesion For

NTIS CRA&I	☑
DTIC TAB	☐
Unannounced	☐
Justification	

By per call
Distribution /

Availability Codes

| Dist | Avail and / or Special |
| A-1 | |

iii
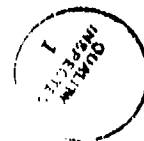
SUMMARY

This program is concerned with the development of an interesting class of artificial dielectrics and a deeper understanding of its electromagnetic properties at high frequencies (centimeter and millimeter wavelengths). This Final Technical Report–Part A deals with essentially non-magnetic composite dielectrics. Part B, which contains classified material, treats magneto-dielectric composites.

A model dielectric consisting of a randomly packed, metal-insulator composite is an example of an inhomogeneous material whose properties have provided problems and challenges for theorists and experimentalists for over 150 years. We have studied the permeability and permittivity at high frequencies on correlated artificial dielectrics with moderately sized metal particles (~1 μm to ~37 μm) randomly loaded into both polymeric and inorganic glassy binders up to 40 vol%. The metal alloy powder, $Ni_{92}Cr_8$, is prepared by gas-water atomization, which provides an oxide coating for interparticle isolation (= the correlation). The powder is ferromagnetic below about 160K, which enables a low-temperature magnetic measurement of volume loading, p, while leaving a "non-magnetic" composite at room temperature. Non-percolating composites with p ranging from 0.1 to 0.4, for separate size fractions (in μm) of –10, +10-20, +20-37, were examined from about 1 GHz to 20 GHz and for selected samples at ~35 GHz and ~90 GHz.

The complex permeability results are in very good agreement with induced magnetic dipole (eddy current) calculations as a function of frequency and particle diameter. Permittivity results (real part) are independent of particle diameter and essentially constant with frequency. Their dependence on loading is compared to the classical Maxwell/Clausius-Mossotti dipolar calculation, to the ordered array models with higher-order multipole interactions pioneered by Rayleigh and completed recently by Doyle and McPhedran et al., as well as to a pair-interaction model developed during this program. Comparison is also made to an empirical curve obtained from remarkably ideal experiments of Guillien and of Turner. Our permittivity data on another alloy powder system, from work outside this contract, are in excellent agreement with the empirical curve. For the Ni-Cr alloy powder composites, there is a residual upward deviation of ε' vs. p, which is attributed to (detectable) non-spherical deviations in particle morphology.

This research demonstrates that the microwave electromagnetic behavior of non-percolating, artificial-dielectric composites is well understood. Random arrays have their own unique properties, as distinct from ordered arrays. The present study provides a firm foundation

for examining the more difficult metallic magnetic-dielectric composites discussed in Part B of this Final Report.

TABLE OF CONTENTS

TABLE OF CONTENTS (Continued)

TABLE OF CONTENTS (Continued)

LIST OF ILLUSTRATIONS

LIST OF ILLUSTRATIONS (Continued)

LIST OF ILLUSTRATIONS (Continued)

LIST OF TABLES

I. INTRODUCTION

This research is concerned with the development of a novel class of artificial dielectrics and a deeper understanding of its properties at millimeter wavelengths. Our original point of departure was a Radar Absorbing Materials Physics Model developed during a classified program [1]. That study involved experimental measurements in the microwave range of frequencies (centimeter wavelength) over a wide range of parameter space and analysis of the broad data base obtained therefrom. Many of the model features and predictions are, however, relevant to the millimeter wavelength region. Some of the interesting implications of the prior work concern the permittivity behavior of the composite system, one which may be regarded as a new class of oxide-passivated metal-insulator dielectrics.

A somewhat optimistic overview of the research goals for the study was stated in its early stages in question form as follows: How valid is the RAM physics model in higher frequency regimes? Why does the dielectric behavior appear to follow the simple Maxwell approximation, given the pitfalls that often beset metal-insulator composites? Has the artificial (magneto-) dielectric system been optimized in the centimeter wavelength regime? Can composites be fabricated which work well in the millimeter wavelength regime? How do they compare with other materials approaches?

Alternatively, a more formal view of the program can be obtained from the Statement of Work given in the proposal and reproduced below as Table 1. Concurrent with this, we take note of the division of the work and of the reports into two subclasses, one of essentially non-magnetic composite dielectrics and one of composite magneto-dielectrics. Some aspects of the work on the latter are classified. Therefore this Final Report is prepared in two sections, Parts A and B, with the magneto-dielectrics work appearing in the classified section, Part B. The Statement of Work must be considered from that divided point of view.

The notation in the table following Task 4 signals a modification approved by the ONR Scientific Officer (W.R. Schmidt, CDR, USN) during an oral review/site visit on 12 June 1984. It resulted from the early realization that particle size effects and induced eddy currents would be rather important and that these had not been planned for study in the original program plans. An expansion of scope in Tasks 3 and 6 to these ends–i.e., theoretically and experimentally–formed a balance to the suppression of Task 4.

Table 1

STATEMENT OF WORK BY TASK

TASK	SUBCLASS ASSIGNMENT
1. Investigate effect of binder permittivity in artificial dielectrics	A
2. Analyze effects of microstructure control in passivated metal-insulator composites	A
3. Develop alternative theoretical approaches to composite dielectrics	A
4. Search for percolation transition: exploitation and control	removed see note in text
5. Explore alternative passivation coatings/investigate high-frequency properties	B
6. Quantify skin-depth effects in passivated artificial dielectrics	A B
7. Investigate millimeter-wavelength properties of artificial dielectric composites	A B
8. Investigate or simulate temperature dependence of high-frequency properties	B

2

The program plan originally provided for a three-year effort, starting officially on 1 Aug. 1983. The studies under Part A were completed by 30 June 1987 while those of Part B continued into the latter part of 1988. These were "no-cost" extensions. Reasons for the delays in research and in reporting were several: research leaves by the principal investigator, measuring equipment problems, and considerable difficulties in the preparation and/or acquisition of desired materials. We regret these substantial delays. However, we believe that we have completed the tasks of the work statement and contributed to understanding and progress in a number of the designated areas of research. We trust the reader will concur after examination of these final reports.

The principal investigator under this contract has benefitted from major and minor contributions from a number of collaborators and consultants. It is a pleasure to acknowledge their help, as listed here with their areas of contributions:

L.M. Levinson, for original program planning and helpful counsel

W.G. Moffatt for alloy preparation

S.A. Miller with D.N. Wernple for alloy powder preparation by gas-atomization and exploration of alternative coatings

A.E. Berkowitz and J.L. Walter with J.J. Rogers and W.E. Rollins for experimental research on the spark erosion method of alloy powder preparation

R.W. Harrison, D.B. Lindeman, and J. Murphy for consultation on and preparation of polymeric composites (GE Aircraft Engine, Cincinnati);

M.P. Borom with L.E. Szala for searching for alternative inorganic binders and preparing composites thereof

S.P. Yu and J.P. Quine for consultation on microwave measurement techniques

W.B. Westphal, Prof. F.R. Morgenthaler, and E. Maxwell (MIT, during leave 9/83-1/84) for discussions on high frequency measurements and on artificial dielectrics

J.O. Hanson for microwave measurements, K_α band, (GE-Re-Entry Systems, Philadelphia)

D.W. Forester and F.J. Rachford for consultation and measurements both at centimeter and millimeter wavelengths (Naval Research Laboratory)

D.R. Kelland for consultation on fine particle separation (National Magnet Lab., MIT)

H.J. Patchen for a wide range of important measurement responsibility for the principal investigator including thermomagnetic, microwave and Mossbauer spectroscopy

Prof. W.T. Doyle for major contributions in the modeling of random artificial dielectrics (Dartmouth)

Prof. W.P. Wolf for a wide range of consultations on physics and measurements (Yale).

II. DEVELOPMENT OF AN ARTIFICIAL DIELECTRIC

With the initial emphasis of the program on the dielectric aspects, an important phase has been the development of a suitable laboratory artificial dielectric. The model of a dielectric which consists of a series of metallic globules separated from each other by insulating material goes back at least to Faraday in 1837. An excellent history of inhomogeneous media concepts has been recorded by Landauer [2].

II.1 Criteria

Our criteria were that the metal (alloy) powder be non-magnetic at room temperature but ferromagnetic at low temperature to facilitate determination of the volume loading, p. The latter quantity is key to quantifying the dielectric behavior. We also required that the powder be capable of developing a thin insulating oxide layer on each particle. We contrast this with some other work in which researchers have encouraged formation of a thin oxide coating in powder preparation to discourage initial agglomeration but kept it thin enough to allow metal-to-metal contract between the particles under sufficient pressure [3].

The choice of candidate alloys thus involved magnetic and metallurgical consideration. Added to these was the challenge of fine metal powder preparation. For this task we made use of our gas-atomization facilities. In this process [4] molten alloy is forced through a specially designed nozzle, and the liquid stream is disrupted by high-velocity gas blasts to create fine droplets. These solidify as they descend in a large volume settling chamber. In one of our facilities liquid-substrate quenching is a special feature; i.e., a blast of water spray follows the gas jets (see Figure 1).

II.2 Consideration of Candidate Metallic Systems

Desirable alloy systems were therefore such that one of the elemental components would tend to form a stable and at least partially protective oxide. Some usual examples of this category are Al, Cr. and Y. Folding these in with the magnetic considerations yielded several suggestions, e.g., Ni with Cr, Gd with Y, and (Cu-Ni) with Al. The first two systems are reasonably well known magnetically in handbooks [5] or in more recent research [6], while the third has had little exploration [7]. The Gd-Y combination was quickly rejected (by our metallurgical colleagues) as
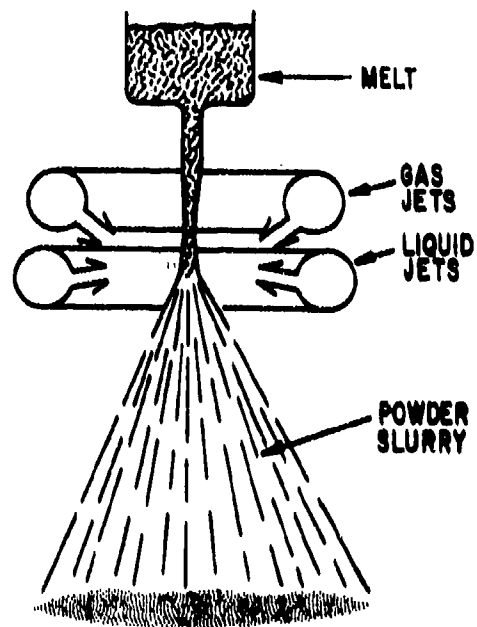
Figure 1.   Gas-liquid atomization

explosively undesirable. Although the solubility of Al in the Ni-Cu host is modest, at about 10 at% (~5 wt%), there appeared to be a fair prospect of a Curie point below room temperature. We chose to prepare an exploratory ingot with the composition (by weight) Ni90Cu5Al5. Finally for Ni-Cr, the wide range of solubility and well-known magnetic properties enabled us to specify "with confidence" an ingot composition of Ni92Cr8 with every expectation of a Curie point near 240K, and a low temperature saturation magnetization of about σ_∞ (0K) = 22 emu/g.

II.3 Magnetic Characterization of Candidate Metallic Systems

Thermomagnetic scans, magnetization vs. temperature at 50 Oe, along with low-temperature (6K, 20K) saturation magnetization data, were measured. For this purpose we have a vibrating sample magnetometer system with capabilities from 4K to 1370K (~1000°C) and fields up to 25 kOe. The scans for Ni-Cr are shown in Figure 2. As for the Ni-Cu-Al ternary (not shown), its T_c centered at 256K, but there was a risk of some residual undesirable ferromagnetism at room temperature. The opposite problem presented itself with the ingot Ni92Cr8. Both the Curie point and the magnetization fell short of confident expectations by a factor of 2! In searching for the "fault" here, we verified the chemical composition of the ingot, and also prepared a second ingot with composition Ni94Cr6. Its T_c, measured as 237K, again compares poorly with the literature value of 335K! At this point we were facing an unexpected, annoying, and delaying problem. A resolution of the dilemma was clearly warranted because this Ni-Cr system remained the most attractive of the ones considered as candidates.

II.3.1 Exploration of Magnetic Characterization Problems

The solution of the problem and the "validation" of our own work came from a detailed look at the published literature both backward from the handbook data and forward to the present time via a library bibliographic search. The magnetic measurements cited in the standard references [5] are based on experimental work from the Strasbourg laboratory directed by P. Weiss, a world-famous organization that set most of the standards for current magnetics research. In studying the primary sources, the research of Marian [8] and Sadron [9], we found that they used identical alloy samples which had been prepared earlier by Šafránek [10], also at Strasbourg. In the preparation, he had been concerned with the purity of the available starting materials, especially the chromium. Indeed, he ultimately prepared his own Cr by an electrolytic process, to combine with high-purity Mond nickel. Satisfactory metallurgical micrographs were shown, indicating single-
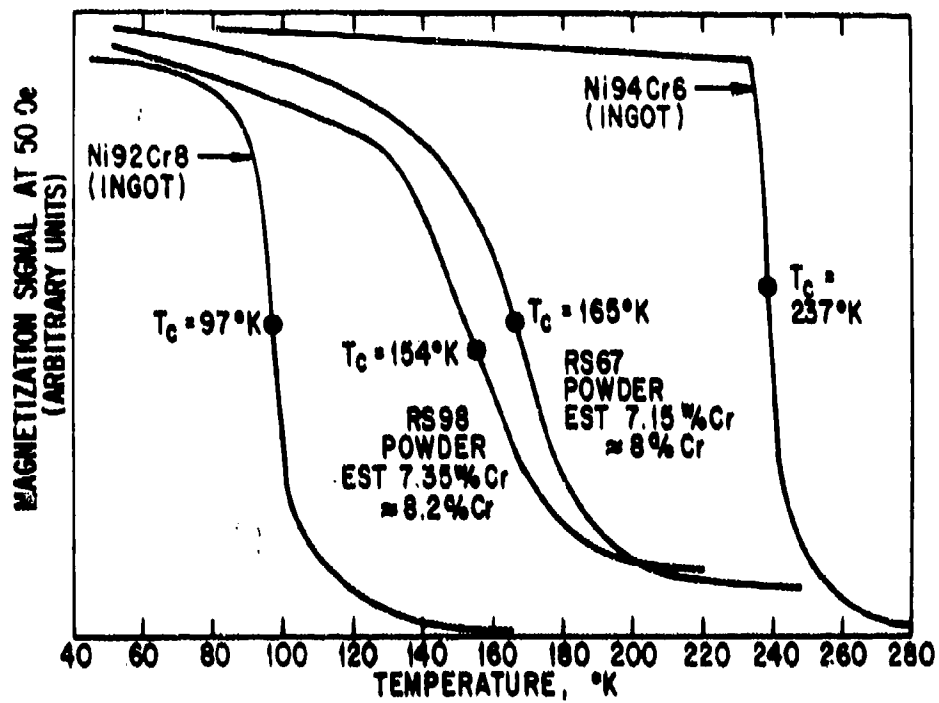
Figure 2. Thermomagnetic analysis of Ni-Cr ingots and atomized powders

7

phase alloys. Inasmuch as our Curie points were markedly lower, a suspicious investigator may still want to raise the purity question. How much residual Fe or Co in either component would be needed to shift the results into "accord"? More tolerance is in order with regard to the magnetic saturation because the French workers had to extrapolate downward from 110K toward absolute zero. However, their results are 40% to 100% greater than ours!

As one looks forward from the standard references into the most recent two decades, a different picture emerges. A group at Leiden [11] in 1962 noticed some differences in saturation magnetization for alloys of 5.6 at% and 9.1 at%, and in an estimate of T_c for the former alloy, but politely called these "small discrepancies." Next, a rather thorough investigation in 1972 at Strasbourg by Besnus et al. [12] (on newly prepared samples and including low-temperatures) presented results which differed quite a bit from the early data though not quite as much as the Leiden results. They diplomatically omitted to mention that they differed from their colleagues of an earlier generation! The emerging picture is displayed in Figure 3 for Curie points and in Figure 4 for saturation magnetization. (Compositions are in atom percent, as used by these research workers. In the region of interest to us, i.e., 6-8 wt%, the amount in at% is about one integer higher). More recently a study from Japan [13] gave results in close agreement with Besnus et al., and did make a significant graphical display of the differences with the early work. Lastly, Simpson and Smith in 1982 reported especially on compositions with quite low Curie points [14], in close agreement with our measurements.

While examination of the comparative results in Figures 3 and 4 does not fully settle the question of which set is correct, the existence of a major discrepancy with the early work is established. The present work on the several ingots sets the base line for subsequent magnetic evaluation of powder properties and ultimately, for our original goal, of volume loadings in artificial dielectric composites.

II.4 Preparation and Magnetic Characterization of Metal Powder

At this stage we were ready for powder preparation. We anticipated (correctly) that there would be some composition shift in this step toward a higher Curie point, and thus we selected the ingot Ni92Cr8 (about 9 at% Cr) in order to keep the alloy non-magnetic at room temperature.

Two atomization trials of the Ni92-Cr8 alloy were performed. In both cases the melt was atomized while at a temperature of 1870K by argon gas at 4.28 MPa. The high melt temperature
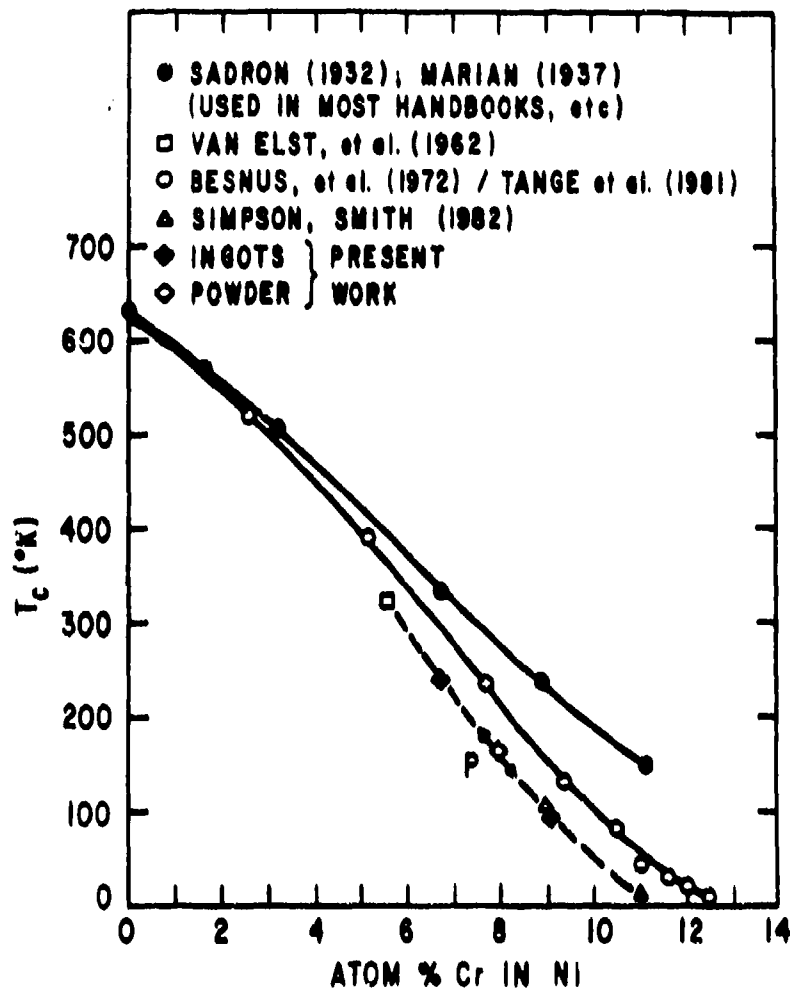
Figure 3. Ferromagnetic Curie points as a function of composition in Ni-Cr solid solution alloys including work of other investigators as well as present results
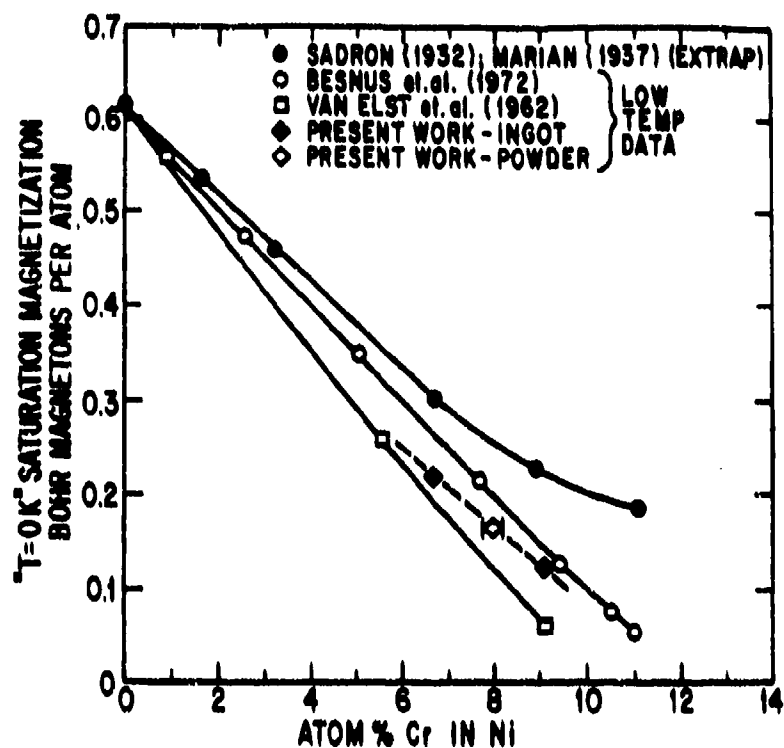
Figure 4. Saturation magnetization per average atom vs. composition for Ni-Cr alloys including available literature
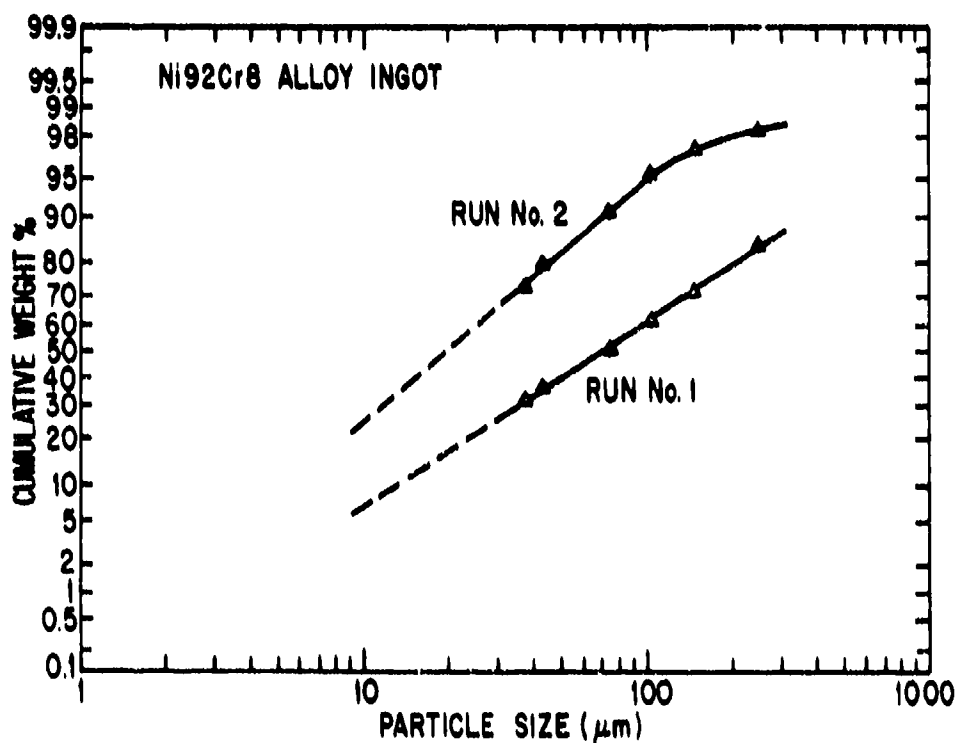
Figure 5. Particle size distributions from two gas atomization runs on $Ni_{92}Cr_8$ alloy

10

was employed to reduce the melt surface tension and melt viscosity while the high gas pressure resulted in a high gas jet velocity. (Mach Number ~3.2). Previous analysis has shown that fine powder sizes are favored by increased gas velocity and decreased melt surface tension and melt viscosity.

The two trials were performed using two different versions of the GE-CRD-developed close-coupled gas nozzle. The second run used an improved form of the close-coupled concept, designed to provide increased yields of fine powder.

The results of the two runs are shown in Figure 5. The particle size distributions between 37 μ m and 250 μ m were determined by sieving. The particle size distributions below 37 μ m were obtained by extrapolation, assuming the curves to be log-normal. (This assumption has been verified in other work).

The thermomagnetic scan of this powder (sieved to <37 μ m) is shown in Figure 2 as powder RS67. An average Curie point of 165K results, some 68K upward from the ingot. It is broader, suggesting a range of T_c values. The shift in T_c is presumed to arise principally from the effects of the blast of water spray.

Referring to Figure 3, this T_c translates in composition to about 8 at% Cr or 7.15 $\pm$ 0.2 wt% Cr. Using this composition, there is satisfactory accord of the saturation magnetization "line" in Figure 4 with the "present work" data.

For the practical record, the magnetization values at low temperature (6K or 20K), extrapolated to infinite field, are 21.2 emu/g and 12.0 emu/g for the ingots Ni94Cr6 and Ni92Cr8 respectively. For the RS67 powder we find 16.2 emu/g, and for the RS98 powder prepared later the value is 14.6 emu/g.

II.5 Evaluation of Surface Condition of Metal Powder

The shift in composition during powder preparation corresponds to a net depletion of Cr in the alloy particle. It is tempting to attribute this to an oxide coating of Cr_2O_3. It is much more difficult to examine the surface coating of spherical particles by microprobe techniques than the surface scales on bulk flat samples. Several, moderately successful attempts to do this on these powder spheres are reported herein. Conventional oxidation studies on the Ni-Cr system, albeit

11

under isothermal conditions, indicate a moderately complex scaling with NiO, Cr_2O_3, Ni-Cr spinel oxide and other components [15].

If we naively (and tentatively) hold to a view that the coating may be Cr_2O_3, we can estimate its thickness from a mass balance. Using a mean diameter of about 23 μ m we calculate a shell coating whose thickness is about 0.1 μ m, which is not unreasonable. A sketch of this rough calculation is as follows:

$$[(w\,/\,o\text{ Cr in ingot}) \times \text{vol. sphere} \times \rho \text{ alloy}] = [(w\,/\,o\text{ Cr in powder}) \times \text{vol. sphere} \times \rho \text{ alloy}]$$
$$+ [(w\,/\,o\text{ Cr in oxide}) \times (\text{vol. oxide shell}) \times \rho \text{ oxide}]$$

vol. sphere $= 4\pi r3\,/\,3$; vol. shell $= 4\pi r^2 \Delta r$

$$\Delta r = \left\{ \frac{\langle w\,/\,o\text{ Cr in ingot} - w\,/\,o\text{ Cr in powder} \rangle \times \langle \text{diam.} \rangle \times \rho \text{ alloy}}{(w\,/\,o\text{ Cr in oxide}) \times 3 \times 2 \times \rho \text{ oxide}} \right\}$$

Let us examine our first attempt with microprobe techniques on the Ni-Cr powder. As-prepared powder was pressed onto and into an aluminum substrate block for examination by Auger electron spectroscopy. The count rates for the various elements, Ni, Cr and O, were monitored as a function of sputter time. The latter is proportional to depth into the particle being examined, as material is sputtered away. The probe spot used was smaller than the particle diameter (from the powder size fraction +20, - 27 μ m). Count rates are expressed in atomic percent, after appropriate scaling in the instrument (Physical Electronics Model 600 Auger Microprobe). The "depth" probing may not be completely simple because the pressure used in preparing the specimen may have deformed the spherical alloy particle. As an alternative, we hoped to obtain a profile on a polished particle as the probe traversed the edge coating.

The depth profile by Auger spectroscopy is shown in Figure 6. While not the simple naive picture we hypothesized, it does have features one might expect. At the surface ($t = 0$, sputter time) there is a major build-up of oxygen, from a residual low level representing a sort of background; and a modest, ~50%, build-up of chromium from about 12 at% to about 18 at%. Concurrently, there is a major decrease of nickel, albeit not to the near-zero level hypothesized. We can attempt to rationalize these data in terms of NiO and Cr_2O_3, there being no evidence for Ni metal in the magnetic data. (Oxidation studies of this system [15] always assume that Cr goes to
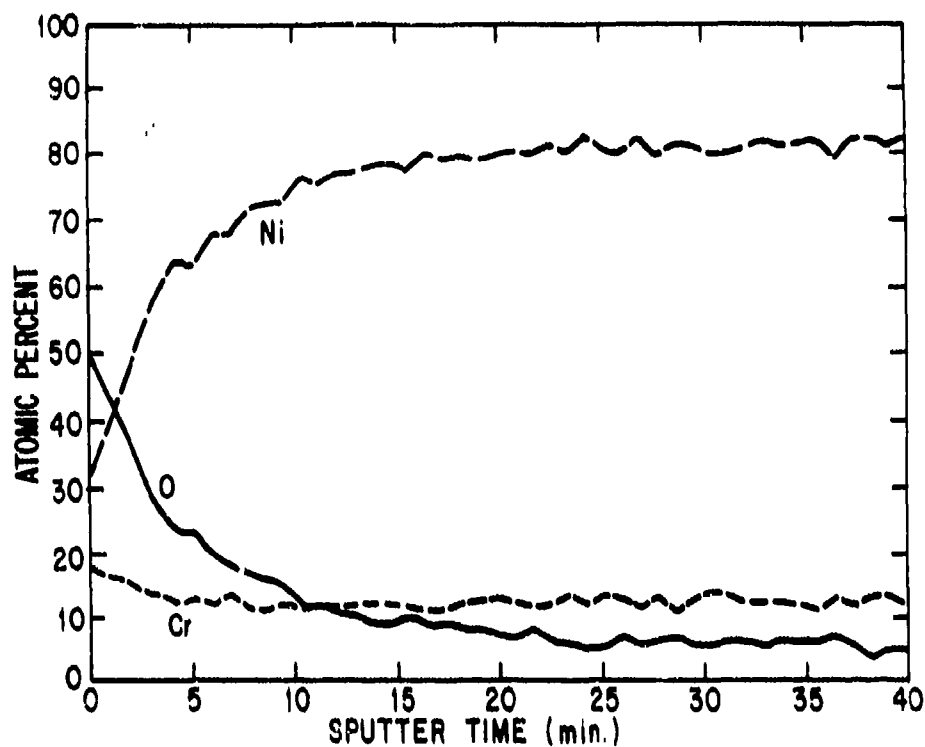
Figure 6. "Depth" profile by Auger electron spectroscopy of Ni-Cr powder compact: composition vs. sputter time (proportional to depth)

Cr_2O_3, or more complex spinels or solid solution). The "surface composition," $Ni_{0.32} Cr_{0.18} O_{0.50}$, is roughly equivalent to $3NiO \cdot Cr_2O_3$, which corresponds to $Ni_{0.27}Cr_{0.18} O_{0.54}$.

If we oversimplify the surface as a uniform shell (again), we can invoke a mass or atom balance to determine how much material is in the shell. Using the chemically and magnetically determined alloy compositions, we write:

$$Ni_{0.91} Cr_{0.09} + 6zO \rightarrow y\ Ni_{0.92} Cr_{0.08} + z\ (3NiO \cdot 1\ Cr_2O_3).$$
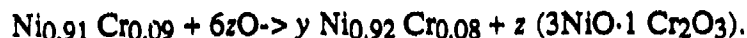
Balance equations for Ni and Cr yield two simultaneous equations in y and z, which are readily solved to yield $y = 0.969$, $z = 0.00625$. Approximately 2% of the original nickel goes into the oxide shell, while about 14% of the original chromium makes the transition. This does confirm the general stronger tendency for Cr to oxidize. Expressing the chemical balance in terms of the mass of one average (23 μm) particle and the number of moles of alloy in that particle, we can obtain the masses of NiO and Cr_2O_3. Converting to volumes (via their separate specific gravity values), and equating their total volume to a "shell" volume, we arrive at the oversimplified thickness of shell of 0.22 μm. This is a factor of two greater than the more naive estimate, but it too is only a rough (albeit reasonable) approximation.

For the second attempt with microprobe equipment, our associate, M.D. McConnell of the Microchemical and Surface Analysis Unit, Materials Characterization Operation, used an alternative technique. The Ni-Cr alloy particles were copper-coated by electroless plating for edge retention, and pressed together to develop an apparently continuous copper matrix. This compact could be polished to expose the particle cross section, and then a traversing scan by Auger electron spectroscopy might reveal an edge coating. The results of such a scan at 8000X embracing parts of two spherical particles are shown in Figure 7. Signals for Ni and O are shown, that for Cr being too weak or overlapping with the others. There is a clear buildup of oxygen at the particle edges. Its thickness could approach 0.5 μm, but care should be taken with that interpretation without details on the beam spot size.

The present evidence permits us to conclude with confidence that there is an oxide coating on the particles, one which is probably responsible for the high dc electrical resistance measured crudely on compacts of the powder (cf. next section). However, we cannot conclude the exact chemistry or microstructure of the shell itself. Conventional isothermal oxidation studies of Ni-Cr alloys [15] show that the nature of the oxide coating is rather sensitive to the Cr content and to the oxygen partial pressure, as well as to temperature and time. At our level of Cr, it seems quite

14
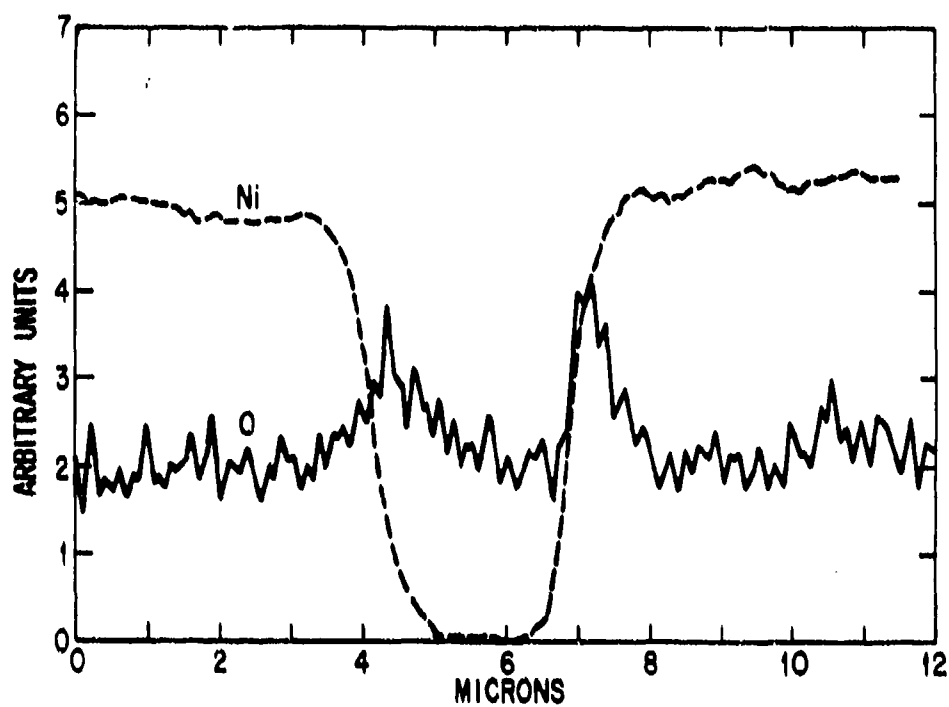
Figure 7.   Auger electron spectroscopy microchemical scan for Ni and O across Ni-Cr powder particles ($20 < d < 37$ μm) embedded in copper matrix

possible that the coating would contain precipitates of Cr_2O_3 in a NiO host, but that is still conjecture [16]. The conditions of temperature and partial pressure of oxygen in the gas-water atomization spray are poorly known.

II.5.1 Resistance Tests of Metal Powder Compacts

As a final practical acceptance test for the alloy powder, we attempted to verify that the powder particles were electrically insulated from each other. Conceptually, a check of resistance in powder compacts appears simple. In practice, it is less so. A simple device was constructed consisting of solid copper electrodes which can slide into a plastic cylinder, 1.25 cm inner diameter. We used this with a digital multimeter capable of measuring up to 20 MΩ resistance. A small amount of alloy powder in the cylinder gave erratic results, dependent on pressure, time, powder column height, etc. Confirmation of this behavior was found in the literature. Ottavi et. al. [17] describe a conceptually elegant experiment to study percolation concepts; i.e., at what composition do continuous electrical paths develop when various mixtures of conducting and insulating spheres are studied? Their experiments were carried out with monodisperse 5 mm diameter plastic spheres, a fraction of which had been electroplated with a thin copper coating. It is helpful to quote from their paper, as follows: "In order to obtain stable conductance measurements we find it necessary to apply pressure to the piston bearing the upper electrode. This lack of stability is not that due to fluctuations introduced by the randomness of the mixture. Indeed, even if the system is reduced to only two spheres, the measured resistance is not constant in time, or reproducible between trials, unless a sufficient force (about 10 kgf) is applied... We observe, moreover, a hysteresis phenomenon..."

Following these hints, we obtained roughly the same behavior. Powder column height was kept to 1.0 to 1.2 mm. Significant arm/body pressure, with some electrode piston rotation, was employed. These included a hydrogen-reduced ferromagnetic metal powder and a deliberately well-coated magnetic metallic powder. Under these conditions, we obtained the results given in Table 2. On the basis of these results, we conclude that the gas-atomized Ni-Cr powder prepared from the ingot Ni92Cr8 should meet the insulated particle criterion for our artificial dielectric.

16

II.6 Particle Size Separations and Morphology

As mentioned in the Introduction, particle size effects turn out to be more important than originally anticipated. Separation of -325 mesh (<37 μm) Ni-Cr powder from gas atomization preparation run RS-67 was carried out (somewhat tediously) using laboratory sieves until about 200 grams were obtained. The yields were as follows: 29 g at < 10 μm, 65 g at 10 < d < 20 μm and 114 g at > 20 μm. The possibility of invoking arch type methods for millimeter wavelength evaluations of composites at NRL necessitated large samples and hence greater quantities of powder. From the later atomization run RS-98, about 1400 g of -325 mesh powder was air-classified under a subcontract to Alpine American Corp. of Natick, MA. The yields obtained were as follows: 550 g at < 10 μm, 185 g between 10 and 20 μm and 670 g between 20 and 37 μm.

We show some SEM photographs in Figure 8 of the Ni-Cr powder from preparation run RS-67, for two powder particle size ranges, as classified. In each case there are a number of rather smaller particles than called for in the nominal range, but they do not represent a significant weight or volume fraction of the batch. The other feature of note is the occurrence of some elongated particles among the majority of spherical ones. This is more pronounced in the fraction with larger sizes. At present, we have to live with this, but this fact is important to know, both as a reference and as possible perturbation on the interpretation of data.

II.7 Preparation of Artificial Dielectric Composites – Polymeric Binder

II.7.1 Selection of Binder

One goal of the program (Task 1 of Table 1) was the investigation of the effect of binder permittivity in artificial dielectrics. Our plans called for two different insulating binders, one of which would be a polymeric material for which ε is typically 3 $\pm$ 0.5. The second would be an inorganic binder for which ε may be in the range 5 to 10. For the former, there is an easy choice for a laboratory system, i.e., polyurethane, known commercially as Permuthane™ (Division of Beatrice Foods, Corwin St., Peabody, MA. 01960). It has been used extensively in laboratory research test composites by ourselves and our collaborators at GE Aircraft Engine, Evendale, Ohio, who actually prepared our test specimen coupons. Efforts at preparing a suitable inorganic binder are described below in Section III.

17

Table 2

RESISTANCE OF ALLOY POWDER COMPACTS

Sample-Powder	Approx. Resistance
Ni-Cr $< 37\mu$m	10^5-10^6 Ω
Reduced Magnetic Metal $< 37\mu$m	10^1 Ω
Well-Coated Magnetic Metal $14 < d < 27\mu$m	$> 10^7$ Ω

Table 3

DESCRIPTION OF POLYURETHANE
TEST COUPONS (ALLOY-Ni$_{92}$Cr$_8$)

Sample #	Alloy Particle Size (in μm)	Nominal Alloy Volume Loading, p	Measured Volume Loading, p
ONR 1	—	0	—
ONR 2	+20 - 37	0.40	0.413
ONR 3	+20 - 37	0.30	0.307
ONR 4	+20 - 37	0.20	0.200
ONR 5	+20 - 37	0.10	0.112
ONR 6	+10 - 20	0.40	0.396
ONR 7	-10	0.40	0.384
ONR 8	-10	0.20	0.208

II.7.2 Preparation of Polyurethane Test Specimens

For our initial series of measurements, a set of nine test coupons was prepared. These involved several particle sizes, for reasons which will be explained in a later section. The basic specifications are given in Table 3, including measured values of p determined as described below.

The preparation followed guidelines for curing the polymer as prescribed by the manufacturer. Suitably chosen amounts of alloy powder and binder powder were combined and blended for several hours. The mixture was leveled into a 2.5 cm x 5 cm (1 in. x 2 in.) die to a thickness such that the final coupon would be ~1 mm (~0.040 in.) (In later work somewhat thicker samples were used for lower frequency measurements.) The loaded cold die was placed on hot press platens, then with increased pressure, raised to a curing temperature of 177°C where it was held for 5 min. It was subsequently cooled under cold running water.

The weighing calculations were based on a cured Permuthane density of 1.06 to 1.11 g/cm^3. (For sample ONR 1, we determined 1.11 g/cm^3.) These densities, as well as those for the composites are obtained from dimensions on regular shapes and weight. This avoids the possible problems of porous media, etc., but does permit small uncertainties in the determinations. For the alloy, we used a density of 8.79 g/cm^3 based on the magnetic determination of composition and an x-ray lattice parameter value of $a_0 = 3.529 \pm 0.006A$.

II.7.3 Evaluation of Volume Loading

As indicated in Section II.1.1 we place emphasis on a straightforward and non-destructive approach to determining the volume loading, p, of metal in the artificial dielectrics, as a guide to analysis of their electromagnetic properties. Our approach to this is through magnetic measurements at low temperature, having chosen an alloy metal that has its Curie point below room temperature.

A few simple formulas are helpful here. The subscripts a,b,c and h will refer to alloy, binder, composite and holes or voids respectively. Although we use the symbol p to designate volume loading in the bulk of this report, for this discussion we shall use the symbol f with the superscript w or v to indicate weight fraction or volume fraction. The symbols σ, M and P designate magnetization per gram, magnetization per unit volume (e.g., cm^3) and specific gravity (or density in g/cm^3).

19
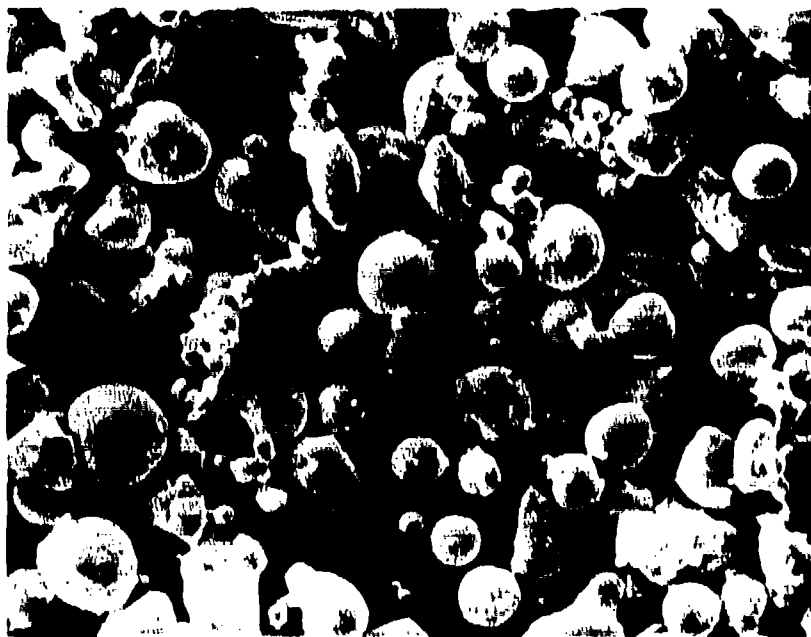
Figure 8. Scanning electron micrographs of Ni-Cr alloy powders from gas atomization preparation run RS-67. Magnification: 1000X. Top photo, nominal 10 μm < d < 20 μm; bottom photo, nominal 20 μm < d < 37 μm.

For specific magnetization, or magnetization per gram, of composite we write

$$\sigma_c = \sigma_a f_a^w + \sigma_b f_b^w + \sigma_h f_h^w,$$

but obviously

$\sigma_h = 0$ and f_h^w at all times, and thus $f_a^w + f_b^w = 1$. Therefore, we have

$$\sigma_c = \sigma_a f_a^w + \sigma_b (1 - f_a^w).$$

This expression becomes trivial but useful when one notes that $\sigma_b = 0$ in most cases of interest. Therefore the formula for weight fraction of alloy becomes $f_a^w = \sigma_c / \sigma_a$. The measurement of σ_c along with a knowledge (or independent measurement) of the alloy magnetization gives its weight fraction.

For the volume magnetization and the related volume fractions, we obtain in the same manner

$$M_c = M_a f_a^v + M_b f_b^v + M_h f_h^v,$$

but this time f_h^v may be different from zero although $M_h = 0$ at all times and $M_b = 0$ in most cases of interest. Note also that $f_a^v + f_b^v + f_h^v = 1$, by definition. The formula for volume fraction of alloy, p, is thus

$$p \equiv f_a^v = \frac{M_c}{M_a} = \frac{\rho_c \sigma_c}{\rho_a \sigma_a} = f_a^w \frac{\rho_c}{\rho_a}$$

This requires the additional measurement (or knowledge) of the density of the composite and of the alloy. With these measured values, on whole samples, the results are on firm ground and contain no approximations or idealizations. We discuss determination of the void fraction in the next section.

As for the case of the binder alone, we have obtained more consistent results in determining density in the "primitive" way from dimensions on regular shapes and weight. For many electromagnetic considerations it is the overall volume property which is of interest, so that this simple method which includes voids, cracks, etc., is the proper one. The results for the volume loading determinations are given in Table 3. The agreement between nominal and measured values is very satisfactory and should be characteristic of polymeric-type binders when appropriate care is taken. With other categories of binders such agreement cannot be taken for granted.

II.7.4 Calculation of Porosity

An aspect of the microstructure of composites is the porosity, i.e., the volume fraction of holes or voids. It is straightforward to calculate this quantity using the densities of the separate components and their proportions ascertained from observable measurements. We refer back to definitions of symbols used above for evaluation of volume loading.

Consider a mass m_c of the composite occupying volume v_c. Then

$$v_c \rho_c = m_c = v_c \left(\rho_a f_a^v + \rho_b f_b^v + \rho_h f_h^v \right),$$

but $\rho_h = 0$ of course. Thus we have

$$\rho_c = \rho_a f_a^v + \rho_b f_b^v, \text{ or}$$
$$f_b^v = \frac{\rho_c - \rho_a f_a^v}{\rho_b}$$

But with $f_h^v = 1 - f_a^v - f_b^v$, we can write

$$f_h^v = 1 - f_a^v - \frac{\rho_c}{\rho_b} + \frac{\rho_a}{\rho_b} f_a^v = 1 - \frac{\rho_c}{\rho_b} + p \left(\frac{\rho_a}{\rho_b} - 1 \right)$$

Alternatively, using the formula for p in observables, we obtain

$$f_h^v = 1 - \frac{\rho_c}{\rho_b} + \frac{\sigma_c \rho_c}{\sigma_a} \left(\frac{1}{\rho_b} - \frac{1}{\rho_a} \right).$$

22

The principal sources of error in this determination of porosity are the density values for the binder material and for the composite. By contrast, the alloy density and the various magnetizations (on a mass basis) are sufficiently well known or well measured to be much less important in estimating the possible errors in f_λ^v. Therefore, we can write

$$df_\lambda^v = \frac{\partial f_\lambda^v}{\partial \rho_b}d\rho_b + \frac{\partial f_\lambda^v}{\partial \rho_e}d\rho_e$$

$$= \frac{\rho_e}{\rho_b}\left(1 - \frac{\sigma_e}{\sigma_a}\right)\frac{d\rho_b}{\rho_b} - \left[\frac{\rho_e}{\rho_b}\left\langle 1 - \frac{\sigma_e}{\sigma_a}\right\rangle + \frac{\rho_e\sigma_e}{\rho_e\sigma_a}\right]\frac{d\rho_e}{\rho_e}$$

When we substitute typical numbers into this formula we find: at the $p = 0.4$ level, a 2% error (uncertainty) in ρ_b contributes about 0.01 to df_λ^v and a 1% error in ρ_e contributes a similar uncertainty (0.01) to df_λ^v; at the $p = 0.1$ level each of such a pair of uncertainties (0.01) in df_λ^v follows from 1% errors in ρ_b or ρ_e.

In Table 4 we present the result of the porosity calculation. Other characteristics of these samples such as volume loading and particle size were given in Table 3. The values of porosity are generally small. The scatter between positive and negative values (the latter are meaningless) say more about our uncertainties than about the composite samples. At this stage we conclude that the preparation method is sufficiently in control that porosity is not a significant factor for this set of samples to affect the electromagnetic parameters.

II.7.5   Follow-on Higher-Frequency Test Specimens

We contracted to obtain measurements at 35 GHz at GE Re-Entry Systems Department in Philadelphia. The method was based on the slotted-line technique with a circular waveguide cavity. It has the advantage of requiring a small (0.250 in. diameter), thin disk. This is much less demanding of material than, for example, that required for the arch method. It is also easier to fabricate than the precision (7 mm) coaxial toroid, when the question of machinability arises.

According to the provisions of the contract, millimeter wavelength region measurements for this study are to be performed at the Naval Research Laboratory, Washington, DC. Toward this goal, a visit was made to NRL in February 1985 for discussions with Dr. D.W. Forester and Dr.

23

Table 4

CALCULATED POROSITIES
OF POLYURETHANE
TEST COUPONS

Sample #	f_h^v
2	+0.04
3	−0.05
4	−0.03
5	+0.01
6	−0.04
7	+0.07
8	+0.01

Table 5

DESCRIPTION OF POLYURETHANE TEST COUPONS
FOR NRL HIGH-FREQUENCY MEASUREMENT SAMPLES

- Powder from atomization run RS-98 (Alloy 8.2 at% Cr in Ni; $T_c = 154$ K ± 20)
- All intended for nominal 40% volume loading ($p = 0.40$)
- Two powder particle size ranges chosen

Coupon Slab	Particle Size (μm)	Measured p	Measured Density	Calculated Porosity f_h^v
A Waveguide pieces: K_a, Q, W	< 10 μm	0.36	3.63_4	0.19
B Arch slab	< 10μm	0.27	3.10_0	0.07
C Waveguide pieces: K_a, Q,W	>20-37μm	0.42	4.31_8	0.01
D Arch slab	>20-37μm	0.39	4.04_0	0.08

F.J. Rachford. It was agreed that the measurements would be attempted by several techniques, including the arch method at rather high frequencies (~90 GHz), and waveguide techniques at several high-frequency bands, e.g., K_u (26-40 GHz), Q (40-60 GHz), and W (75-110 GHz). Such a wide range of frequencies, coupled with the particle size effects, offers an exciting prospect for testing our models and amplifying our understanding.

From the discussions at NRL, it was decided to measure rather highly loaded samples, i.e., volume loading of $p = 0.40$. In order to preserve the particle size study, we chose the two extremes, i.e., < 10 μm and 20 to 37 μm. Test coupons of powder (RS-98) with polyurethane binder were prepared according to the above techniques. Two coupons for each particle size were made. One was 4 x 4 x 0.045 in. for preparation of the arch method test piece, and the second was about 1 x 2 x 0.080 in. for subsequent precision cutting of waveguide pieces.

The actual volume loading and estimated porosities were calculated as described above. The results are presented in Table 5. We see that the larger powder size material coupons came quite close to the goals set ($p = 0.4$) while the < 10 μm powder composite coupons fell short.

At millimeter wavelengths, the samples must be cut with high precision. The 3 x 3-in. plate samples for the arch method were trimmed to thicknesses estimated at $(3/4)\lambda_m$, where λ_m is the wavelength in the medium at W band (90 GHz). Estimates for λ_m were arrived at from modeling for μ' and ε' described herein. The formula for the wavelength in the medium is $\lambda_m = \lambda_o / [\varepsilon'\mu']^{1/2}$, where λ_o is the vacuum wavelength. Even more demanding are the samples to fit into the waveguides of the separate bands These desirable thicknesses are again an odd number of quarter-wavelengths. However, for this measurement one refers to the guide wavelength [4], λ_g given by

$$\lambda_g = \frac{\lambda_m}{\left[1 - (\lambda_o / \lambda_c)^2\right]^{1/2}}.$$

where λ_c is the cutoff wavelength of the particular waveguide which is a function of the waveguide dimensions [20]. In some cases we could get by with quarter-wavelength pieces. At higher frequencies, these would be so thin as to force a choice to three-quarter-wavelength thicknesses.

25

II.8   Direct Observations on Composites: Porosity and Particle Aggregation

Can we confirm the calculated conclusion that porosity in the polyurethane artificial dielectric composites is negligible? That would seem to be an easy task in these days when a scanning electron microscope (SEM) is often readily available. However, preparation of samples for observation is a special art which is needed in the case of these polymeric composites. Special equipment was needed, as provided by our associates V.H. Watkins and S.Y. Hobbs of the Polymer Physics Unit. Room temperature microtoming was unsatisfactory because the binder was so soft, but a cold microtoming technique (with the sample at about $-150^{\circ}C$) using a glass knife produced a very satisfactory surface for examination. The apparatus used was an Ultracut E.

For the first sample studied, the as-cut material was lightly coated with Au and Pd (a few hundred angstroms coat) to carry off electronic charge and heat. The SEM pictures shown in Figure 9 for one sample (ONR #2, $p = 0.4$, $20\,\mu m < d < 37\,\mu m$) are clean and interesting. There are faint but discernable circles which are cut(!) sections of the metal powder spheres. Their dimensions correspond to particle sizes used. Note that smaller sizes may be anticipated in the cut, and a few are distorted from the circular cross section. Their identity is confirmed by EDAX (Energy Dispersive Analysis by X-rays) which shows a high count for Ni and a lesser one for Cr on these circles, in contrast to the adjoining matrix. A number of holes are present. Some of these are obviously hemispherical "pull-outs." Others are distorted but with excess lip material suggesting a pull-out. There are many regions densely filled with material of one kind or another. The latter observation is in accord with the calculations suggesting negligible porosity. At this volume loading the metal particle density is sufficiently high that one cannot get a feel for "irregular fluctuations" in the loading.

It is a matter of concern for understanding the electromagnetic properties on a quantitative basis that one look for wide variations in local packing on some moderate length scale. Several workers have pointed out the potentially enormous effects that may arise from agglomeration with electric conduction contact [18] or wide variation in size distribution [19] intrinsically or as a consequence of agglomeration. In addition, as we discuss later herein, if a nominally dilute, low p-value composite has locally densely packed regions (of a size we hope to be able to investigate theoretically), compensated by regions nearly empty of metallic particles, without electric conduction paths in the densely packed regions, there can be some enhancement of electromagnetic property parameters. This arises from a strongly non-linear volume loading dependence of the property.

Figure 9. Scanning electron microscope views of cold-microtomed polymeric composite (lightly coated with Au and Pd): ONR #2 ($p = 0.4$, 20 μm $< d <$ 37 μm). Top photo at 150X; lower photo at 500X.

Subsequently we extended the examination to the more dilute samples of the series (ONR No. 5, $p = 0.1$; ONR No. 4, $p = 0.2$; ONR No. 3, $p = 0.3$; 20 μm < d < 37 μm, alloy RS-67). This time the microtomed samples were coated lightly with carbon to carry off electrons and heat, instead of Au and Pd. The result is a much improved visual contrast, as shown in Figure 10. There is clear evidence for spatial fluctuations in local density of alloy particles. This picture gives a scale to the "clumping." The challenge is whether we can model this in an analytic way. The SEM pictures in Figure 10a also show "crevasse" lines in the matrix that do not appear in the other photos. We (including Watkins and Hobbs) do not know their origin, but think they are not relevant to our problem. Our collaboration with Professor Doyle was initiated in hopes of tackling the clumping in a quantitative way.
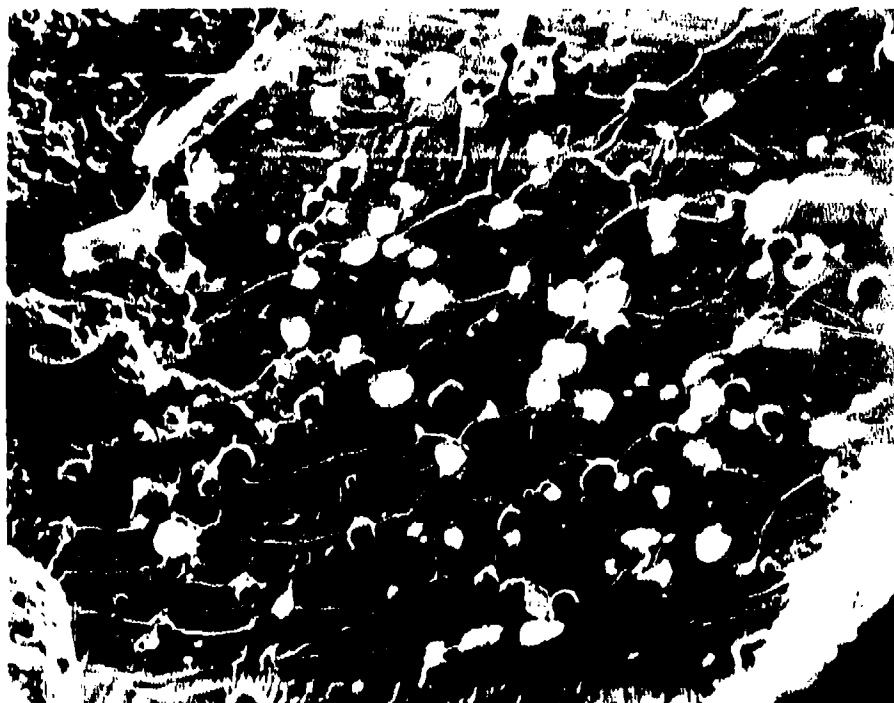
Figure 10a. Scanning electron microscope views of cold-microtomed polymeric composite. ONR #5 ($p = 0.1$, 20 μm $< d <$ 37 μm). Top photo at 150X; lower photo at 500X.
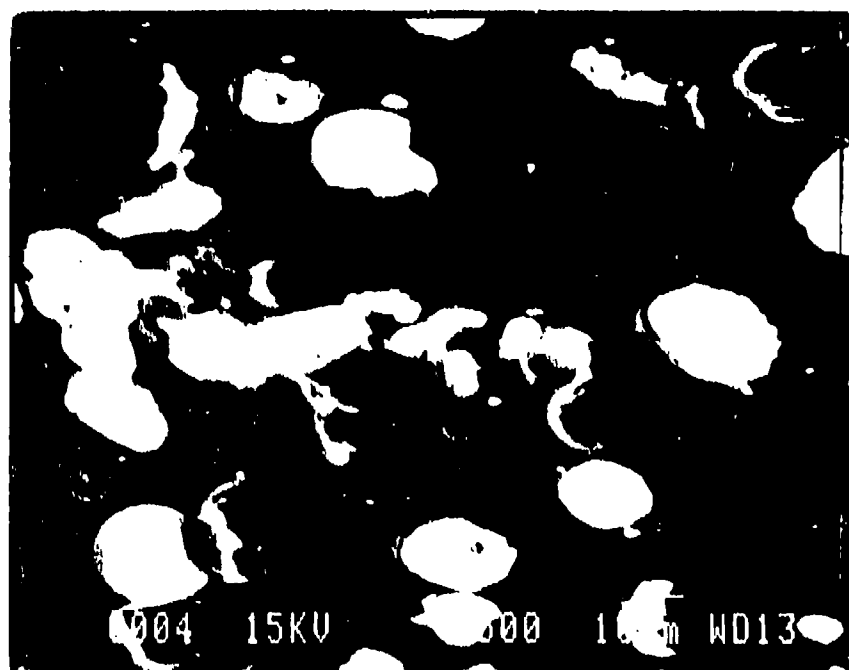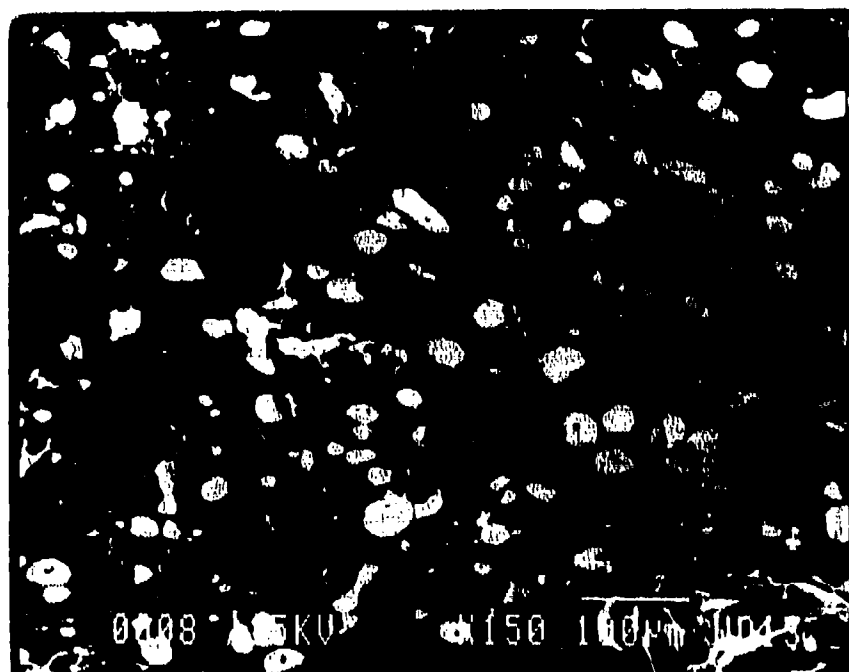
Figure 10b. Scanning electron microscope views of cold-microtomed polymeric composite. ONR #4 ($p = 0.21$, same d). Top photo at 150X; lower photo at 500X.

30
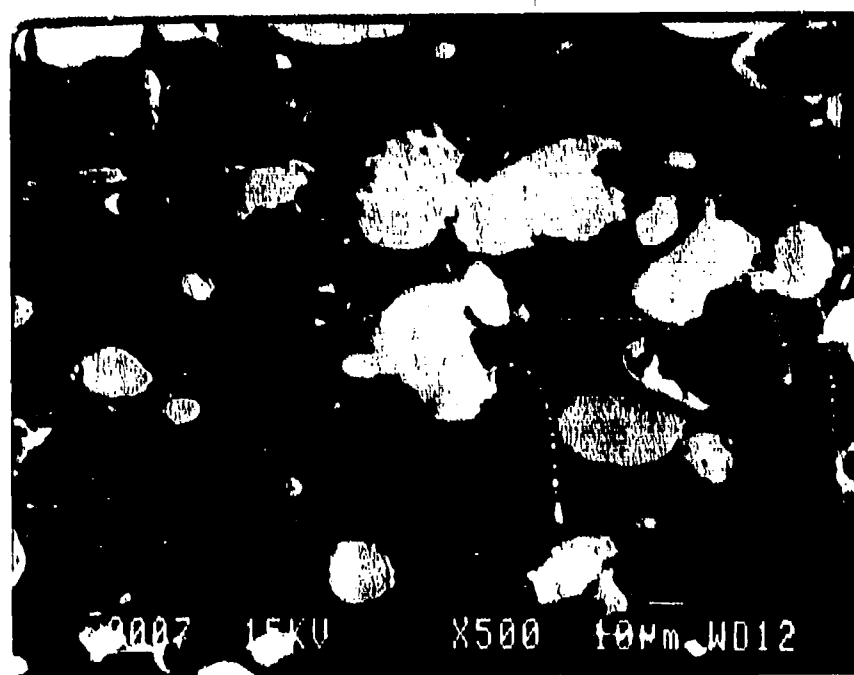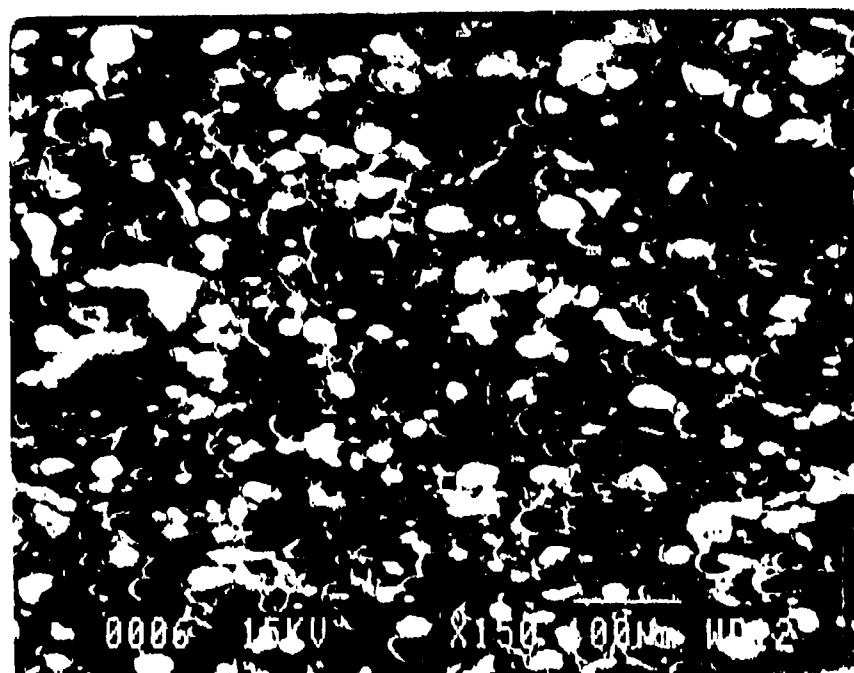
Figure 10c. Scanning electron microscope views of cold-microtomed polymeric composite. ONR #3 ($p = 0.3$, same d). Top photo at 150X; lower photo at 500X.

III. BINDER PERMITTIVITY EFFECTS

An aspect of the modeling analyses of the permittivity of artificial dielectrics is that the dielectric constant of the binder "sets the level" for the dielectric constant of the composite, and in a multiplicative way. This can be expressed quite simply by citing the formula for the Mitoff approximation to the Maxwell (Clausius-Mossotti) formula [21], i.e.:

$$\log \varepsilon' \approx \log \varepsilon'_b + Gp$$

or

$$\varepsilon'_c / \varepsilon'_b \approx 10 Gp,$$

where c and b represent composite and binder, p is the volume loading of the metal or alloy particles (phase a), and G is a constant of value 1.3 Thus choosing a binder with twice or half the value for ε'_b will produce a doubling or halving the value of ε'_c.

The relevance of this effect lies in the role of ε'_c in the wavelength of the electromagnetic radiation in the medium, by the formula given in Section II.7.5. Since electromagnetic applications configurations often are designed with materials of thickness measured in units of the wavelength, the choice of binder could influence the overall weight of the configuration.

As noted in Section II.7.1, one of the tasks was to verify this prediction in the microwave and/or millimeter wavelength regions by comparing artificial dielectric composites with two different insulating binders. (In hindsight, the proposed task was rather naive in that the prediction has been rather well established.) Our plan called for one organic, polymeric binder, for which ε'_b is usually near 3, and a second inorganic binder that could carry an ε'_b value in the range of 5 to 10.

III.1 Criteria

At the outset it is useful to enumerate the requirements of the proposed search. The material and process should maintain the shape (usually spherical) of the alloy particles; they should maintain the essential chemical integrity of the alloy, although some small deviation is

permitted; and they should maintain a condition of electrical isolation of the particles. Beyond these requirements, the resulting product should have sufficient mechanical integrity to permit machining into high-frequency measurement specimens. Even with the last requirement, there are options in that precision coaxial samples for the microwave network analyzer are more demanding of machinability than the thin, solid disks needed for the 35-GHz, slotted-line measurement.

III.2   Extensive Search for Alternative Inorganic Binder

For our first attempt we tried to use a proprietary inorganic binder under development at GE-Evendale. It is intended for a similarly sized but chemically different dispersoid (loading material). Typically, with inorganic binders there is a high-temperature cycle to bring the binder to its final state. In our past experience [1] such a high-temperature excursion may be accompanied by a chemical reaction between binder and dispersoid particle. In the present case we requested four composites, $p = 0.1, 0.2, 0.3$, and 0.4, each with the largest particle size +20-37 μ m of the Ni_{92} Cr_8 powder. In each case, the resulting composite was ferromagnetic at room temperature. Indeed a thermomagnetic scan showed Curie points up to 350°C (pure Ni, $T_c = 358$°C) with strong suggestions of composition variations within the magnetic phase. Under these conditions it is very difficult to know the alloy composition in the composite. Therefore, we could not determine volume loading without destruction and visual or probe analysis of the composite.

The subsequent steps of our search were carried out by our collaborators M.B. Borom and L.E. Szala. Specimens were compounded from a three-component system--paramagnetic Ni-Cr alloy particles as the active component, a choice of two different glasses as the binder, and alumina as an inert filler. Ni-Cr alloy particles of two different particle sizes were used in volume fractions ranging from 15 to 30 vol%. Alumina as an inert, refractory, fine-grained, dielectric material was chosen to keep the metallic particles isolated from one another. Good, high-temperature compressive strength of the alumina contributes to maintaining spaciag of the deformable metallic phase, particularly during sintering or hot pressing. The third component to be considered is the binder. (Electrically, all the nonmetallic components make up the binder, but we are speaking here in the ceramic processing sense). The binder must be sufficiently fluid during processing to flow between the Al_2O_3 and the alloy and create a mechanically strong structure. The binder must flow at a temperature below the melting point of the Ni-Cr alloy, and must also be nonreactive to it. Many glasses with reasonable softening points fit these requirements. Two types of glass were tried: a soda/lime window glass composition designated as Corning code 0800, and a lead-

33

bearing, Owens-Illinois solder glass designated as SG-7. Both glasses have softening points below the melting point of the Ni-Cr alloy.

Powder preparation was accomplished by milling the components in polyethylene jars using 1/4-inch alumina spheres as the grinding material. The alumina, 0.3 μm in size, and the glass were initially wet-milled together in alcohol for 8 to 10 hours to reduce the particle size of the glass and to ensure proper blending of the two components. After the addition of the alloy powder, an additional 1 to 2 hours of milling was performed to disperse the alloy powder. Milling times after the addition of alloy were kept short to prevent erosion of the oxide coating already present on the alloy powder particles. The blended powders were then dried in a rotating evaporator to keep the relatively coarse-grained Ni-Cr in suspension. The dried blends were compacted using standard die and/or isostatic pressing.

Table 6 is a summary of experiments and results. The table is made up of two sections, with the type of glass used being the prominent variable. Samples are listed alphabetically in each section. The major sections are then divided into segments detailing composition and process variables and results.

Sample 0800-A, a blend of 35% Al_2O_3, 35% 0800 soda/lime glass and 30% 20-37 μm Ni-Cr powder, was consolidated by hot pressing at a temperature of 950°C and 600 psi loading. The resultant material shown in Figure 11 appears to meet the requirements of paramagnetism (i.e., not attracted by a small permanent magnet) and is nonconductive; however, the compact has very low strength.

In an attempt to overcome the low strength problems associated with sample 0800-A, a higher hot pressing temperature and loading were employed. It was felt that increasing the temperature to 1300°C and the pressure to 1200 psi would require a more rigid, less deformable composition. This Ni-Cr content was kept at 30 vol%, while the glass content was decreased to only 10%, and the difference made up by alumina (sample 0800-B). As anticipated, use of higher temperatures and pressures corrected the low strength problem associated with sample 0800-A, but created a problem of its own. Because of the elevated temperature and pressure, the alloy became more deformable and sintered into an interconnected network, thus becoming electrically conductive.

Sample 0800-C was prepared keeping the ratio of Al_2O_3 to glass the same as in 0800-B, but reducing the metallic alloy loading to one half the value, i.e., 15%. Hot-pressing conditions

34

Table 6

SUMMARY OF PREPARATION EXPERIMENTS
IN SEARCH OF SUITABLE INORGANIC HOST COMPOSITE

Sample Idel	Glass	Glass Comp. v/o	Matrix: Inert Phase Al₂O₃ v/o	Ratio Inert/Glass	Binder Inert + Glass v/o	Active Particle Conc v/o	Active Particle Size (μm)	Comp.	Hot-Press P (psi)	Hot-Press T_max (°C)	Hot-Press t_min	Sintering T_max (°C)	Sintering t_min	Magnetic Yes	Magnetic No	Electrically Cond. Yes	Electrically Cond. No	Comments
0800-A HP-26-85	0800 Soda/Lime	35	·	1:1	70	30	20-37	NiCr	600	950	2				X		X	Mechanically weak
0800-B HP-23-85		10	·	6:1	70	30	20-37	NiCr	1200	1300	2					X		Very dense microstructure
0800-C HP-25-85		12.5	·	6:1	85	15	20-37	NiCr	1200	1300	2				X	X		
0800-D HP-28-85		10	·	6:1	70	30	<10	NiCr	1200	1300	2				X	X		
0800-E 5-16-85A		10	·	6:1	70	30	<10	NiCr				1000	5	X			X	Compact pre-oxidized to 80
0800-F 5-16-85B		10	·	6:1	70	30	<10	NiCr				1000	5	X			X	No pre-oxidation
SG-7-A HP-30-85	SG-7 Lead-Bearing Solder Glass	21	·	4:1	100	0	—	—	700	650	2			NA		NA		
SG-7-B HP-31-85		20	·	2.5:1	70	30	20-37	NiCr	400	840	2				X		X	Very weak mechanically
SG-7-C 6-11-85		20	·	2.5:1	70	30	20-37	NiCr				1000	5	X		X		
SG-7-D 6-28-85		20	—	0	70	30	20-37	NiCr				1000	5	X		X		Good strength, Blow holes present
SG-7-E 7-17-85		20	—	0	70	30	20-37	NiCr				625	20		X		X	Potential candidate material

35

Figure 11. Optical micrographs of inorganic composite sample 0800-A, with soda-lime glass. Preparation parameters given in Table 6. Magnifications at 200X and 500X.

were identical to 0800-B. These conditions produced a very dense, paramagnetic, nonconductive sample. The process, however, would probably not be suitable because of the low loading of Ni-Cr alloy.

Sample 0800-D differs from sample 0800-B only in that the alloy particle size was reduced from 20-37 to <10 μ m. Composition and processing were the same. A smaller particle size was used in an attempt to increase the loading back to 30% and to achieve a better dispersion of the Ni-Cr alloy throughout the mixture, thus possibly creating less contact between the individual particles. It is very difficult to suspend large particles of a dense material in a fine dispersion of a low-density material. Results of the test were poor. Even though the uniformity of the dispersion of Ni-Cr alloy was greatly increased, the material was highly conductive. The result is shown in Figure 12.

The Ni-Cr alloy powder appears to be too deformable at elevated temperatures to withstand unidirectional pressure of hot pressing. Pressure exerted on the system deforms the spherical metal particles into platelets and increases the chance of contacting and sintering together. Therefore, experiments employing pressureless sintering were designed in an attempt to solve the problem of metal-metal contact during consolidation.

Samples 0800-E and 0800-F were compositionally the same as 0800-D (60% Al_2O_3, 30% Ni-Cr (<10 μ m), 10% 0800 glass). The mixtures were isostatically pressed into 1/2-in. diameter x 5/8-in. long pellets at a pressure of 55 kpsi. In an effort to increase the oxide film thickness on the Ni-Cr particles to assist in preventing metal-metal contact, sample 0800-E was subjected to a preoxidation step by firing the sample to 800°C in air and holding for 10 min. Both samples 0800-E and 0800-F were sintered by heating in helium at ~50°C/min to 1000°C and held at temperature for 5 min. Even though both samples remained electrically nonconductive, the paramagnetic properties of each sample were destroyed. The loss of paramagnetism and development of ferromagnetism were indicated by the ease with which the sample could be picked up and held by a small permanent magnet. Loss of paramagnetic properties was not observed in any of the hot-pressed samples. The change in magnetic properties indicates that the Ni-Cr alloy had been changed compositionally, most likely due to oxidation during sintering and/or preoxidation.

From both sintering and hot-pressing experiments it became apparent that temperatures in excess of ~900°C could be detrimental to the Ni-Cr alloy particles both chemically as well as physically. To reduce the processing temperature below 900°C, a lower softening point glass was

Figure 12. Optical micrographs of inorganic composite sample 0800-D, with soda-lime glass. Preparation parameters given in Table 6. Magnifications at 200X and 500X.

38

selected. The glass selected was a lead-bearing solder glass designated SG-7, which has a working temperature of approximately 600-700°C.

Sample SG-7A, a mixture of 79% Al$_2$O$_3$ and 21% SG-7 containing no metal particles, was hot pressed under a static load of 700 psi. The sample completely densified at 690°C.

Sample SG-7B was formulated with 30% Ni-Cr (20-37 μm). The volume percent of SG-7 was kept at the same level as in SG-7A (20%) and the balance was alumina. The mixture was hot-pressed under a static load of 400 psi. In contrast to sample SG-7A, which glassified at 690°C, no movement of the press rams occurred until 750°C. The final pressing temperature was 840°C. Both the reduced pressure on the sample and the presence of the coarse metal particles probably contributed to the need for higher processing temperature. The density of the resultant compact was excellent. The material was non-conductive and maintained its paramagnetic properties, but as in hot-press experiments the alloy was no longer spherical.

With further evidence that hot-pressing, even at 850°C, deforms the Ni-Cr alloy particles, sintering was again employed. Sample SG-7C is compositionally identical to SG-7B. The material was sintered at a temperature of 1000°C for 5 min in 1 atm of helium. The high temperature was again tried, even though previously unsuccessful, as a direct comparison between the 0800 and the SG-7 glass (via sample 0800-E). The results were nearly the same. The paramagnetic properties were destroyed. The material is nonconductive, but this is primarily because the material is substantially unsintered. A higher content of glass may be required for densification.

After discussions it was decided to relax the potential high-temperature service requirements of the material to see if Ni-Cr could be successfully incorporated in a low-temperature glass matrix without the presence of the refractory alumina phase.

Sample SG-7D is a mixture of 70% SG-7 solder glass and 30% Ni-Cr alloy (20-37 μm). The intent of the experiment was to sinter at ~ 650°C, but due to an error in reading a thermocouple scale, the temperature was raised to ~1000°C. Again, and not surprisingly, the sample failed all the necessary requirements (i.e., it was both ferromagnetic and electrically conductive). Micrographs are shown in Figure 13.

The experiment was then repeated, this time sintering at 625°C for 20 min. The results (samples SG-7E) were quite encouraging. The paramagnetic and electrical conductivity
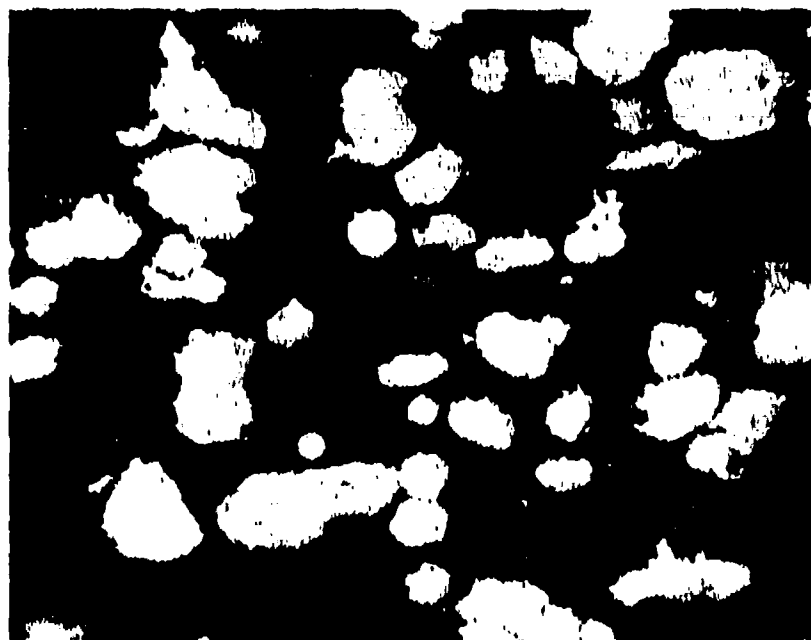
39
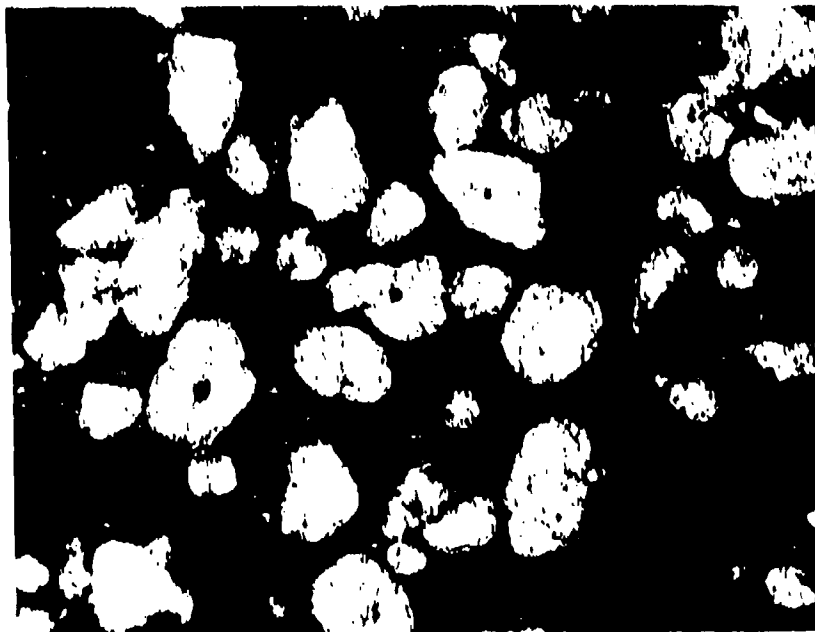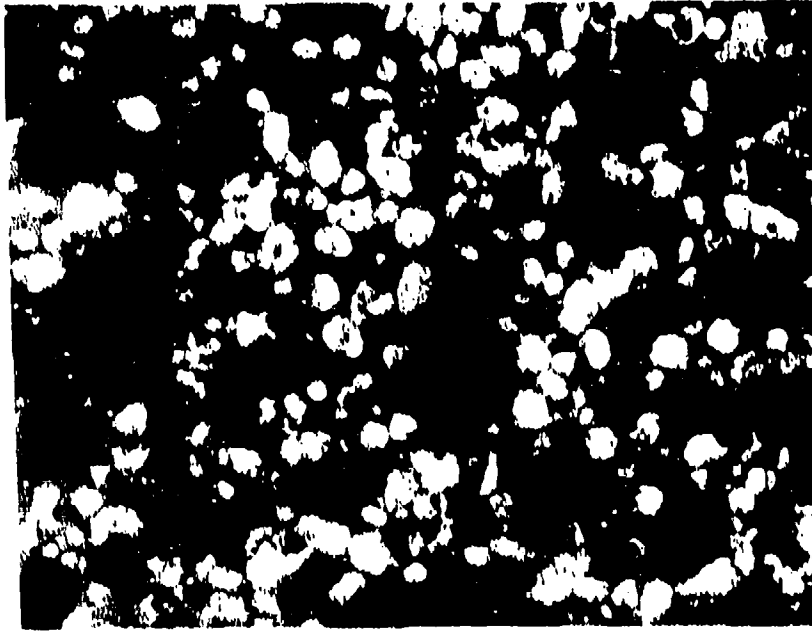
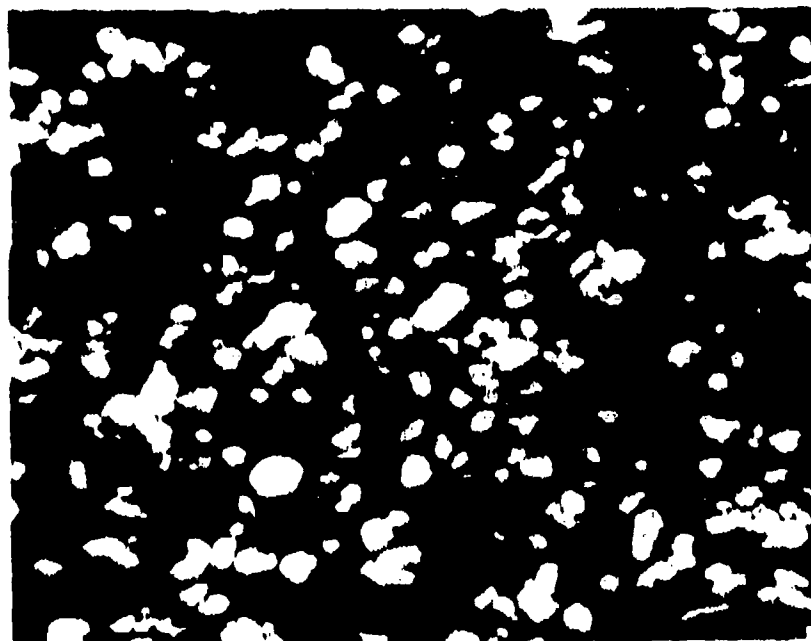Figure 13. Micrographs of inorganic composite sample SG7-D, with lead-solder glass. Preparation parameters given in Table 6. Magnifications at 200X and 500X.

requirements appear to have been met. Microstructural observations in Figure 14 show the material to be quite dense. The Ni-Cr powder has remained substantially spherical, when compared with its starting state in Figure 8.

III.3   Initial Evaluation Measurements

The procedures used to make sample SG-7E were continued so as to prepare a series of three sample pieces with a range of nominal volume loading (p) values. These were evaluated first by thermomagnetic analysis, similar to that shown in Figure 2, which first verified that the desired characteristic of no ferromagnetism at room temperature was retained, and second, provided data on Curie-temperature and low-temperature (6K) saturation magnetization from which the actual volume loading could be calculated. The results are presented in Table 7. The Curie temperatures allow one to determine the alloy composition from Figure 3. The saturation magnetization of the Ni-Cr alloy present in the composite follows from Figure 4, and when combined with densities of alloy and composite the volume loading is obtained from $p = \sigma_c \rho_c / \sigma_a \rho_a$.

The resulting values are quite acceptable for the nominal 20% and 30% loadings. By contrast, that for the nominal 40% samples is poor. Its low density correlates with a microscopic observation of significant porosity. Another interesting point appears in Table 7: The Curie temperatures are all slightly lower, by 15 to 20K, than those shown in Figure 2 for the original as-atomized powder. If we assume that there was no sampling problem, nor a significant variation of T_c with particle size, we are led to conclude that a slight reaction did occur in preparing the composite, which shifted the Ni-Cr ratio slightly toward that of the original ingot. This would not impair the application of this material for our purposes.

The other "evaluation" technique attempted was the preparation, by careful machining, of precision coaxial toroids for high frequency measurements. The results were not a success, in that the composites were very brittle and tended to chip or shatter. Where two toroids were needed for measurement at each volume loading, we were lucky to obtain one, and that one might have had small chips at its corners. Therefore, we confined this series to the 35-GHz measurements, which require only a single solid disk for the slotted-line technique.

41

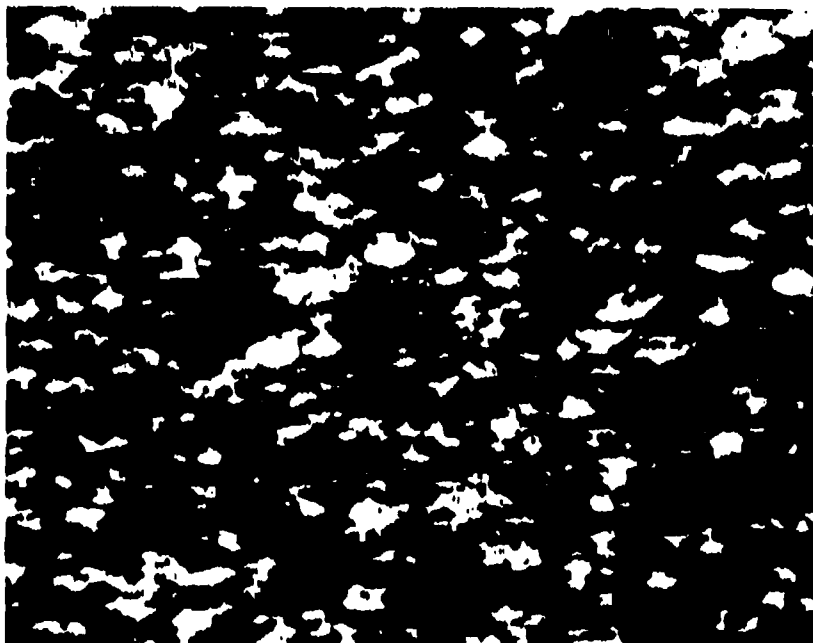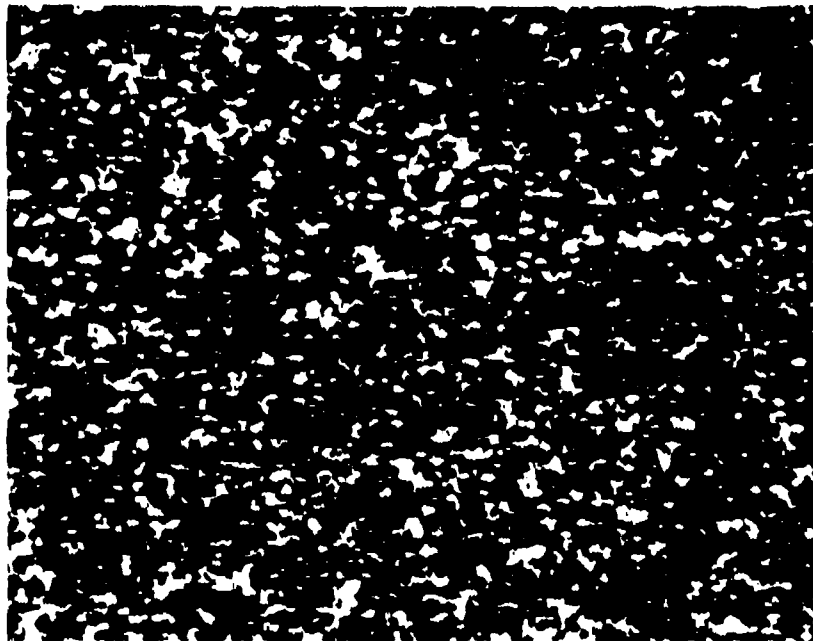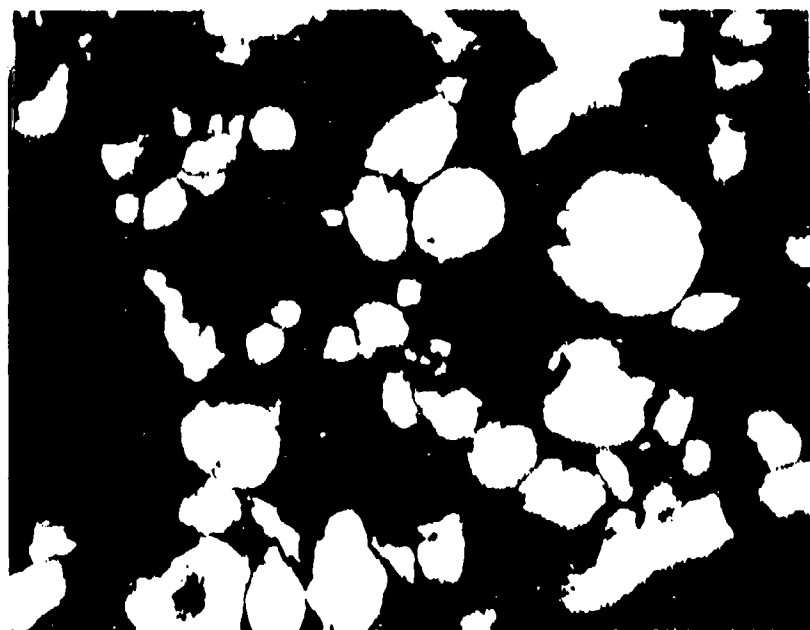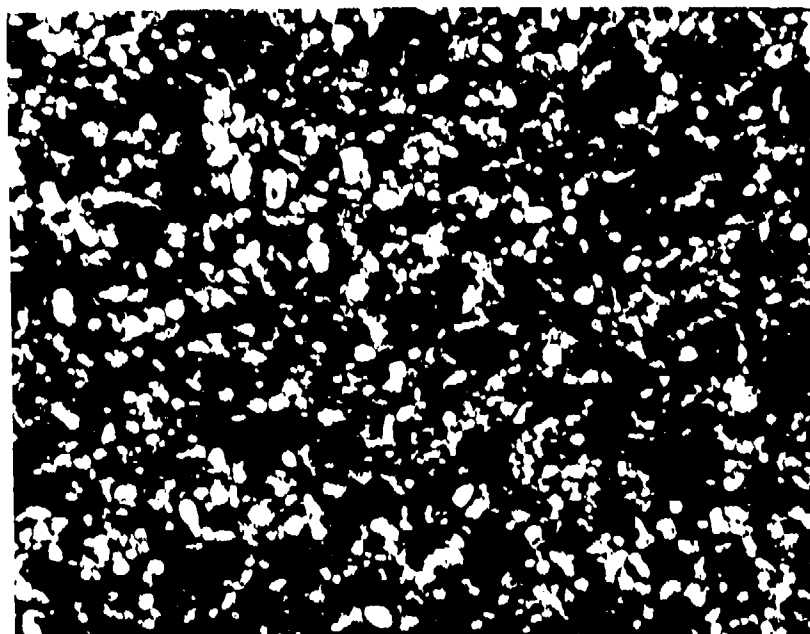**Figure 14.** Micrographs of inorganic composite sample SG7-E, with lead-solder glass. Preparation parameters given in Table 6. Magnifications at 100X and 500X.

Table 7

THERMOMAGNETIC EVALUATION PARAMETERS
OF INORGANIC COMPOSITES PREPARED WITH LEAD-SOLDER GLASS
BY LOW TEMPERATURE SINTERING

Sample Ident (Powder Source)	Nominal Alloy (vol%)	Curie Temp.	Sat. Mag. σ_m (6 K) (emu/g)	At% Cr	Specific Gravity	Measured Vol Load (p)
SG-7-S (RS-67; $10 < d < 20$)	20	143 K ±21	5.30	8.2	4.47	0.18
SG-7-E (RS-98; $20 < d < 37$)	30	137 K ±23	6.75	8.4	5.01	0.27
SG-7-H (RS-67; $10 < d < 20$)	40	147 K ±26	8.97	8.2	4.23	0.28

IV. THEORETICAL APPROACHES/MODELING

In this section we address the challenges posed in Task 3 of the Statement of Work (Table 1). Despite the "classical" background of artificial dielectric composites [2] in the nineteenth century, the subject remains quite alive today. There have been several conferences in recent years on the properties of heterogeneous media [22,23]. In addition to the obvious dielectric or permittivity behavior, this particular class of mixture also can exhibit permeability phenomena. We begin our discussion on this point.

IV.1 Magnetic Dipole and Particle Size Effects

At first consideration it might seem that purely electric dipole phenomena would fully describe the high-frequency response of an artificial dielectric composed of strictly non-magnetic materials (in contrast to prior work on artificial magneto-dielectrics [1]). Indeed this appears to have been the initial point of departure for analysis over the past rather active decade of research on selective absorbers of solar and infrared radiation [24, 22]. However, it was quickly realized that, if the diameter of the conducting particle is not negligible compared to the skin depth, there is a second, rather classical, mechanism for absorption arising from the effects of the magnetic field of the incident radiation. In the time-varying magnetic field, there will be an induced eddy current magnetic polarization and an eddy current loss. The effective permeability of the composite artificial dielectric will thus not be unity even though the dc permeability of the constituents may be exactly unity. These magnetic effects are size-dependent while the electric dipole polarization and loss phenomena are not. Indeed the magnetic contribution dominates for metallic particles above about 50 Å in size [24, 25]!

As noted in Section I, this feature was not in our original plans. The calculations presented below show that much interesting behavior occurs in relevant frequency and particle size ranges. Therefore we put emphasis on obtaining and measuring different powder size fabrications (Section II). This is the expansion of scope noted in Section I.

IV.1.1 Magnetic Polarizability of a Single Particle

The magnetic response of an isolated isotropic conducting sphere has been discussed nicely by Landau and Lifshitz [26]. Following their notation,

44

$$M = \alpha H$$

where M is the magnetization (magnetic moment per unit volume), H is the external magnetic field and α is the (complex) magnetic polarizability. For a sphere they derive (with $\alpha = \alpha' + i\alpha''$),

$$\alpha' = -\frac{3}{8\pi}\left[1 - \frac{3\delta[\sinh(2a/\delta) - \sin(2a/\delta)]}{2a[\cosh(2a/\delta) - \cos(2a/\delta)]}\right]$$

and

$$\alpha'' = -\frac{9\delta^2}{16\pi a^2}\left[1 - \frac{a\sinh(2a/\delta) + \sin(2a/\delta)}{\delta\cosh(2a/\delta) - \cos(2a/\delta)}\right]$$

where δ is the skin depth given by

$$\delta = \frac{c}{\sqrt{2\pi\sigma_{RL}\omega}} \quad \text{in cm (with cgs units)}$$

or

$$\delta = \frac{1}{\sqrt{\pi f \mu_o \sigma_{RL}}} \quad \text{in m (for practical or SI units)}$$

In these expressions $\sigma_{RL} = 1/\rho_{RL}$ is the electrical conductivity (in appropriate units), f the frequency and μ_o the permeability of free space ($4\pi \times 10^{-7}$ henry/m).

In Figure 15 we plot $-\alpha'$, the (negative) real part of the conducting sphere magnetic polarizability as a function of a/δ, the radius divided by the skin depth. In the low frequency (or small particle size) limit, $\delta \gg a$, this component decreases as $(a/\delta)^4$. At the other extreme, it reaches a finite value, $\alpha' = -3/8\pi$, corresponding to the magnetic behavior of a superconducting sphere [26].
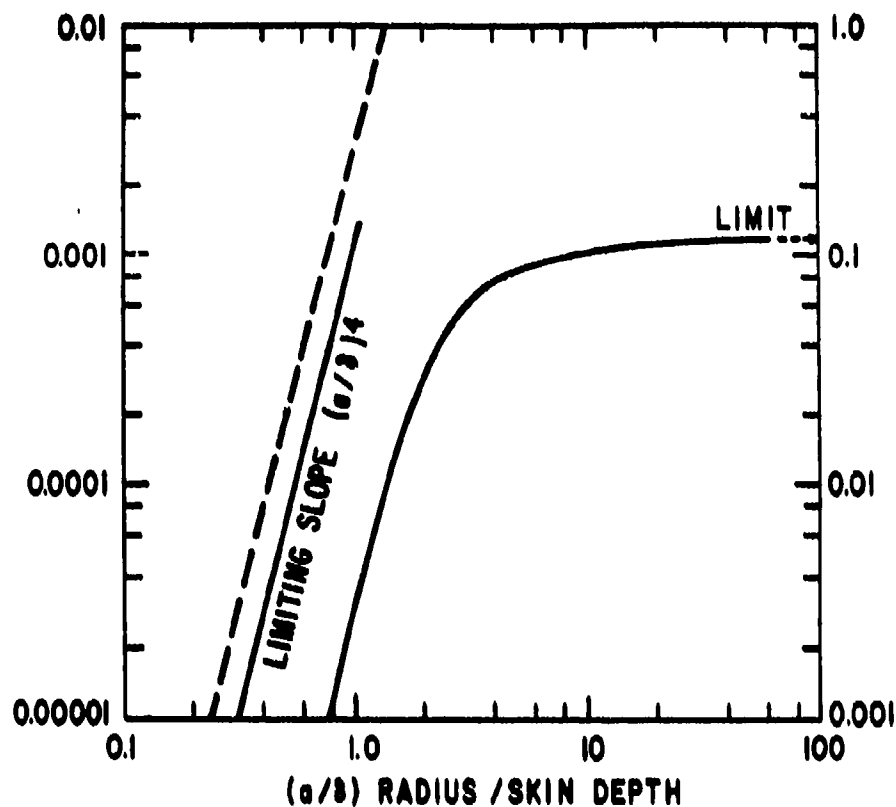
Figure 15. Magnetic polarizability of a conducting sphere. Negative real part, $-\alpha'$, vs. the dimensionless ratio of sphere radius to skin depth.
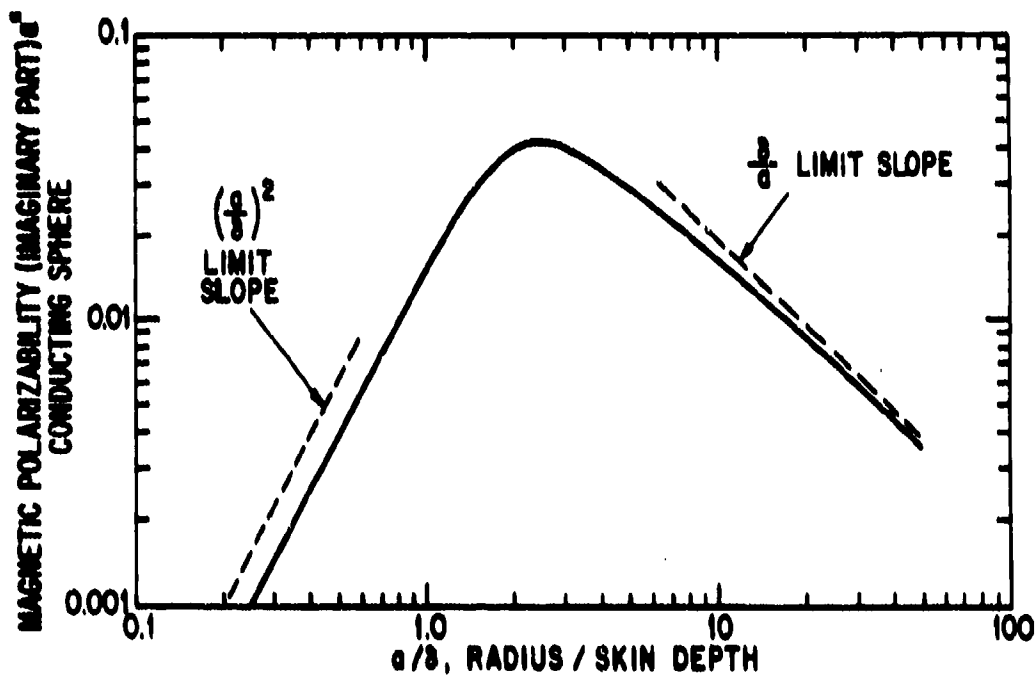
Figure 16. Magnetic polarizability (imaginary or loss part) of conducting sphere in time-varying field. α'' vs. (a/δ)

46

In Figure 16, the imaginary part of the magnetic polarizability is presented, again as a function of a / δ. This quantity is intrinsically positive. It vanishes in both of the extremes of small or large radius (or frequency); in the former the limiting behavior is as $(a / \delta)^2$, while in the latter it decreases in proportion to (δ / a). The maximum loss occurs at $a / \delta = 2.3$, while remaining above half its maximum for the (a / δ) range of 1.2 to 7.

IV.1.2   From Single Conducting Sphere to Composite

The magnetic polarizability formulas given in the preceding section pertain only to the spherical shape and the externally applied magnetic field. In describing magnetic properties in general, as well as in the present case of a dispersion of small magnetic particles, one must proceed carefully in accounting for the various demagnetizing effects, internal and external fields, etc. For example, in the present case one may have to distinguish between the demagnetizing coefficients of the overall composite sample, of the individual particle, and of the cavity "constructed" around the particle in analyzing for interactions between the particle's dipole moment and the magnetization of the particles. In our model, the latter interactions are considered in the mean-field approximation, which is accurate in the dilute limit. (We shall describe some of its weaknesses in a later section when we deal with the dielectric behavior). As another example, particularly relevant to conventional magnetic materials, i.e., ferromagnetic ones, the quantity of fundamental importance is the intrinsic or internal property, be it susceptibility, permeability, or polarizability.

For the artificial dielectric composites studied here, we have the simple case of spherical particles (demagnetizing coefficient = $4\pi 3$), spherical cavity (same), and overall sample configurations, for which we can ignore demagnetization. The latter come about because the measurements are carried out with closed flux configurations (toroid in a co-axial line) or thin slabs with the incident H-field parallel to the slab plane.

Having hoisted the flags of caution, we shall not repeat the derivations which may be found in appropriate textbooks, but shall merely present some key formulas. The intrinsic (or internal) magnetic susceptibility of the sphere (relative to the internal field) is related to the polarizability derived above as:

$$\chi_i = \frac{\alpha}{1 - 4\pi\alpha / 3}.$$

47

For a composite of spherical particles with volume loading, p, the susceptibility relative to an externally applied field is:

$$\chi_{ext} = \frac{\chi_i p}{1 + \frac{4\pi}{3}\chi_i - p\left\langle \frac{4\pi}{3} - N_s \right\rangle \chi_i}$$

where N_s is the demagnetizing coefficient for the overall composite sample shape. In the common case herein, we have $N_s = 0$, and thus we obtain

$$\chi_{ext} = \frac{p\chi_i}{1 + \frac{4\pi}{3}(1-p)\chi_i} \quad .$$

Upon substituting the relation between χ_i and α, this formula becomes

$$\chi_{ext} = \frac{p\alpha}{1 - \frac{4\pi}{3}p\alpha} \quad .$$

This appears so simple that one presumes it could have been found more directly. However, we feel the excursion into details and warnings is appropriate. Finally for the permeability, we have, by definition, $\mu_{ext} = 1 + 4\pi\chi_{ext}$ and then

$$\mu_{ext} = \frac{1 + 2\left\langle \frac{4\pi}{3} \right\rangle p\alpha}{1 - \frac{4\pi}{3}p\alpha} \quad .$$

At this point we take note that α and hence μ are complex, with the forms $\alpha = \alpha' + i\alpha''$, $\mu = \mu' + i\mu''$. Making these substitutions and continuing the manipulation, we obtain

$$\mu_{ext} = \frac{1}{D}\left\{ 1 + \frac{4\pi}{3}p\alpha' - 2\left\langle \frac{4\pi}{3}p \right\rangle^2 \left[(\alpha')^2 + (\alpha'')^2 \right] \right\},$$

$$\mu_{ext}'' = \frac{4\pi p\alpha''}{D}$$

48

with

$$D = 1 - 2\left\langle 2\frac{4\pi}{3}\right\rangle p\alpha' + \left\langle \frac{4\pi}{3}p\right\rangle^2\left[\langle\alpha'\rangle^2 + \langle\alpha''\rangle^2\right] \quad .$$

In Figures 17 and 18 we show the behavior of μ'_{em} and μ''_{em} for values of p from 0.1 to 0.5. As will be discussed later, the empirical limit for random packing of monodisperse spheres is about 0.63, but in practice one rarely goes much beyond about 0.5. In Figure 17, we note that the negative real polarizability manifests itself in a substantial lowering (diamagnetic tendency) of μ' from unity. In Figure 18, the family of curves for μ'' are straightforward reflections of the behavior of α'' (as given in the formula). These formulas and graphs are in a universal dimensionless form, expressed in terms of α / δ. It remains to demonstrate that the changing properties are relevant to the materials and electromagnetic parameters of this investigation.

IV.1.3 From Model Composite to Practical Application

At this point we transform the model calculations, expressed in dimensionless ratios of material parameters, into real units that are measurable. The major parameter is the resistivity, followed by particle sizes and frequencies of interest. The resistivity, ρ_{el}, for the alloy $Ni_{92}Cr_8$ is 55×10^{-8} Ωm [27]. When this is substituted into the formula for skin depth, δ, we obtain at 10 GHz, $\delta = 3.7$ mm. Proceeding a step further with the consideration that peak α'' (and μ'') occurs at $\alpha / \delta = 2.3$, we find that "important" sphere diameters, d_c are as follows:

$d_c = 17$ μm at 10 GHz
$d_c = 7.6$ μm at 50 GHz
$d_c = 5.4$ μm at 100 GHz

Obviously there is relevance for a powder with particles below 37 μm (-400 mesh).

We show in Figures 19 and 20, the calculated model behavior for μ' and μ'' for this alloy composition, for a volume loading, $p = 0.4$, and for various sphere diameters of interest, i.e., 5, 10, 20, and 30 μm (Similar calculations for other p-values are presented below). It should be noted that our calculations above have been in the cgs system for which μ', μ'' are dimensionless. As we move closer to real electrical measurements in the "more practical" mks SI system, these

49
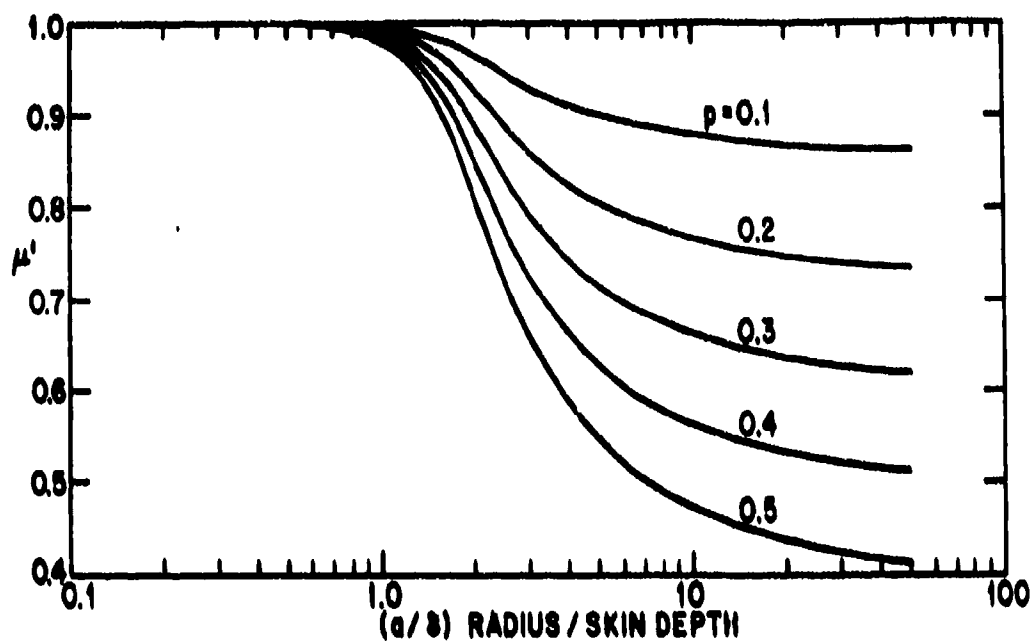
Figure 17. Magnetic polarizability (real part) calculated for composites of conducting spheres at various volume loadings, p. μ'_{ext} vs. (a/δ)
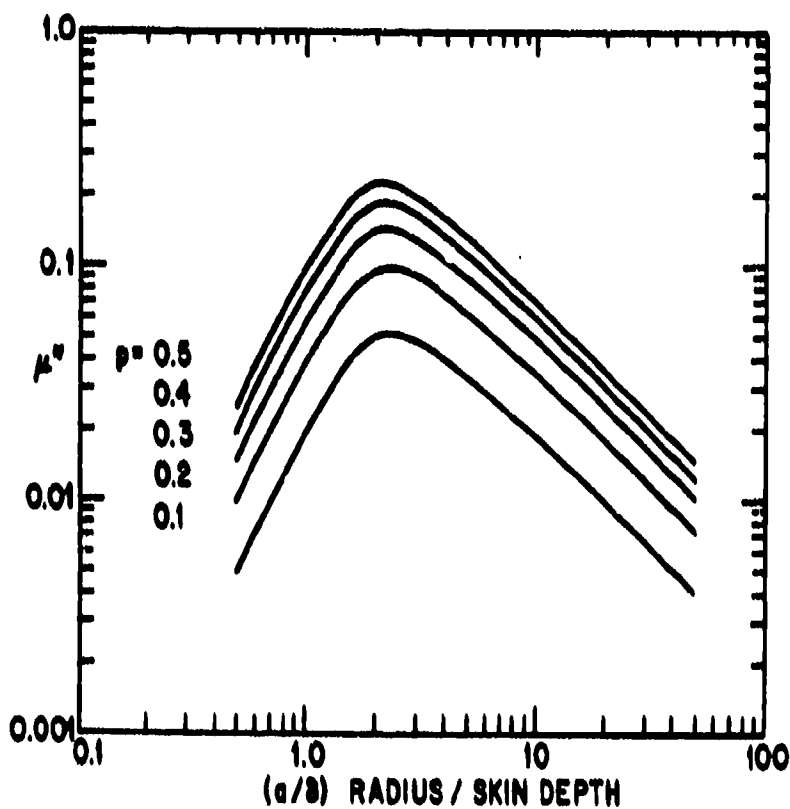
Figure 18. Magnetic permeability (imaginary part) calculated for composites of conducting spheres at various volume loadings, p. μ''_{ext} vs. (a/δ) .
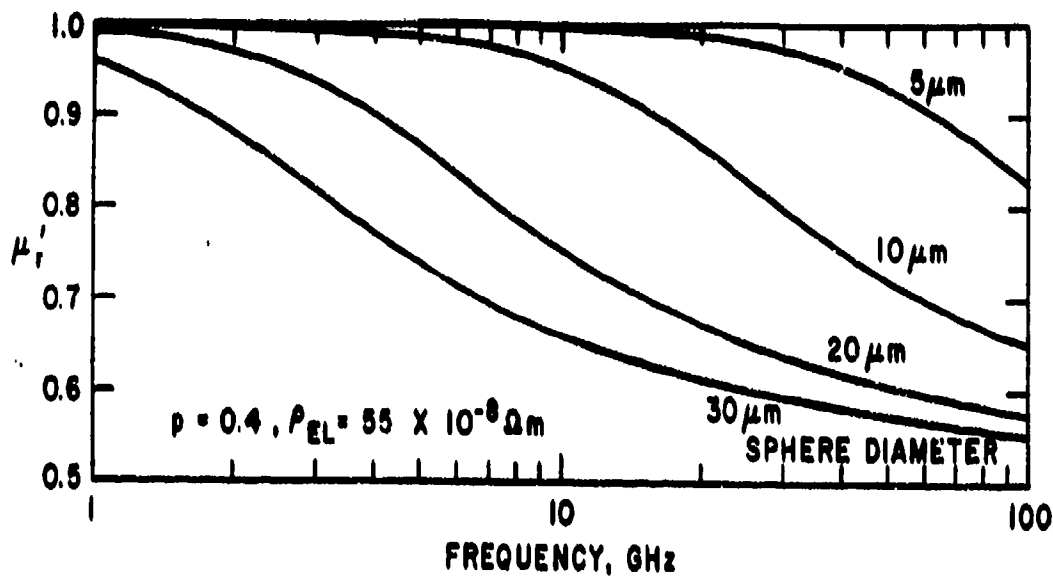
Figure 19. Relative real magnetic permeability, μ_r', vs. frequency calculated for composites of conducting spheres of various diameters; composite loading volume, $p = 0.4$; sphere alloy resistivity, $\rho_{EL} = 55 \times 10^{-8}$ Ωm.
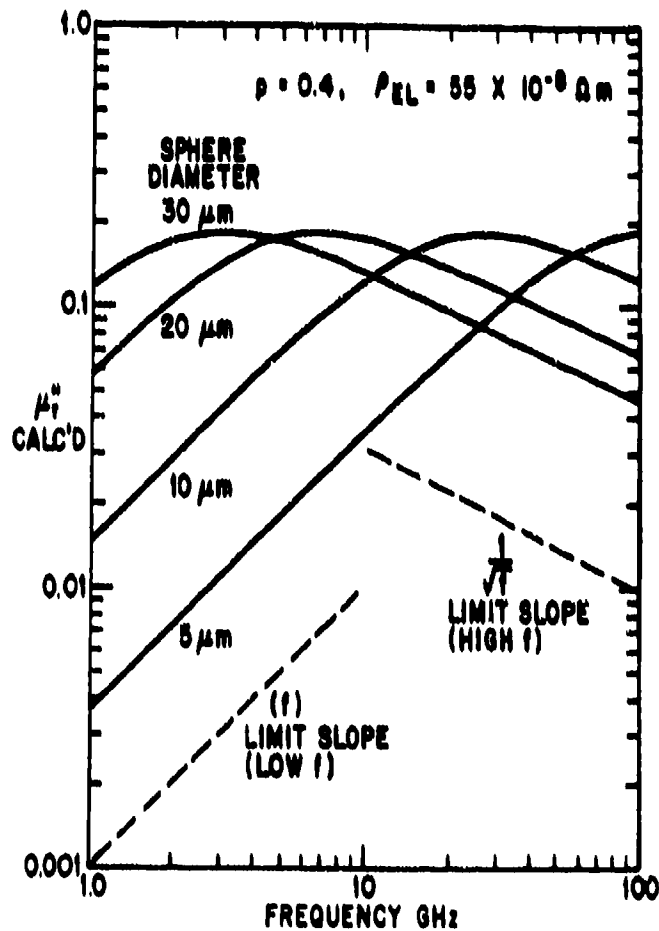
Figure 20. Relative imaginary magnetic permeability, μ'', vs. frequency calculated for composites described in Figure 19.

51

expressions or graphs of μ', μ'' (and later of ε', ε'') are to be considered as relative to the permeability (or permittivity) of free space. In other words we have $\mu'_r = \mu' / \mu_o$, etc.

The qualitative remarks made for Figures 17 and 18 remain true for these figures. However, the separation of the features for the various sphere diameters is rather dramatic. It certainly invites experimental demonstration in that the range of sizes and of frequencies for this investigation spans the calculated behavior very nicely. It is for these reasons that we prepared samples with different particle sizes (and volume loadings) as listed in Table 3; i.e., -10 μm, + 10-20 μm, and + 20-37 μm.

It is instructive to extend the critical diameter/frequency consideration somewhat further on either end. If we move to the far-infrared, to a frequency of 1 THz (1×10^{12} Hz) alternatively expressed in wave numbers as 33 cm^{-1}, the critical diameter for maximum absorption in this alloy would be 1.7 μm, which is in line with predictions for such research [25]. This domain is of interest for selective absorbers of solar or infrared radiation. At the other extreme that of low frequency, the critical diameter at 10 kHz is 1.7 cm. This is the regime for induction heating!

In each of these two limiting regions one is unlikely to find results obtained and presented in terms of the complex permeability (and permittivity). Instead the focus is on absorption per se, because of measurement techniques as well as because of practical interest. For these reasons, measurements of the permeability reported here make a useful contribution to the understanding of artificial dielectric materials in the microwave frequency region, and they relate to the nearby far-infrared region also. At present, we are aware of only one report which presents these kinds of measurements and analysis. It deals with systems of millimeter-sized ferromagnetic steel spheres over the kilohertz and megahertz frequency range [28].

There is yet another interest in such model results, a technological one. The RAM physics model [1] predicts that high frequency loss in a magneto-dielectric should become negligible beyond certain frequencies and/or temperatures (depending on material parameters). When the induced magnetic effects are included, one may expect to find lossy properties outside the limits indicated previously.

IV.2   Alternative Approaches To Composite Dielectrics

The model dielectric of interest herein represents one limit in the properties of inhomogeneous media (or composite materials) which have provided problems for theorists and engineers for over 150 years [2]. It is relevant to note that for composite materials the calculations of dielectric constant, magnetic permeability, electrical conductivity, thermal conductivity and diffusion properties can often be formulated in precisely analogous ways. Thus there is an extensive common literature for such phenomena from which one can readily apply theoretical and experimental results to the various properties.

There is a basic distinction between several classes of models of heterogeneous dielectric media. More modern theory follows the work of Bruggeman [2, 29]. This is a symmetrical (two-component) effective medium model wherein particles of type 1 are mixed randomly in some proportion with those of type 2, so that each may be surrounded by particles of both types. If one type is conducting and the other insulating, there will be a percolation threshold composition at which conducting paths are established. The volume loading for this to occur is about 0.15 to 0.2. This model is often labeled EMA (eff. med. approx.). The upper inset in Figure 21 depicts this topology, and the curve shows the dramatic change that occurs at percolation according to one mathematical model.

In another (older) class of model one assumes that particles of type 1 are completely surrounded by material of type 2. It is clearly necessary to specify whether metal has been added to a dielectric host or vice versa, i.e., the model is unsymmetrical. This class of model is associated with the names of Maxwell, Maxwell-Garnett, Clausius and Mossotti, and Lorentz and Lorenz. It too is really an effective medium (or molecular field) model. It is variously called by any of the names just cited, e.g., MGT, CM, etc. Real-life examples of this model are ordered (cubical) arrays of spheres in a different medium, or an otherwise correlated medium such as coated spheres in a random arrangement, with each metal particle surrounded by a concentric dielectric coating. The lower right inset in Figure 21 describes this model, and the curve for its behavior is indicated. Our coated alloy particles fall into this class of composites.

In recent years, rigorous calculations (and some measurements) of the ordered arrays have appeared [30, 31, 32, 33], and these have relevance for the random coated array. Features of these theories are the significant effects of higher order multipoles beyond the dipole-dipole model and the (obvious but sometimes ignored) maximum packing limits. Re-examination of the earlier data
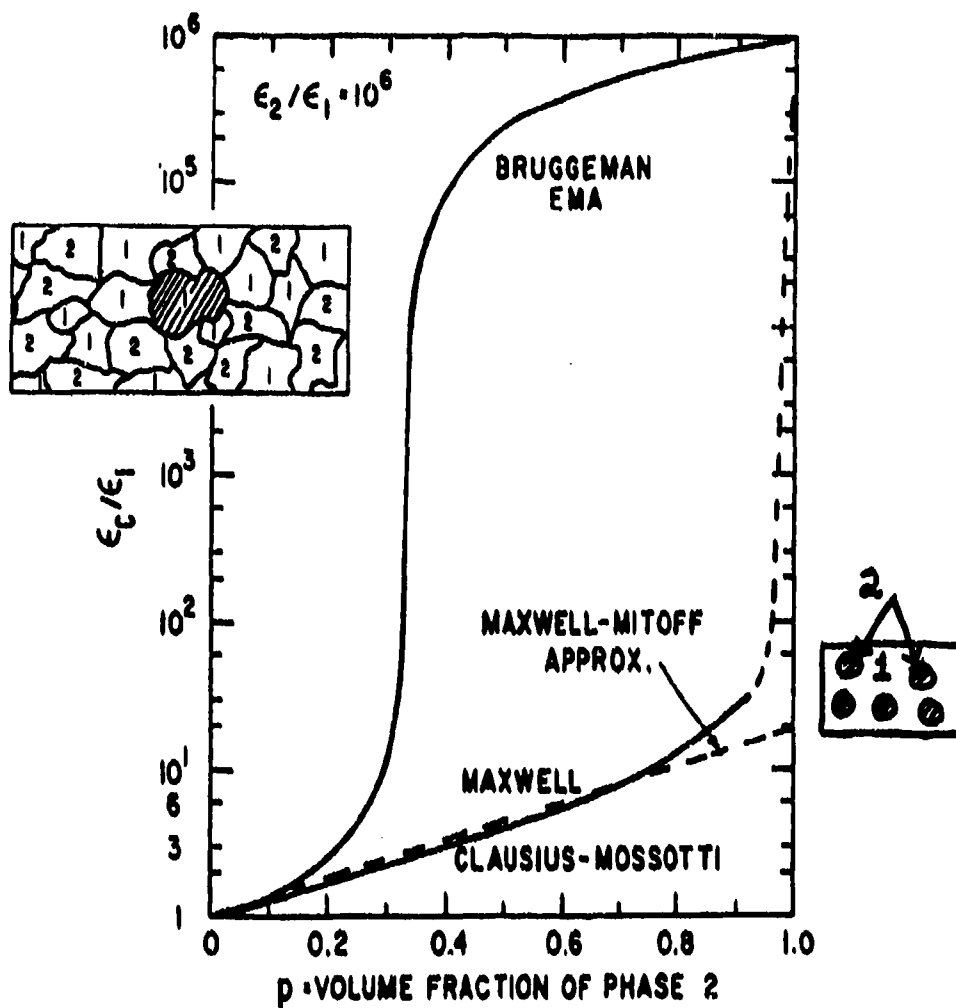
Figure 21. Comparison of classical dielectric models of percolating (Bruggeman) vs. non-percolating (Maxwell/Clausius-Mossotti) systems.

[1] confirms the potential applicability of these recent calculations, and deviations therefrom cast some light on the microstructure of the random coated arrays.

IV.2.1 The Maxwell (MGT, CM) Model

An excellent derivation of the formulas for this model with emphasis on the concepts and approximations is presented by Landauer [2]. A contrasting experimentally oriented discussion on methods of approximating the behavior of two-phase (heterogeneous) systems has been developed by Mitoff [21].

Mitoff's report also calls attention to a very simple method described by Lichtenecker [34] for approximating the properties of two-phase systems, particularly when the properties of the two phases are not very different. Although the method is not fundamentally correct, it is easy to use and does agree with experimental results.

Lichtenecker's rule states that a plot of log k (k being the property value or "constant" for the composite) versus volume fraction p of phase 2 in phase 1 is a straight line between the end values. A graphical comparison with a correct treatment, such as Maxwell's (discussed below) shows that the difference between the two is insignificant with respect to experimental accuracy where the constants of the two phases are within an order of magnitude of each other.

Maxwell derived an equation which, at infinite dilution, exactly describes the k of a mixture of spheres with property constants k_1 and k_2, ($k_2 > k_1$). While he used k_c and k_d for the continuous and the discontinuous phases, Mitoff recasts this into two expressions:

$$k = k_2 \left[\frac{k_1 + 2k_2 - 2(1-p)(k_2 - k_1)}{k_1 + 2k_2 + (1-p)(k_2 - k_1)} \right]$$

for phase 2 being the continuous phase; and

$$k = k_1 \left[\frac{k_2 + 2k_1 - 2p(k_1 - k_2)}{k_2 + 2k_1 + p(k_1 - k_2)} \right]$$

for phase 1 continuous. It assumes that the discontinuous phase consists of spheres and that the spheres are separated enough not to disturb the lines of "flux" around a neighbor. It has been shown by experiment to be quite accurate up to 10% dilution and is a fair approximation in some cases even up to 50%.

An alternative writing of the second of the above equations may be more familiar to some. Thus for the Maxwell, Maxwell-Garnett, Clausius-Mossotti model we also have

$$k = k_1 + \frac{3pk_1(k_2 - k_1)}{(1-p)k_2 + (2+p)k_1}$$

When $k_2 >> k_1$ and p is small (low-concentration) this formula reduces toward

$$k = k_1(1 + 3p)$$

Although equations of the general type above have been available for many years, they have seen little use, probably because they are not the kind one keeps in one's head for a quick approximation. Mitoff's report, however, shows that a very simple treatment applies when the two (separate) pr ...ties are very different. This is precisely the region for which the simple Lichtenecker method does not apply.

For large differences, extending to a number of orders of magnitude, one adopts the procedure of plotting log k/k_1 versus volume fraction. From Mitoff, we obtain Figure 22, presenting the Maxwell curves for k_2/k_1 ratios from $10^{0.3}$ to 10^6. The upper curves represent phase 2 continuous and the lower ones phase 1 continuous. The straight line, L, represents the Lichtenecker approximation. One notices that when k_2/k_1 is less than 10, the mathematically defensible Maxwell treatment is not much different from Lichtenecker's.

Mitoff goes a step further in observing that the limiting behaviors in Figure 22 for large differences ($k_2 >> k_1$) are really straight lines with slopes that do not involve the property constant of the discontinuous phase. He obtains the relationships:

$$\frac{\Delta \log_{10}\langle k / k_2 \rangle}{\Delta(1-p)} \cong -0.65 \quad (k_2 = k_c)$$

and

$$\frac{\Delta \log_{10}(k/k_1)}{\Delta p} \cong 1.3 \ (k_1 = k_c)$$

These are shown graphically on Figure 23. So long as the k's are very different, one expects the points to fall on these straight lines, especially at volume fractions close to the k_c side.

Mitoff compares this approximate method with the complete Maxwell equation and with Lichtenecker's rule for a wide range of ratios of k_2/k_1. He shows that for one-order-of-magnitude difference or more the first or upper straight line for $k_2 = k_c$ is useful even out to rather high volume fractions of the discontinuous phase. At less than an order-of-magnitude difference, Lichtenecker's line is a good approximation to the Maxwell equation while the others are not.

Inspection of Figure 22 shows that the Maxwell (MGT, CM) expressions continue analytically across the whole range of volume fraction, p. That the curves are shown dashed at extreme p values is a recognition of two points: one is the assumption of non-contact, translated as meaning a dilute system; the second is the fact that the volume loading of uniformly sized spheres in random packing cannot exceed 0.63, and reaches this only under specially favorable conditions. We return to this point below. Nevertheless the Maxwell (MGT, CM) formula is useful, as is the Mitoff approximation when used with care.

There are two applications of practical interest for this discussion. The upper branch curves of Figure 22 (or their analytic expression) successfully describe the effects of porosity in a host medium. The second application of special interest is that of a coated sphere. It connects to a designated task of Table 1, i.e., "Analyze the effects of microstructure control in passivated metal-insulator composites."

In Section II.5 we examined the surface condition of the metal powder and concluded that there is an insulating oxide coating of about 0.1 to 0.2 μm thickness. It would be rash to call this a passivating layer, however. This conclusion derives from the considerable reaction suffered by this alloy powder when composite preparation using an inorganic binder was attempted, as discussed in Section III.

The presence of the insulating coating is very significant for the electromagnetic behavior, especially for the dielectric properties (See Figure 21). Loosely speaking, it prevents the individual metal particles from shorting to each other. More elegantly, it means we have a correlated
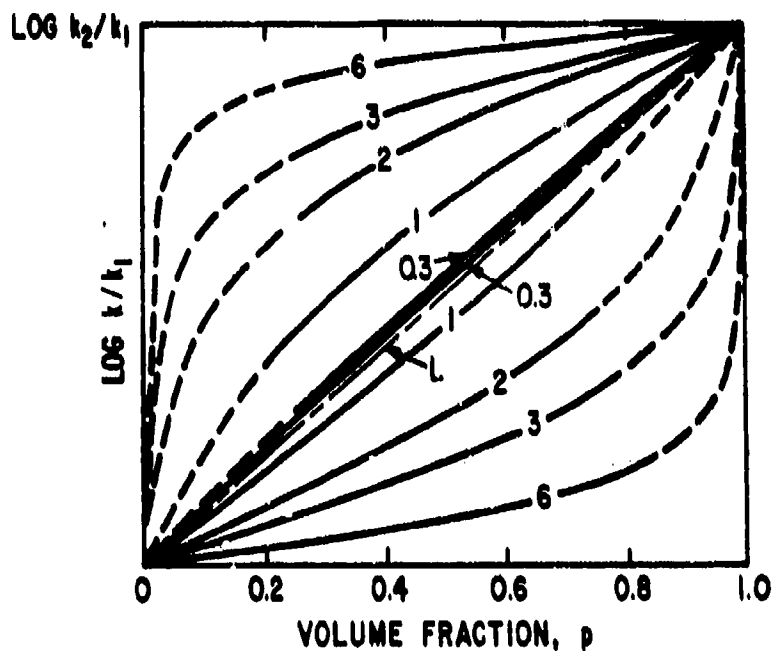
Figure 22. Maxwell (MGT, CM) equations for mixtures, on a semilog plot. Upper set is for Phase 2 continuous; lower set is for Phase 1 continuous; L is Lichtenecker's approximation. (The number on each curve signifies the power of ten in the ration k_2/k_1.) (From Reference 21)
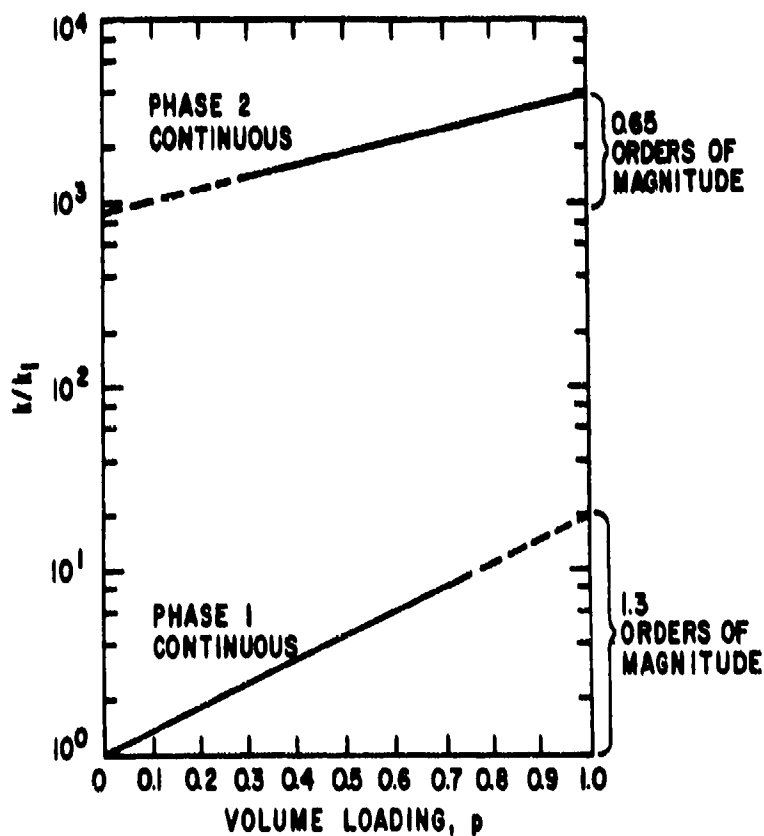
Figure 23. Mitoff's graphical approximations to the Maxwell (MGT, CM) equations for $k_2 \gg k_1$. (From Reference 21)

58

heterogeneous medium in which conducting particles are completely surrounded by insulating material. This restricts the theoretical approach to describing the dielectric behavior. Volume loadings up to or approaching the packing limits can be achieved with coated particles (spheres) without the establishment of conducting paths, i.e., percolation.

With a coating on the conducting sphere, as well as a binder material, the resulting composite is a three-phase medium. However, it is possible to replace the coated sphere combination by a single, slightly modified, dielectric sphere, at least in our frequency regime. An apparently direct application of the Maxwell (MGT, CM) expressions yields [35] the single dielectric constant

$$\varepsilon_{ct} = \varepsilon_1 \left[\frac{2\varepsilon_1 + \varepsilon_2 + 2Q^3(\varepsilon_2 - \varepsilon_1)}{2\varepsilon_1 + \varepsilon_2 - Q^3(\varepsilon_2 - \varepsilon_1)} \right]$$

where

$$Q = 1 - (t/a)$$

with t the coating thickness and a the sphere radius. For $\varepsilon_2 \gg \varepsilon_1$, medium 1 being the insulating coat, this reduces to

$$\varepsilon_{ct} = \varepsilon_1 \left[\frac{1 + 2Q^3}{1 - Q^3} \right]$$

For our estimated coating thickness of 0.1 μm, on a sphere of average diameter 23 μm, we find $\varepsilon_{ct}/\varepsilon_1 = 115$. For simplicity we take ε_1 for the coating as that for Cr_2O_3, i.e., 11.1, from which $\varepsilon_{ct} = 1276$. This value for ε_{ct} is still so much greater than that for typical binders that the model calculations are unaffected.

IV.2.2 The Bruggeman Effective Medium Approximation

We described the initial elements of this EMA model in IV.2 above. A visual image is presented in Figure 21 (after Landauer [2]). The two components are mixed randomly. The shaded crystallite of type 1 (of volume fraction, p) is surrounded by crystallites of both types. In

the analysis [2], the surrounding (two-phase) material is imagined as a single medium of uniform properties. The homogeneous dielectric constant ε_B in this case arises from the solution of a quadratic equation which, assuming spherical particles, is:

$$p\frac{\varepsilon_B - \varepsilon_1}{2\varepsilon_B + \varepsilon_1} + (1-p)\frac{\varepsilon_B - \varepsilon_2}{2\varepsilon_B + \varepsilon_2} = 0$$

At quite low cc. ntrations, p, the EMA and the Maxwell-CM give identical results. The EMA has the appealing as; cct of treating particles of types 1 and 2 on an equivalent basis (hence a symmetrical theory).

As we have discussed above, our artificial dielectric is one with a correlation between the two phases of the medium. This rules against the use of the EMA model and in favor of one for which the metal is embedded in the insulating medium (thanks to the coating).

An interesting and distinctive feature of the EMA is that it predicts a metal-insulator or percolation transition. In this version it occurs at $p = 1/3$, while in other theories this value can be as low as $p = 0.15$. (For quasi-two-dimensional mixtures, the values are somewhat higher). A good illustration of this prediction experimentally is shown in Figure 24 [36]. For these samples the critical percolation fraction (vol. loading) is about 0.20. This demonstration is a convincing argument against the EMA class of model for the artificial dielectrics of this study.

IV.2.3 Exact Calculations for Arrays of Spheres

Concurrent with the interest in random heterogeneous media is an attention to the equivalent problem for ordered arrays of (conducting) elements. Lord Rayleigh in 1892 showed a significant advance beyond Maxwell's work when he took into account induced octupole moments. The ordered array lends itself to a more rigorous formulation of the problem. The subject received a technical boost with the suggestion of Kock [37] that artificial dielectrics (of the ordered type) could be used as microwave lenses. There has since been a great deal of engineering interest, involving a variety of conductor shapes [38]. We have found particularly useful a paper by Kharadly and Jackson [30] both for the (lossless) effective permittivity calculations and measurements, and for discussions of the dielectric loss. Most recently, with modern computers, one can carry out numerical calculations of these problems to arbitrary precision limits which were totally unattainable heretofore [31-33, 39,40].
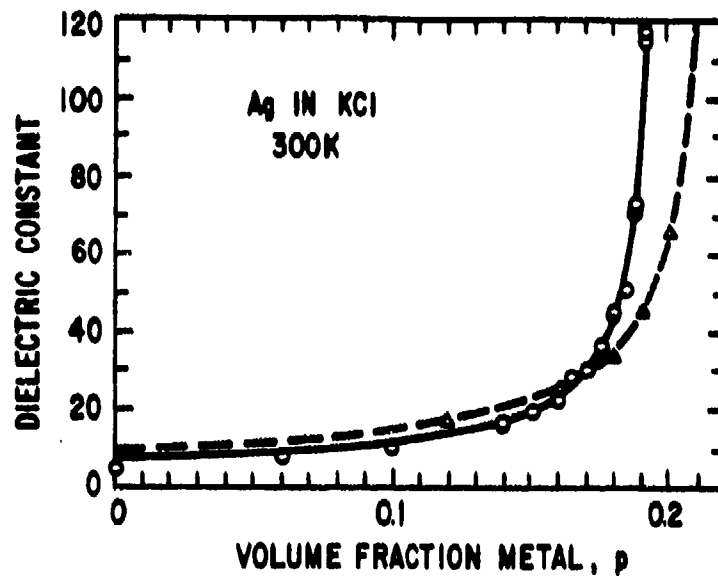
Figure 24. The dielectric constant of several Ag-KCl samples as a function of metal volume fraction, p. (From Reference 36)
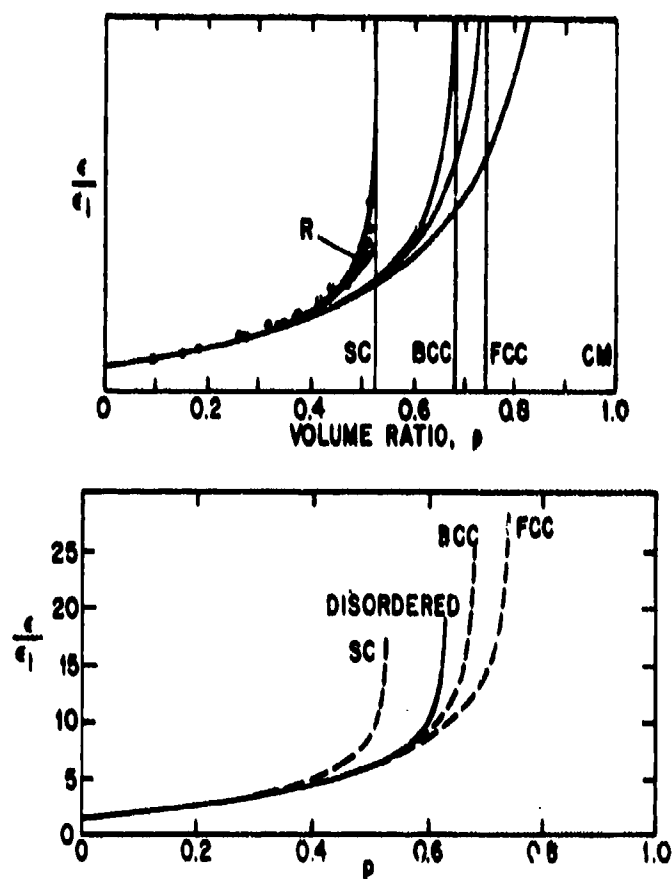
Figure 25. Dielectric constants for cubic lattices as calculated in Reference 31 (upper) and References 32, 33 (lower)

61

As noted above, the higher order multipoles (beyond the dipole terms of the Maxwell/CM theories) have an important effect as the spherical conductors get closer at increased p. A measure of the success of the calculations is that the calculated permittivities exhibit an anomaly at the critical volume loading where the spheres just touch, in contrast with the Maxwell (MGT, CM) models. The conceptual drama of this feature shows in the simplicity of a confirmatory experiment for the body centered cubic lattice [33]. It suffices to construct only a one-eighth portion of a unit cell using conducting and insulating plates plus two one-eighth sections of metal ball bearings! The metal-insulator "anomaly" or transition when they touch is thus lattice dependent. This follows from the 3-dimensional packing limits for hard, uniform spheres, as follows.

> simple cubic $p = \pi / 6 = 0.52$
> body centered cubic $p = \pi\sqrt{3} / 8 = 0.68$
> face centered cubic $p = \pi\sqrt{2} / 6 = 0.74$
> or hexagonal close-packed

In Figure 25 we reproduce the results of the calculations, the upper from Doyle [31,39] and the lower from the Australian group [32,33,40]. The Maxwell-CM curve in the upper portion agrees with the exact calculations out to $p \approx 0.35$ for SC and to $p \approx 0.5$ for BCC and FCC. This provides the justification for the reasonable success in our prior work. It was the right type of model and a not-bad approximation. On the other hand, the Maxwell/CM model fails to diverge until p tends toward unity. The line marked R is the Rayleigh calculation for the SC lattice (corrected [31]) showing some multipole effects but failing to diverge at the contact limit. In addition experimental data are included for the SC lattice which are in line with the exact results.

The calculations of the Australian group in the lower portion of Figure 25 agree in detail with those of Doyle, since the methods of attack were equivalent. They have added another curve estimated by scaling arguments and intended to apply to a random or disordered array. The empirical packing limit in this case (as noted above) is $p = 0.63$, although that limit is tricky to reach and values nearer to $p = 0.60$ are more likely. They even express this curve with a closed approximate formula as follows:

$$\varepsilon = 0.05398 - 2.0675 \times \ln(0.63 - p).$$

IV.2.4   Reanalysis of Prior ε' Results

In our prior study [1] we obtained dielectric measurement data on a composite system of magnetic metal particles in the same polyurethane binder as employed herein (we call this the B-series). The particles were reasonably spherical and had an insulating coating as manifested by a resistance test (cf. the last entry in Table 2). The composites studied had (magnetically measured) volume loading ranging from about $p = 0.25$ to $p = 0.50$. It is instructive to re-examine those data in the light of the preceding discussion, especially as regards exact calculations for arrays, inasmuch as the prior analysis had considered only the Maxwell (MGT-CM) model.

In Figure 26 we display that ε' data in comparison with the Maxwell-Mitoff approximation. The various data symbols refer to particle groups with differing average sizes and size ranges. Most, but not all, of the groups have data that are approximated by the solid line drawn as a guide to the eye. (We cannot really explain that "maverick" group, but we note that it was comprised of the widest range of particle sizes of the set, about a factor of four from the largest diameter to smallest.) We confess that in the prior analysis [1], we were so infatuated by the potential of the Mitoff approximation line (of predetermined slope – see Section IV.2.1) that we used that line fitted to the lower p-values of the B-series data set. (Those p-values are not really very low!) In that case, in the limit of $p = o$, the line came close to but still deviated from the separately measured binder value, ε_b. In the greater wisdom of hindsight, Figure 26 fixes the Mitoff line to originate at the binder value. We strongly infer from this presentation that upward deviations from the Maxwell/Clausius-Mossotti model occur experimentally at lower values of volume loading, p, than we suspected earlier.

Finally, we offer a comparison of the experimental representation with some of the better theoretical models. This is shown in Figure 27 where the dashed line portrays the behavior of most of the B-series, apart from the maverick set. All are plotted as a ratio to the binder ε_b' value.

One comparison is to the predicted behavior for a simple cubic array (S.C.) calculated on a rigorous model [31, 32], which is the array diverging at the lowest p-value ($p = 0.523$). The second comparison is to the quasi-empirical, quasi-theoretical model for a nonpercolating random composite [33]. This idealized random model was constructed to diverge at the empirical packing limit for random systems, $p \approx 0.63$ and fit to a logarithmic divergence that appears to describe the rigorously calculated array models.
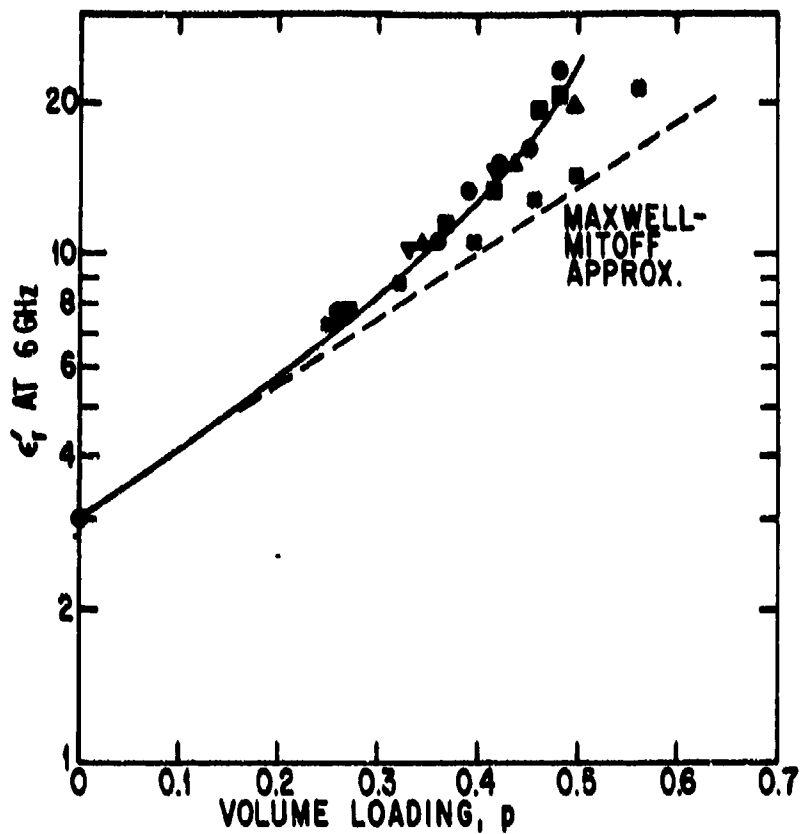
Figure 26. Relative permittivity, ε_r', vs. volume loading, p, for B-series composites. Data from Reference 1.
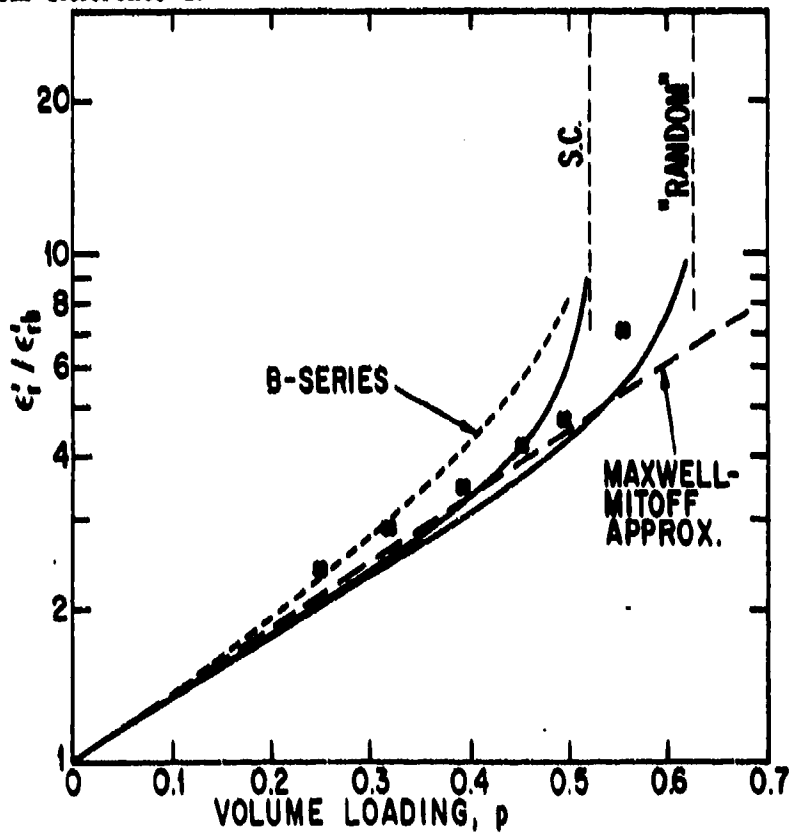
Figure 27. Comparison of experimental studies of ε_r' vs. p for random composites with some theoretical models

64

The data curve mimics the upward curvature of the better theoretical models but precedes their predictions noticeably. In discussions with our consultant, Professor W.T. Doyle of Dartmouth College, he suggested an attractive explanation based on the marked non-linearity of the ε' vs. p curves. In contrast to the lattice arrays of particles, one could have fluctuations of volume loading in a randomly packed composite. Indeed such is the norm in random systems, but we imagine that on some spatial scale it can make a difference. (Note: Our use of semilogarithmic coordinate paper hides some of the non-linearity.) It is reasonably clear that there is room for improved modeling.

IV.3 Improved Modeling of Randomly Packed Artificial Dielectrics; Pair Interaction Model

In discussion with W.T. Doyle, we conceived of an instructive but very much simplified approach to the problem of randomly packed artificial dielectrics. The germ of the idea comes from inspection of a micrograph of one of our actual composites of Ni-Cr particles in polymer at 10% volume loading (Figure 10a), in comparison with a schematic diagram used by microscopist-ceramists to estimate porosity shown in Figure 28. In a limited, but incorrect sense, the schematic diagram may be termed an "idealized random" composite with the volume loading as indicated. While there is no periodicity, it lacks the density fluctuations of a truly random loading. On the positive or idealized side, the particles (= dots) never touch or coalesce until the packing limit is reached! This would be about 63%, for a 3-D random array. Thus this "random" schematic actually represents a correlated medium. In fact, such an assumption of a correlated medium was included [41] in the "estimated calculation" for a random or disordered array carried out by the Australian group [33] by using scaling arguments on the rigorous results for an ordered array.

In contrast, when one examines the micrograph of the actual composite (Figure 10a), local clustering is quite evident. This comparison led us to consider a model based on pair interactions. Professor Doyle's report on this model, performed as a subcontract, follows.

IV.3.1 Introduction

The average permittivity of an inhomogeneous medium composed of spheres of one substance embedded in a continuum of a different material (cermet topology) is, in general, a complicated function of the permittivities of the constituents, the volume filling factor, particle
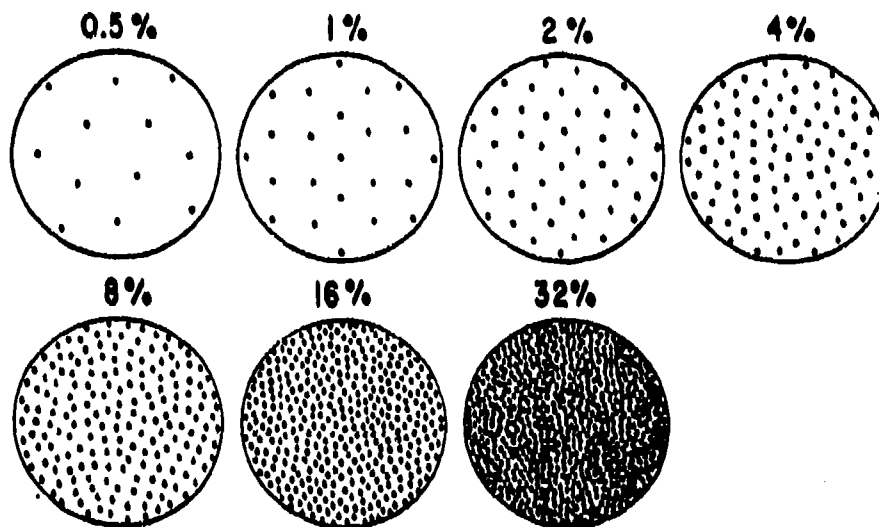
Figure 28. Schematic diagram of "idealized random" composites adapted from figure used by microscopists to estimate porosity (For comparison with actual composite in Figure 10a.)

shape and size, and the details of the particle distribution function. Although the permittivities may be complex and depend upon frequency, we shall be concerned only with perfectly conducting particles in the electrostatic limit.

In the simplest case of a regular array of spheres of uniform size the permittivity may be computed exactly [31-33]. When one or the other of the various parameters has a non-zero variance, the problem becomes substantially more difficult. If all parameters exhibit wide variances, the problem is essentially intractable. Fortunately, in practice, it is possible to obtain nearly mono-disperse distributions of good spheres. However, even an array of uniform sized spheres presents difficulties when the spheres are randomly distributed in space. For such media the permittivity may be calculated only approximately.

If only dipole interactions are present, the permittivity of an isotropic medium is given by the well-known Clausius-Mossotti relation. For regular arrays this case occurs in the limit of low filling factors. For random distributions close encounters can occur even with low filling factors, and corrections may be necessary even with low particle densities. Experiments with nominally "random" media often exhibit substantial departures from the predictions of the approximate formulas, usually of the kinds to be expected from enhanced particle interactions due to particle clustering.

IV.3.2   Clustering Effects

In a neutral dielectric medium only dipole and higher multipolar interactions exist, and all depend inversely upon increasing powers of the distance between the particles of the medium. As a consequence, the multipole interactions grow rapidly with increasing volume filling factor. Because they are positive, all multipole contributions lead to an increase in the dielectric constant with decreasing interparticle distance. A macroscopic manifestation of this is a strong non-linearity of the dielectric constant when plotted as a function of volume filling factor. All experiments and physically valid theoretical approximations show this nonlinear behavior. An immediate consequence of this simple arithmetic fact is that any departure from strict constancy of the density of the medium leads to an enhancement of the dielectric constant.

Density fluctuations are inescapable in a random medium. They occur statistically, if for no other reason, although there are often stronger variances associated with fabrication, such as incomplete stirring, particle cohesion, settling, substrate distortion, interparticle forces, and other

factors. Any or all of these density fluctuations can be expected in any given sample, and all can lead to an increase in the measured macroscopic average dielectric constant. We shall refer to all such enhancements as "cluster effects."

The problems associated with an unrestricted density variation are formidable, if not actually unsolvable. In this report we shall examine one of the simplest types of clustering effect: the permittivity enhancement produced by the presence of a population of close pairs of particles in a medium consisting of perfectly conducting monodisperse spheres. We shall only consider interactions between isolated pairs of particles. All larger clusters of particles and large-scale density fluctuations will be ignored.

The interaction of an isolated pair will be treated exactly, including the effect of all higher multipoles mutually induced by the partners on each other. As will be seen, the pair interaction leads to an enhancement of the effective polarizability of the pair. Once the pair polarizability has been found, the pair may be treated as a molecular dipole in calculating the dielectric constant of an ensemble of mixed isolated particles and pairs.

IV.3.3   Pair Polarizabilities

Laplace's equation is separable in bispherical coordinates, so the problem of two conducting spheres in a uniform external field may be solved exactly. Using this coordinate system Levine and McQuarrie [42] obtained series expressions for the total polarizability of a system of two spheres with arbitrary separation. We follow their treatment here.

The polarizability of the pair may be written

$$\alpha_{pair} = \alpha_1 + \alpha_2 + \alpha_{12} \tag{1}$$

where $\alpha_1 = \alpha_2 = R^3$ is the polarizability of either of the two identical isolated spheres, and α_{12} is the incremental polarizability caused by each sphere's total field on the other. Since the solution is exact, this enhanced polarization includes the effect of all higher multipoles induced on these two spheres in a uniform external field.

68

The polarizability tensor of a pair is axially symmetric, so there are two independent components $\alpha_{12,L}$ and $\alpha_{12,T}$, longitudinal and transverse to the pair axis, respectively. The average polarizability of an ensemble of pairs with axes distributed isotropically is given by

$$\alpha_{12,0} = \langle \alpha_{12,L} + 2\alpha_{12,T} \rangle / 3 \tag{2}$$

For an isotropic random medium $\alpha_{12,0}$ is the important quantity.

The polarizabilities $\alpha_{12,T}$ and $\alpha_{12,L}$ are given by

$$\alpha_{12,T} = 2R^3 \sinh^3 \eta_o \sum_{s=2}^{\infty} (-1)^{s-1} (\sinh s\eta_o)^{-3} \tag{3}$$

and

$$\alpha_{12,L} = 4R^3 \sinh^3 \eta_o \left\{ [S_o(\eta_o)S_2(\eta_o) - S_1(\eta_o)S_1(\eta_o)] / S_o(\eta_o) \right\} - 2R^3 \tag{4}$$

where η_o is defined by

$$\cosh \eta_o = \frac{r}{2R} = \chi \tag{5}$$

The pair separation parameter $\chi = r / 2R$ is determined by the interparticle center-to-center distance, r, and the sphere radius, R. The functions are given $S_o(\eta_o), S_1(\eta_o)$, and $S_2(\eta_o)$ by

$$S_k(\eta_o) = \sum_{t=0}^{\infty} \frac{(2t+1)^k}{\exp[(2t+1)\eta_o] - 1} \tag{6}$$

The polarizabilities obtained with Equations (2) through (4) (normalized to R^3) are tabulated in Table 8 and shown graphically in Figure 29. From the figure it is clear that a substantial enhancement of the dielectric constant can occur in the presence of many closely spaced pairs. For spheres in contact, all of the incremental polarizabilities are of the same order of
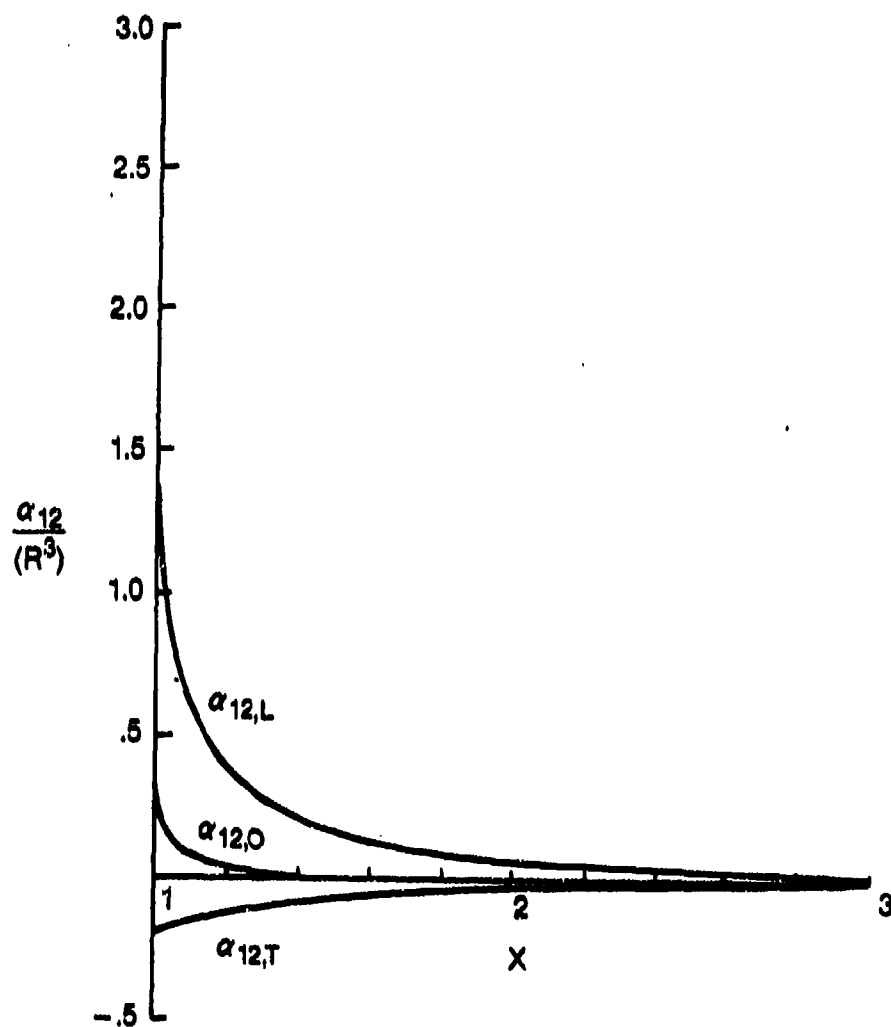
Figure 29. Incremental polarizabilities, α_{12} (normalized to R^3), vs. separation parameter, $\chi = r/2R$.

magnitude as the polarizability of an isolated sphere. The average polarizability, $\alpha_{12,0}$, which determines the dielectric constant of a random distribution, drops off very rapidly with increasing separation of the spheres in a pair.

IV.3.4 Dielectric Constant

The values given in Table 8 are for pairs of particles. The incremental polarizabilities per particle are half as large as the tabulated values. To find the average effective polarizability of a particle of the medium we must add one half of the incremental polarizability for a given pair, $\alpha_{12,0}(\chi)/2$, with separation parameter χ, to the isolated sphere polarizability, R^3, and then average over all pairs in the medium. Thus

$$\langle \alpha \rangle = R^3 + 1/2 \int n_2(\chi) \alpha_{12,0} d\chi \qquad (7)$$

where $n_2 = N_2/N$ is the fraction of particles that are members of pairs, χ is the interparticle distance parameter, and R is the particle radius.

Equation (7) shows that we need further information about the particle distribution in order to calculate the effective polarizability. This kind of detailed structural knowledge is required with any approximation higher than the dipole approximation. In the present case we must know, or make some assumption about, the number of pairs present for each value of the separation parameter $\chi = 2R$.

The simplest assumption we can make regarding $n_2(\chi)$ is that all of the pairs have the same separation, $\langle \overline{\chi} \rangle$, say. Then we have

$$\langle \alpha \rangle = R^3 \left[1 + n_2(\overline{\chi}) \alpha_{12,0}(\overline{\chi})/2R^3 \right] \qquad (8)$$

so that there are only two adjustable parameters: the fractional number of particles in pairs, $n_2(\chi)$, with the effective separation parameter $\overline{\chi}$. The value of $\alpha_{12,0}(\overline{\chi})$ is taken from Table 8, using the appropriate average particle separation parameter $\overline{\chi}$.

Table 8

INCREMENTAL POLARIZABILITIES, α_{12}, PER PAIR (NORMALIZED TO R^3) AS A FUNCTION OF THE SEPARATION PARAMETER, $x = r/2R$

Subscripts T, L, and O designate the transverse, longitudinal
and average composites, respectively. (Sphere radius is R, and
interparticle separation, center-to-center, is r.)

x	$\alpha_{12,T}$	$\alpha_{12,L}$	$\alpha_{12,O}$
5.00000	-0.0020	0.0040	0.0000
4.00000	-0.0039	0.0078	0.0000
3.00000	-0.0092	0.0187	0.0001
2.00000	-0.0307	0.0648	0.0012
1.90000	-0.0356	0.0762	0.0016
1.80000	-0.0417	0.0904	0.0023
1.70000	-0.0492	0.1086	0.0034
1.60000	-0.0586	0.1323	0.0050
1.50000	-0.0704	0.1641	0.0078
1.40000	-0.0853	0.2083	0.0126
1.30000	-0.1043	0.2729	0.0215
1.20000	-0.1285	0.3757	0.0396
1.10000	-0.1591	0.5695	0.0838
1.09000	-0.1625	0.5998	0.0916
1.08000	-0.1660	0.6336	0.1005
1.07000	-0.1696	0.6719	0.1109
1.06000	-0.1733	0.7159	0.1231
1.05000	-0.1770	0.7673	0.1377
1.04000	-0.1809	0.8291	0.1558
1.03000	-0.1848	0.9066	0.1790
1.02000	-0.1887	1.0107	0.2111
1.01000	-0.1928	1.1730	0.2625
1.00900	-0.1932	1.1959	0.2698
1.00800	-0.1936	1.2210	0.2779
1.00700	-0.1940	1.2487	0.2869
1.00600	-0.1944	1.2797	0.2970
1.00500	-0.1948	1.3152	0.3085
1.00400	-0.1953	1.3569	0.3221
1.00300	-0.1957	1.4078	0.3388
1.00200	-0.1961	1.4746	0.3608
1.00100	-0.1965	1.5766	0.3945
1.00090	-0.1965	1.5908	0.3992
1.00080	-0.1966	1.6064	0.4044
1.00070	-0.1966	1.6236	0.4101
1.00060	-0.1967	1.6429	0.4165
1.00050	-0.1967	1.6650	0.4239
1.00040	-0.1967	1.6910	0.4325
1.00030	-0.1968	1.7229	0.4431
1.00020	-0.1968	1.7649	0.4571
1.00010	-0.1969	1.8299	0.4787
1.00009	-0.1969	1.8391	0.4818
1.00008	-0.1969	1.8492	0.4851
1.00007	-0.1969	1.8604	0.4889
1.00006	-0.1969	1.8730	0.4931
1.00005	-0.1969	1.8874	0.4979
1.00004	-0.1969	1.9046	0.5036
1.00003	-0.1969	1.9257	0.5106
1.00002	-0.1969	1.9540	0.5200
1.00001	-0.1969	1.9983	0.5348
1.00000	-0.1969	2.8082	0.8048

The effective polarizability is then used in the dipole approximation for the dielectric constant. The Clausius-Mossotti expression

$$\varepsilon = \varepsilon_o \left(1 + \frac{4\pi N \langle \alpha \rangle}{1 - \frac{4}{3}\pi N \langle \alpha \rangle} \right) \qquad (9)$$

is consistent with our assumption that only pairs and isolated spheres are present.

IV.3.5 Comparison with Prior Experiment

Our results apply to a suspension of conducting spheres in the long wavelength (electrostatic) limit with intermediate filling factors. Although the Clausius-Mossotti expression for isolated spheres is independent of the sphere size, the pair calculations assumed equal-sized spheres, so we should restrict our comparison to fairly mono-disperse samples. Some of the older literature reviewed by DeLoor [43] report dielectric constant enhancements that can be attributed to cluster effects. The measurements of Guillien [44] on emulsions of Hg in oil are of particular interest, because both particles and host are liquids, so that the particles are exceptionally smooth and spherical. We shall first compare our calculations with Guillien's low frequency results and with the microwave measurements reported in our prior study [1].

The largest possible isotropic dielectric constant enhancement obtainable with isolated pairs occurs when all of the spheres form pairs in contact. The number of isolated spheres is then zero, and the number of pairs is maximum, provided that no sphere is permitted more than a single point of contact. From Table 8 we see that at contact, the average polarizability per sphere is equal to $1.4024\,R^3$. The solid lines in Figures 30 and 31 show the Clausius-Mossotti results, with and without pairing. The bottom curve is the Clausius-Mossotti result, with no pairs present. The upper two curves show the pair-enhanced dielectric constant according to two extreme assumptions about the dependence of the pairing probability upon particle density, as discussed next.

In the topmost curve of Figures 30 and 31 we assume that pairing probability is independent of particle density, i.e., $n_2 = 1$. One conspicuous consequence of this assumption is that the derivative of the curve of dielectric constant versus filling factor is larger than the Clausius-
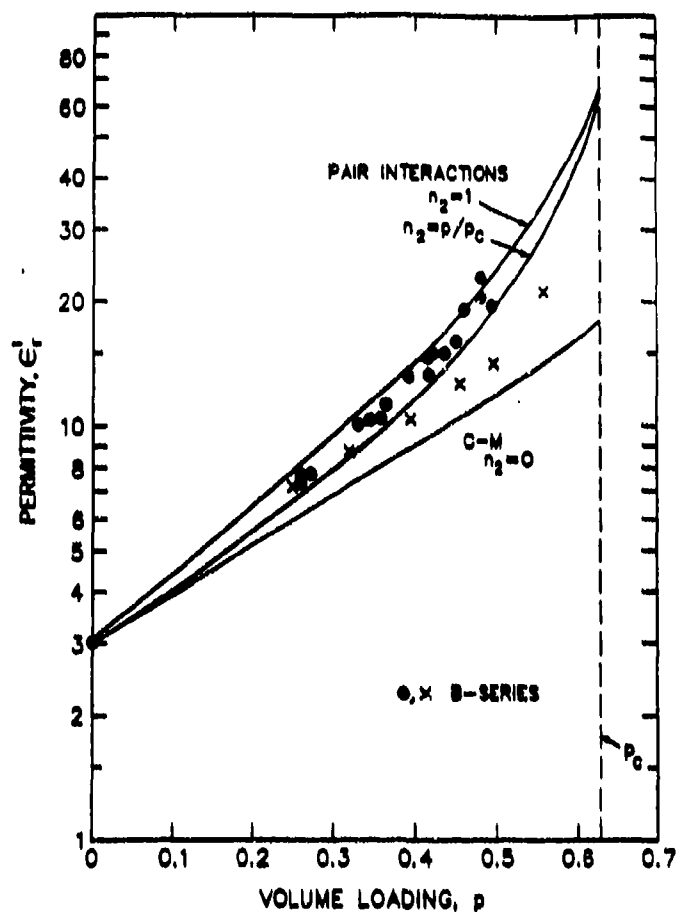
73

Figure 30. Dielectric constant, ε_r', vs. volume loading, p. Calculated models with and without pairing, n_2. Experimental data from Reference 1.
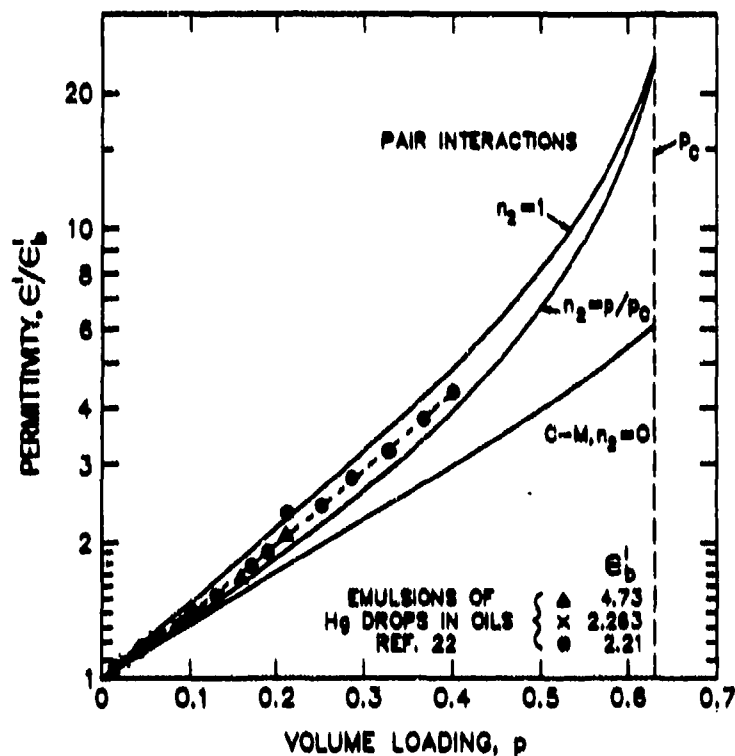

Figure 31. Reduced permittivity, $\varepsilon' / \varepsilon_b'$, vs. volume loading, p. Calculations as for Figure 30. Data for *spherical* drops of Hg in heavy oil, from Reference 44.

Mossotti value $3\varepsilon_o$ at p = 0. This is admittedly an extreme assumption, in that complete pairing is assumed even in the limit of very small filling factor. Such a high clustering tendency may be appropriate for cohering particles that resist breakup by stirring. Some of the experimental data seem to involve some low density clustering. Whether or not such media exist, the example serves to show that even clusters as small as pairs can produce significant effects.

Another simple case is obtained by assuming that the pair density is simply proportional to the filling factor p. Assuming that $n_2(\chi) = p/p_c$, we have

$$\langle \alpha \rangle = R^3 \left[1 + \alpha_{12,0}(1) p / 2 p_c R^3 \right] \tag{10}$$

Setting $p_c = 0.63$, the value appropriate for a random medium, we get the middle curves in Figures 30 and 31. This is a more natural assumption for non-cohering particles, since for such materials one would expect the pair density to go to zero in the limit of low filling factors. With this assumption there are no pairs present at zero filling factor, so the initial slope is equal to $3\varepsilon_o$ in agreement with the Clausius-Mossotti result.

The calculated curves are the same in Figures 30 and 31 except for normalization. The points shown are the experimental results. Figure 30 shows microwave measurements on solid particles from Reference 1. Microscopic examination showed the samples to be relatively mono-disperse distributions of nearly spherical particles. Figure 31 shows Guillien's measurements on Hg emulsions in oil [44]. The similarity of the experimentally measured dielectric enhancements of the solid samples in Figure 30 and the liquid sample in Figure 31 is worth noting, since the Figure 31 liquid sample presumably exhibits an enhancement produced by density variation alone, uninfluenced by a distribution of particle shape.

IV.3.6   Conclusions (Doyle Subcontract)

Using the polarizabilities in Table 8, together with Equations (7) and (9), one could easily calculate the dielectric constant in the presence of an arbitrary distribution of pair densities. However, calculations based on detailed assumptions regarding the pair distribution would require a correspondingly detailed microscopic sample characterization.

In the absence of a detailed sample characterization, we can estimate the magnitude of the pair contributions to dielectric enhancement by assuming that all of the pairs have the same (average) separation parameter. Then only the product of the pair density and the incremental polarizability enters the generalized Clausius-Mossotti relation (9) via Equation (8). In general, a range of densities and incremental polarizabilities yield the same enhancement.

Isolated particle pairs can give rise to a substantial enhancement of the long wavelength dielectric constant of a medium of metal spheres. Large enhancements require large numbers of close pairs. For spheres in contact, the incremental polarizability is of the same order of magnitude as that of a single isolated particle. Whatever the actual pair distribution, only very close pairs make a significant contribution to dielectric constant enhancement.

IV.3.7   Further Experimental Comparisons with Models

In the preceding section we have seen that pair interactions alone can produce permittivity enhancements (above the Clausius-Mossotti values) as large as those often observed in random metal-particle composites. The example shown in Figure 31 is striking because of the ideal materials of that experiment [44]; i.e., both phases liquid and perfect sphericity guaranteed for the metal particles. It would be foolish to put heavy weight on one or the other of the two limiting calculated models, inasmuch as the assumption of isolated pairs quickly breaks down with increasing packing. The apparent trend toward convergence between experiment and model is success enough in an otherwise almost intractable problem. For recent samples of the difficulty in treating the theoretical problem with rigor, see Reference 45.

Subsequent to Doyle's report we encountered another ideal experiment, in the chemical engineering literature on electrical conductance [46]. Beds of solid resin spheres (0.2 to 1.0 mm diameter) were fluidized by aqueous solutions of sodium chloride. By varying resin material as well as saline concentration, a wide range of intrinsic conductivity ratios could be attained. Volume fractions ranging from as low as 0.04 to as high as 0.6 were achieved. Conductivity measurements were carried out at 1.6 kHz using specially prepared electrodes in the fluidized bed. Turner's work provides a nice overlap as well an extension of the range studied by Guillien [44].

In Figure 32 we show the superposition of the reduced permittivity and reduced conductance data in comparison with several model calculations. First one should observe the rather smooth overlap between the two sets of experiments. Together these data sets provide an
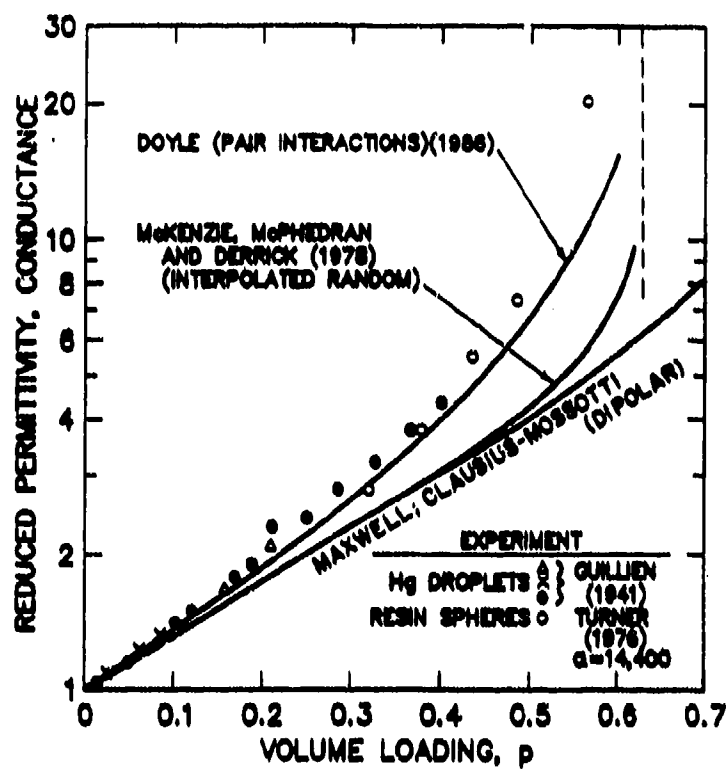
Figure 32. Reduced permittivity or conductance data from several ideal experiments (References 44 and 46) compared with several multipole models and the classical dipole model.

empirical reference solution to the problem of an artificial dielectric composed of non-percolating ("coated") randomly arranged, spheres. Second, we note again how well the oversimplified pair interaction model ($n_2 = p/p_c$), comes close to describing these experimental observations. This is in strong contrast to the quasi-empirical, quasi-theoretical model of McKenzie et al. [33], which accounted for higher order multipoles but was keyed by scaling to the packing limit at $p_c = 0.63$. The base reference curve, the dipolar-only model of Maxwell and Clausius-Mossotti, is also shown. Our delight with this modeling success led us to describe it at an APS meeting [47].

V. MEASUREMENT RESULTS: PERMITTIVITY AND PERMEABILITY

In this section we present the experimental results obtained during this program and compare them with the model behaviors discussed in Section IV, some of which had some other experimental support and some of which had none. We begin with a description of the several experimental equipments employed, along with a few examples of typical measurement outputs (Section V.1). We continue with presentation of results for the polymeric binder artificial dielectrics based on Ni-Cr alloy powders (Section V.2). This is followed with some permittivity results from polymeric binder composites obtained separately on an IR&D program using another coated alloy powder. This series provides an instructive comparison with the Ni-Cr series, a comparison which turns out to be key in validation of the model behaviors. (Section V.3). Finally we present our limited results on composites fabricated with the alternative inorganic binder (Section V.4).

V.1 Measurement Equipment and Examples

High frequency measuring equipment for this study involved a considerable variety of approaches, as well as experiments in three laboratories.

V. 1.1 Evaluation at Centimeter Wavelengths; f < 20 GHz

For the centimeter wavelength range f < 20 GHz, several "Network Analyzers" were employed: a somewhat antiquated one at GE-CRD, based on the rather old (mid 1960's) HP (Hewlett-Packard) 8410 system, and two versions of the new HP8510 family of equipment.

Measurements of the constitutive parameters, complex μ, and complex ε, were first made in centimeter wavelength range ~6-18 GHz at GE-CRD with equipment based on a Hewlett-Packard 8410 system. (In principle the range of frequency covered can extend lower, but in our practice it did not go lower than 6 GHz.) The major building blocks of the system were the 8620A Sweep Generator, the 8410A Network Analyzer, the 8411A Harmonic Frequency Converter, the 8412A Phase-Magnitude Display, the 8746B S-Parameter Test Set, and the 905A Coaxial Sliding Load for calibration runs.

Analog-to-digital converters, together with a data logger and a T.I. Terminal made it possible for the Network Analyzer to interface with a CRD mainframe computer. Any given frequency band of the 8620A Sweep Generator could be swept with a step size of 0.1, 0.2, 0.5, 1, 2, or 5%. Steps of 1% were chosen for this characterization work. This enabled many data points to be taken so that spurious points were of less significance and confidence could be generated that just cannot be obtained when widely separated spot frequency measurements are taken. This "overview" approach was facilitated by a screen display of the calculated μ and ε values from which display a hard copy could be obtained. Smoothing by visual inspection and/or a drawing curve or straight edge completed the process. Alternatively, a tabulation of the measured values could be obtained.

Several methods of measuring the complex permeability and permittivity are suitable for use with a network analyzer. Of these, the reflection technique (S_{11} scattering coefficient) employing first a single-thickness, then a double-thickness sample placed in front of an RF short was the technique used at this stage.

Since the S-parameter terminals of the network analyzer have precision APC-7-type coaxial connectors, the sample holder was made to interface as smoothly as possible with this type of connector. The precision outer (0.2756-in., 7 mm) and inner (0.1197 in.) conductors are available commercially and were used to construct the coaxial line sample holder. The dimensions of a toroidal sample are 0.275 in. O.D., 0.120 in. I.D., and about 0.040 in. thick. (The sample thicknesses of the pair used for a particular set must be identical). An attempt was made to permit no more than 0.001 inch clearance between the sample and its holder. In Figures 33 and 34 we show examples of these measurements for μ' and μ'' in the 6-12 GHz band for sample ONR #2; p = 0.41, sphere diameter in the ranges 20 μm to 37 μm. In Figure 35, we show real permittivity data for three loadings of this same size, again over the same frequency range, $p \approx 0.2$ to $\approx$ 0.4. The figures show the plotted data and the smooth curves used for subsequent evaluation.

During a visit to NRL in November 1985 to discuss millimeter wavelength experiments, we brought our 7 mm diameter coaxial toroids for possible confirmatory measurements on their newer HP Series 8510A analyzer. Through the cooperation of Dr. F.J. Rachford and with the help of S. Browning, it proved possible to measure all eight members of the series (Table 3) from zero-loading p, up to $p \approx$ 04. In most cases, more than one toroid was measured. The range of measurements was 250 MHz to 18 GHz, but owing to thickness effects, the results were most useful between 2 GHz and 18 GHz.

80
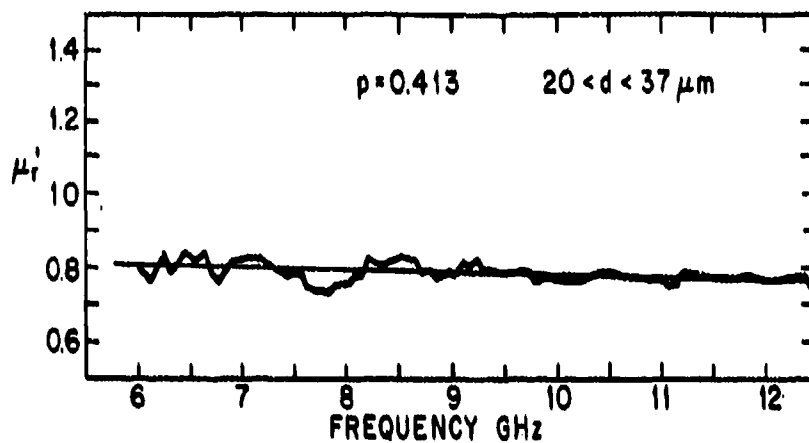
Figure 33. Relative real permeability measurements, μ_r', vs. frequency; range 6-12 GHz, Sample ONR #2, $p = 0.411$, sphere diameter $20 < d < 37$ μm. Measurements on HP8410 system.
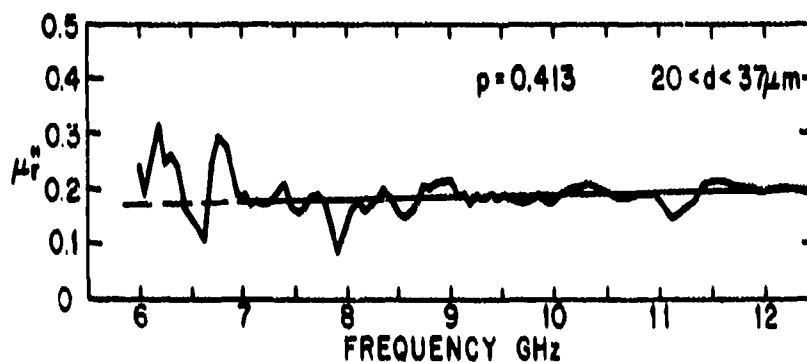

Figure 34. Relative loss permeability, μ'', vs. f; same equipment and frequency range as in Figure 33.
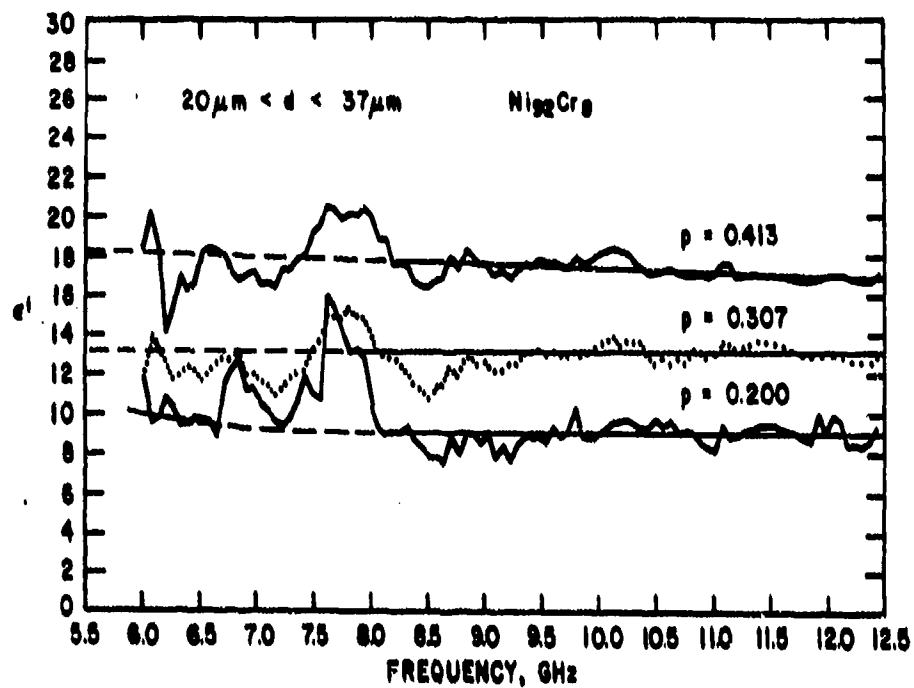
Figure 35. Relative real permittivity, ε_r', vs. frequency; range 6-12 GHz. Samples ONR #2,3,4. Measurements on HP 8410 system.

An example of the quality of this work is shown in Figure 36 for the sample ONR #2, with a volume loading $p = 0.41$ of alloy particles in the size range 20 μ m < d < 37 μ m. The whole series was measured in about four hours! The overall quantity and quality of the results inspired us to present a brief report at the March 1986 meeting of the American Physical Society [48] with focus on the permittivity behavior as a function of loading. These results will be shown in Section V.2.

The performance of the NRL instrument left such a profound impression on us that we were able to convince our management to order similar equipment in mid-1987. (This was forced by the terminal illness and breakdown of our older 8410 system.) The system obtained is the HP8510B comprised of the HP8510B network analyzers, the HP8341B synthesized sweeper (10 MHz – 20 GHz), the HP8515B S-parameter test set and an HP Model 9000 series 300 computer. A coaxial sample 9000 Series holder in the form of a 10 cm APC-7 Beadless Air Line was used in this work. The measurement procedure is described in an HP Product Note [49], following a concept first outlined by Nicholson and Ross [50]. The S-parameters measured provide information on the complex ratios of energy passing in various directions. A single sample is sufficient when complex data are obtained both in transmission and reflection. With phase and amplitude for each, we have enough information for a determination of all four constitutive parameters. We were able to get up to speed on this machine in fairly short order thanks to a software package we purchased from Innovative Measurements Solutions of Atlanta, GA, with the advice and assistance of our colleague R.E. Latta of GEAE-Evendale, OH.

We have since come to understand some mildly deprecatory remarks by Rachford and Browning about the quality of their November 1985 data, in response to our joyous praise thereof. Thus we now understand that data acquired more slowly, with repeat data averaging, forward and reverse propagation direction averaging, as well as very careful attention to sample fit and thicknesses, and to calibrations, can produce even better results. After the period of this report, we were able to measure one of the original samples on our new HP8510-B Network Analyzer. Typical very good results for the same sample #2 are shown in Figure 37. Unfortunately, most of the original samples had lost their mechanical integrity by the time of this measurement, so the full series could not easily be repeated. (The polyurethane binder is intended for laboratory model composites and was chosen for ease of fabrication rather than long-term durability.) It should be stressed that the showing of comparative data is not done in a sense of competition, but rather to illustrate the potential of the modern instrument.
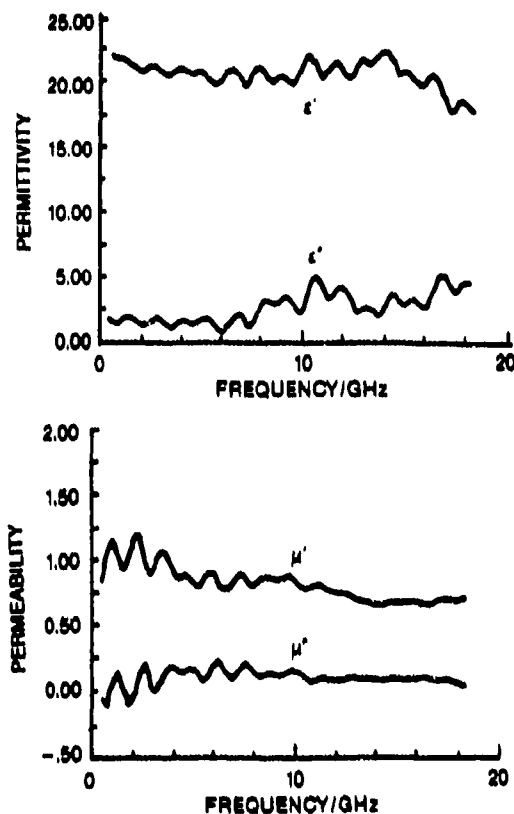
Figure 36. Example of constitutive parameter data obtained on the HP 8510A network analyzer at NRL for sample #2, $p = 0.41$, 20 μm < d <37 μm.
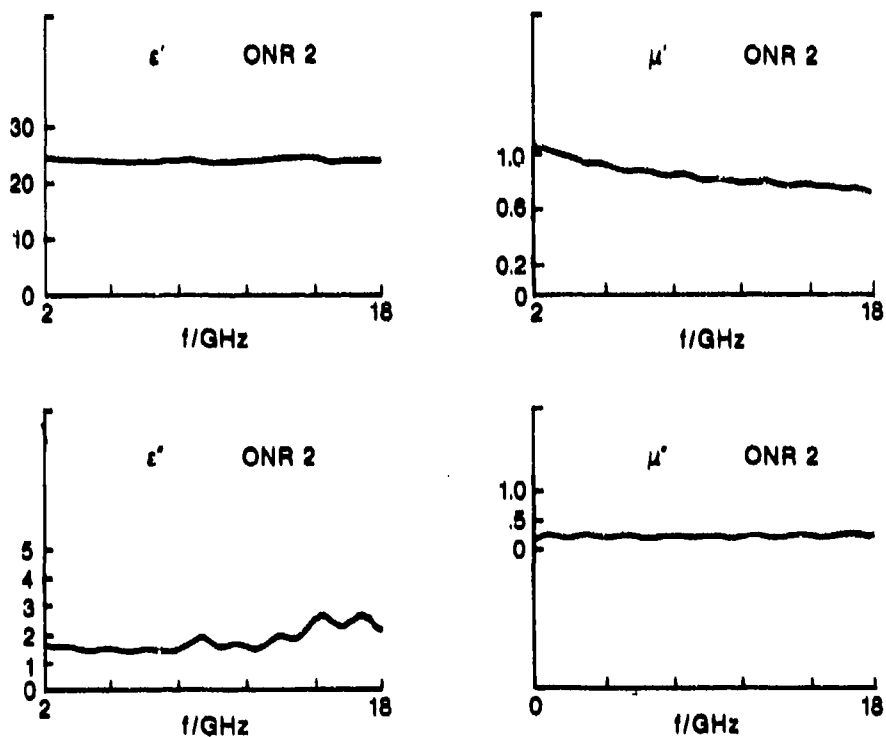

Figure 37. Example of same data as in Figure 36, on toroid from same sample material, as obtained with greater care on the HIP 8510B network analyzer at GE-CRD.

With data of the attractive quality shown in Figure 37, we could not resist upgrading the results already obtained, even though contract time and funds had run out. A limited series of new samples was prepared, and results from these are presented in Section V.2.

V.1.2 Evaluation at Higher Frequencies: $f > 20$ GHz

Initially it was planned in the contract proposal that all measurements above the centimeter wavelength range ($f > 18$ GHz), specifically at 35 and 94 GHz, would be carried out at the Naval Research Laboratory within the limits of their equipment and scheduling. After our first visit/discussion at NRL in February 1985, we were somewhat dismayed by their requirement of a 5 in. x 5 in. seamless square sample for the 35 GHz measurement in the arch method. Fortunately we were able to contract with our colleague, J.O. Hanson, at GE Re-Entry Systems Department in Philadelphia for fixed frequency (35 GHz) measurements using a slotted line technique [51] with a circular waveguide cavity (see Section II.7.5). Measurements at NRL were to be attempted by several techniques, including the arch method at rather high frequencies (~90 GHz), and waveguide techniques at several high-frequency bands, e.g. K_α (26-40 GHz), Q (40-60 GHz) and W (75-110 GHz).

A considerable effort was expended at NRL on this project by Rachford. Satisfactory results were obtained for the waveguide samples at K_α band, as judged by consistency with the lower frequency data and the overlapping experiments at 35 GHz by Hanson. Most of the remaining effort was directed toward obtaining free space transmission on an x-ray diffraction table for fixing the various angles needed in the analysis. The samples had been cut to thickness suitable for W-band. There were a few successes in the W-band range, but when these samples were used at K_α or Q bands, the results were unsatisfactory.

An example of success at W-band, the data for a $p = 0.39$, $20\ \mu$m $< d < 37\ \mu$m composite are shown in Figure 38. The permittivity value of about 20 agrees with Figure 35 and 36 and the relative permeability of about 0.6 will turn out (below) to fit well with other results (also cf. Figure 36). Implicit in the general fit of the permittivity is the condition that the dielectric behavior of the permuthane binder at ~ 100 GHz is essentially the same as the lower frequencies. This is nicely confirmed by direct measurements at NRL on a polyurethane slab supplied by us. Rachford reports a nearly constant value for ε_r' of 2.6 when fitting data from 75 to 100 GHz. This is quite close to the lower frequency values of 2.8 and 3.0 previously obtained. If we had full confidence in the accuracy of the slightly lower value, it would imply an 8% reduction in the composite ε_r' at
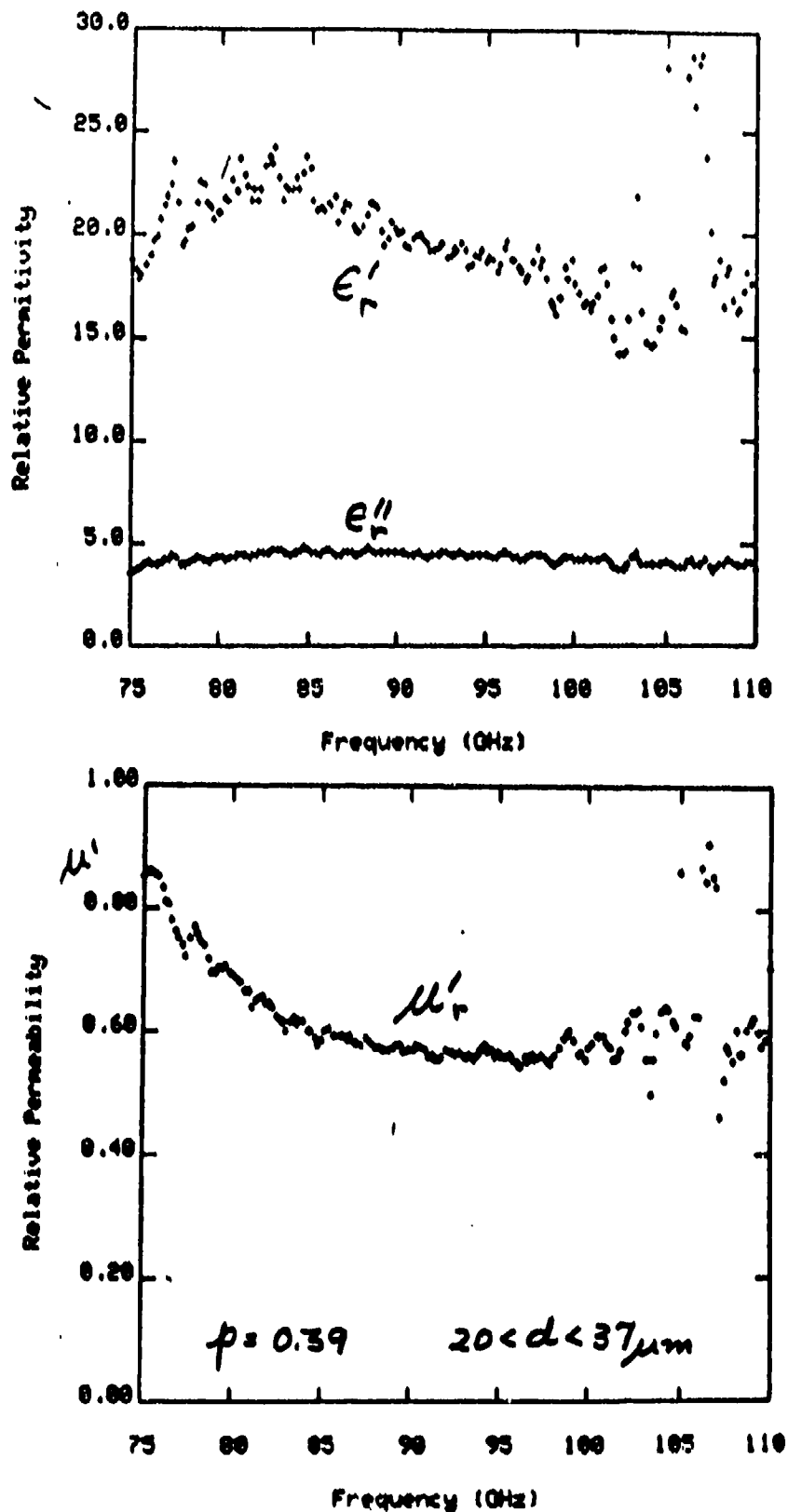
85

Figure 38. Permittivity and permeability vs. frequency in W-band for $Ni_{92}Cr_8$ alloy powder (20 μm < d < 37 μm) in polyurethane, p = 0.39, as measured at NRL.

86

that frequency relative to a low frequency value. However, while this spread is within the scatter limits of the experimental results, such a decrease is in line with the trend for this material at lower frequencies seen in other work at our laboratory.

Returning to the waveguide measurements, several techniques were employed. The "most acceptable" results came from analysis of network analyzer measurements of the amplitude and phase of the transmitted signal S_{21} for single and double thicknesses. When reflection measurements S_{11} with and without a short circuit backing were included, there was considerably more frequency dependence to the calculated ε and μ values than with the other experimental set, as well as more than the "expected" dependence, based on the lower and higher frequency data already explored.

In Figure 39 we show permittivity and permeability results obtained by fitting to the observed S_{21} parameters for a $p = 0.42$, $20~\mu$m $<$ d $<$ 37 μm composite sample in the K_u band. The ε'_r value of 24.5 is in excellent agreement with other results and the μ'_r behavior will be seen as satisfactory. A similar success was obtained for the smaller particle, d $<$ 10 μm, $p = 0.36$ sample in this same frequency band, from the S_{21} parameters. Deviations from "perfect" agreement are within the scatter band of general results.

V.2   Results – Polymeric Binder Composites with Ni-Cr Alloy Powders

In presenting these experimental results obtained with Ni-Cr powders in polyurethane, we start with the permeability measurements. At this stage we also include comparison with the modeling of magnetic dipole and particle size effects from Section IV.1. We follow with presentation of permittivity measurements, but defer comparison with models until Section V.3.

V.2.1   High-Frequency Permeability Results and Model Comparisons

We now present the ensemble of permeability data superposed on model calculations of the type illustrated in Figures 17-20. These include the results obtained during the contract term plus the additional measurements with the CRD-HP8510B system which we just couldn't resist doing. The former group includes the frequency and size-dependent results from the 2-18 GHz range from the NRL HP8510A, in addition to our earlier data obtained from the outdated HP8410 system, the just described K_a band results, and the 35 GHz fixed frequency measurement, and the
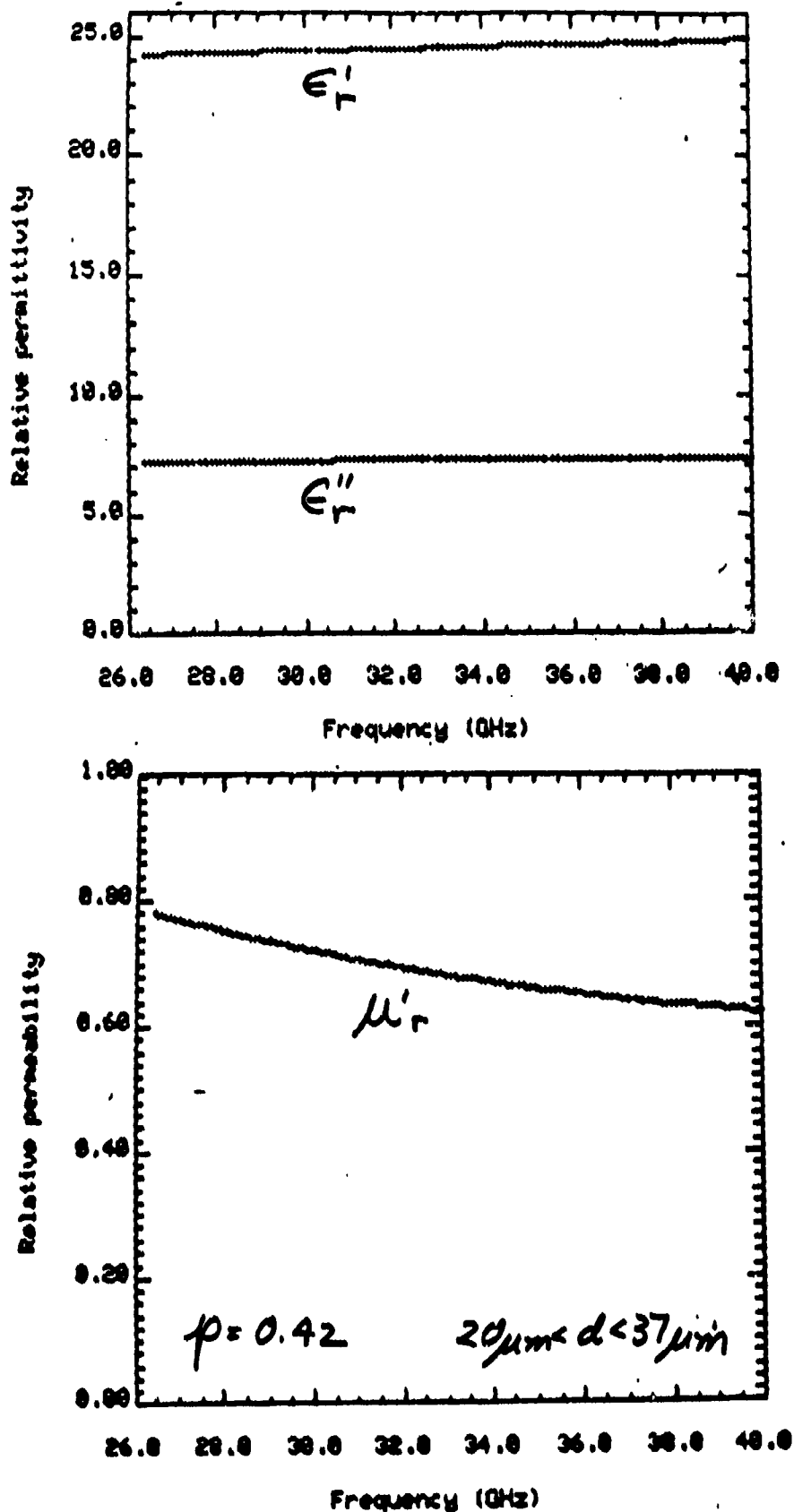
Figure 39. Permittivity and permeability vs. frequency in K_a-band for $Ni_{92}Cr_8$ alloy powder (20 μm < d < 37 μm) in polyurethane, p = 0.42, as measured by waveguide techniques at NRL.

one data group ($p = 0.4$) from W-band (75 to 110 GHz). (Loss permeability, μ_r'', was not measurable in the NRL experiments above 20 GHz.) The gathering together of all these results introduces some small confusion on some graphs, since scatter is inevitable. (The worst is for $p = 0.4$ which embraces all three particle sizes.) Consequently we plot separately the results from the CRD-HP8510B, but pair these graphs with their counterparts from the earlier data sets.

We also confess that we did not directly measure the volume loading, p, values on the final set as would have been obtained using low-temperature saturation magnetization data (σ_s at 6K), the method described in Section II.7.3 herein. Instead for this set only, we used the ε_r' values referred to the ε' vs. p data base on similar composites (from the following subsection) to estimate p values and to verify that these were adequately close to the nominal intended loadings. (The discussions to follow on permittivity will validate this estimation procedure.)

The pair of graphs of μ_r' vs. frequency, $p = 0.1$, data superposed on model calculations are presented as Figures 40 and 41. The three symbols for data in Figure 41 represent three measurement frequency bands for which we usually changed sample thickness in order to improve the quality of the results. These bands, naturally each with its own calibration runs, were 0.045 to 2 GHz, 1 to 5 GHz, and 5 to 20 GHz. Sample thicknesses should, at most, barely exceed $\lambda_m / 4$ (see Section II.7.5), at the highest frequency of a measurement range. On the other hand, a desirable but not mandatory minimum thickness would be $\lambda_m / 10$ at the lowest frequency of a range. When compromises are made for reasons of time efficiency, it is this desired minimum thickness which can be relaxed with only a modest sacrifice in data quality.

The graph pairs for μ_r' vs. frequency continue through Figure 47. Since the follow-up series (for the HP8510B) was not complete, not all the prior cases of volume loading and particle diameter (or frequency range) were duplicated. However, the trends to agreement as a function of frequency and/or particle size are qualitatively confirmed in the earlier data sets, and rather nearly quantitatively confirmed without spurious inflection points in the follow-up data sets. In Figure 47, the upward offset for d < 10 μm, f-range from 5 to 20 GHz, is attributed to a small error in the calibration. If the offset is ignored, as it should be in such a case, the predicted curvature is well reproduced.

The graph pairs for the loss or imaginary part of the permeability μ_r'', follow in Figures 48-55. The relative smoothness of the follow-up measurement curves from the HP8510B, in comparison to erratic waviness in the earlier sets of data, is a further testimonial to the instrumental

89
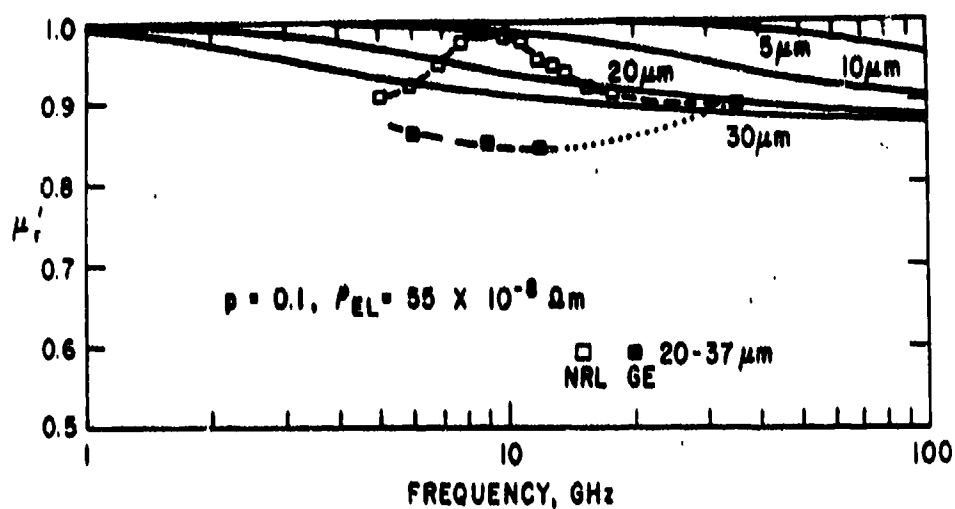
Figure 40. Comparison of experiment and model calculations: μ'_r vs. frequency, $p = 0.1$, for Ni$_{92}$Cr$_8$ alloy powder in polyurethane, from measurements at GE and NRL
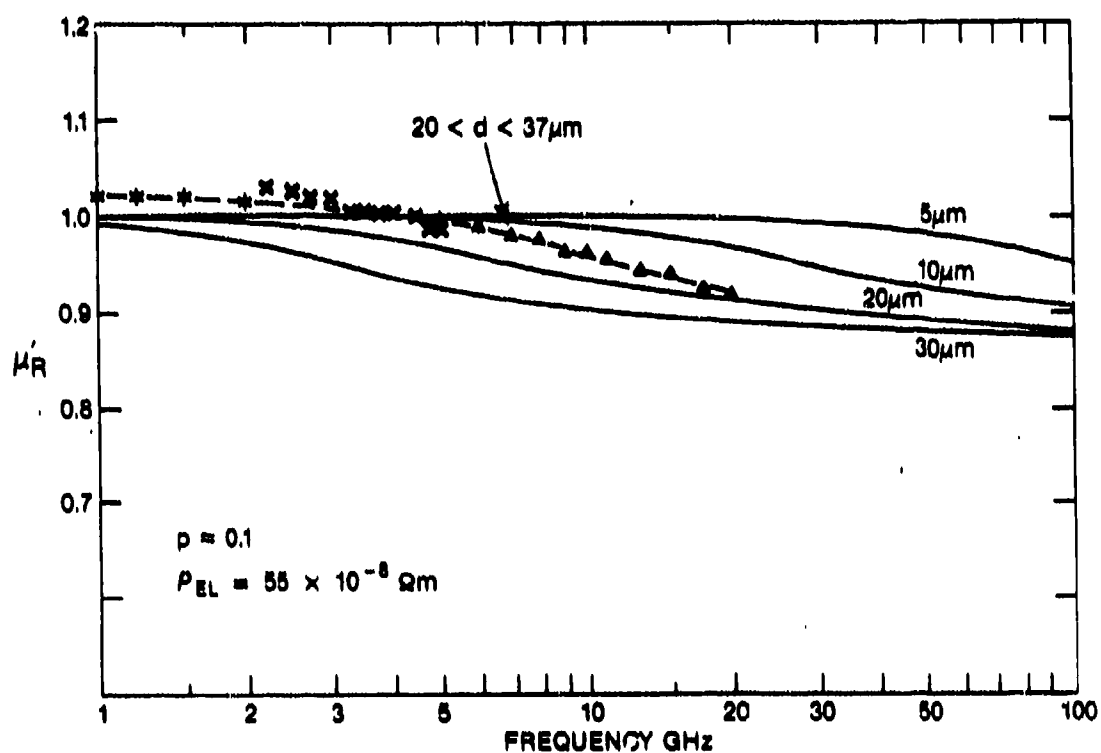
Figure 41. Follow-up measurements on HP 8510B: μ'_r vs. frequency, superposed on model calculation, equivalent composite to Figure 40.

Figure 42. Comparison of experiment and model calculations: μ_r' vs. frequency, $p = 0.2$; material system of Figure 40. Measurements at GE and NRL.

Figure 43. Follow-up measurements on HP 8510B: μ_r' vs. frequency, superposed on model calculation; composite equivalent to counterpart in Figure 42.

91

Figure 44. Comparison of experiment and model calculations: μ'_r vs. frequency, $p = 0.3$; material system of Figure 40. Measurements at GE and NRL.

Figure 45. Follow-up measurements on HP 8510B: μ'_r vs. frequency, superposed on model calculation; composite equivalent to counterpart in Figure 44.

92
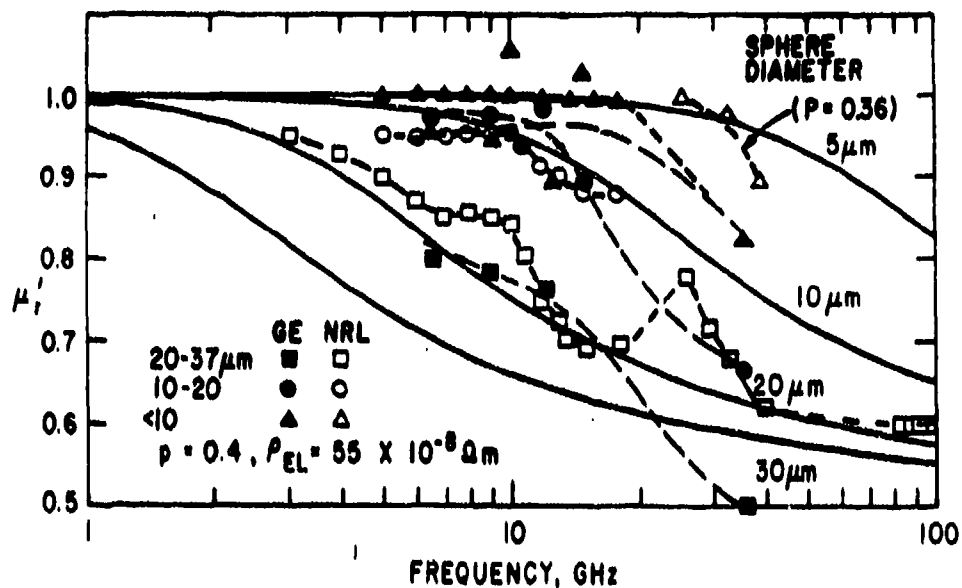
Figure 46. Comparison of experiment and model calculations: μ_r' vs. frequency, $p = 0.4$; material system of Figure 40. Measurements at GE and NRL.
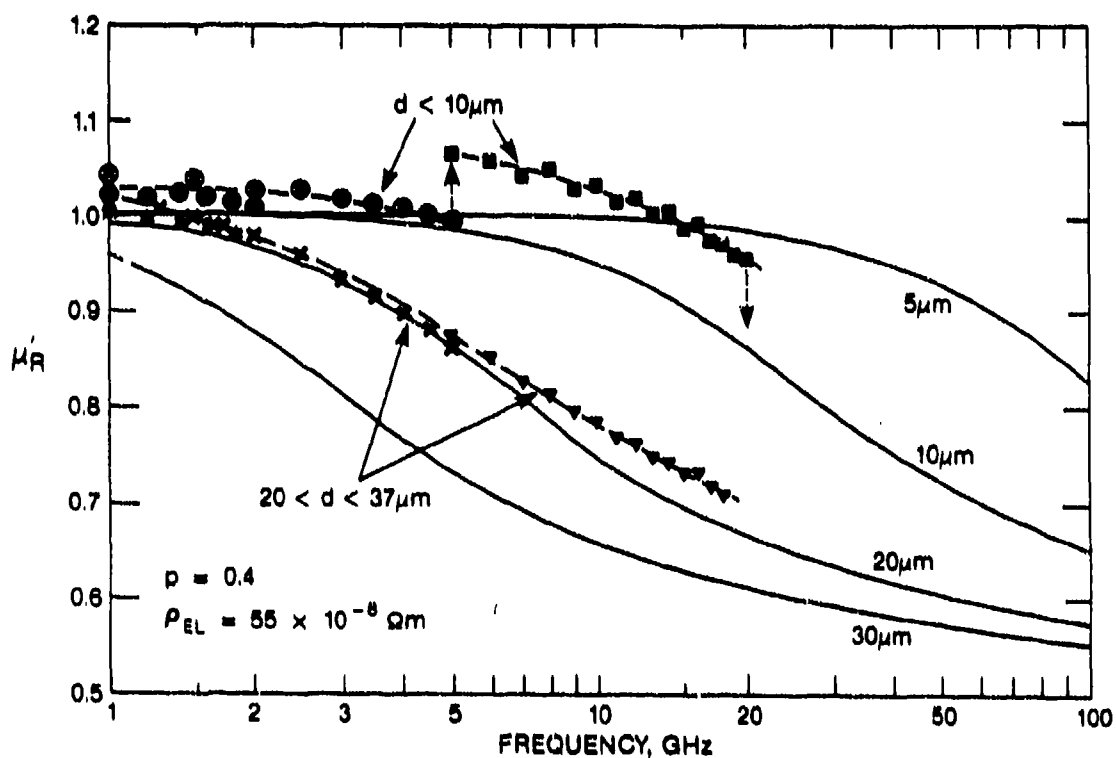
Figure 47. Follow-up measurements on HP 8510B: μ_r' vs. frequency, superposed on model calculation; composite equivalent to counterpart in Figure 46.
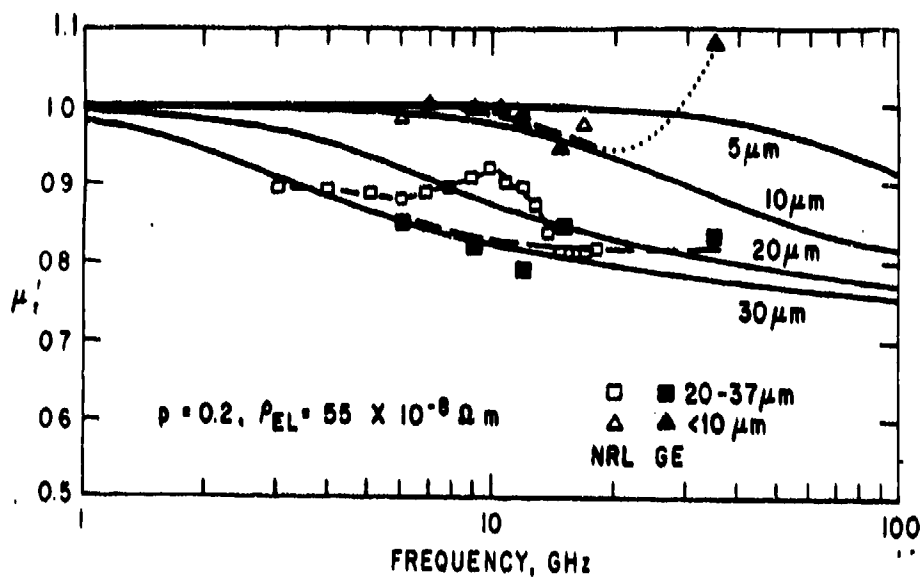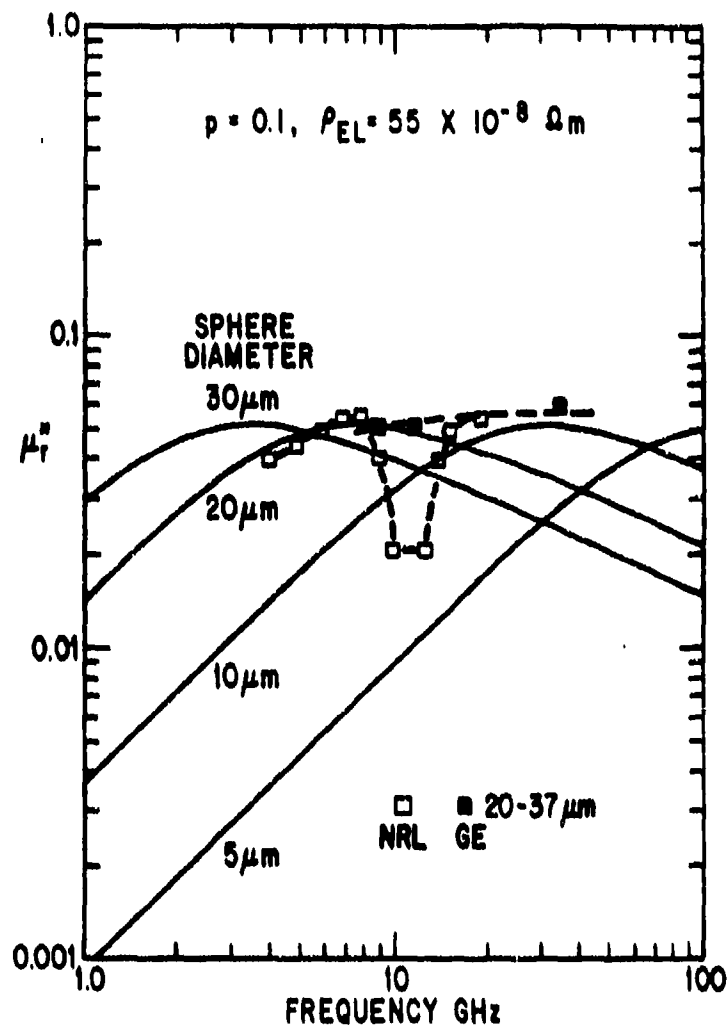
Figure 48. Comparison of experiment and model calculations: μ_r'' vs. frequency, $p = 0.1$; material system of Figure 40. Measurements at GE and NRL.
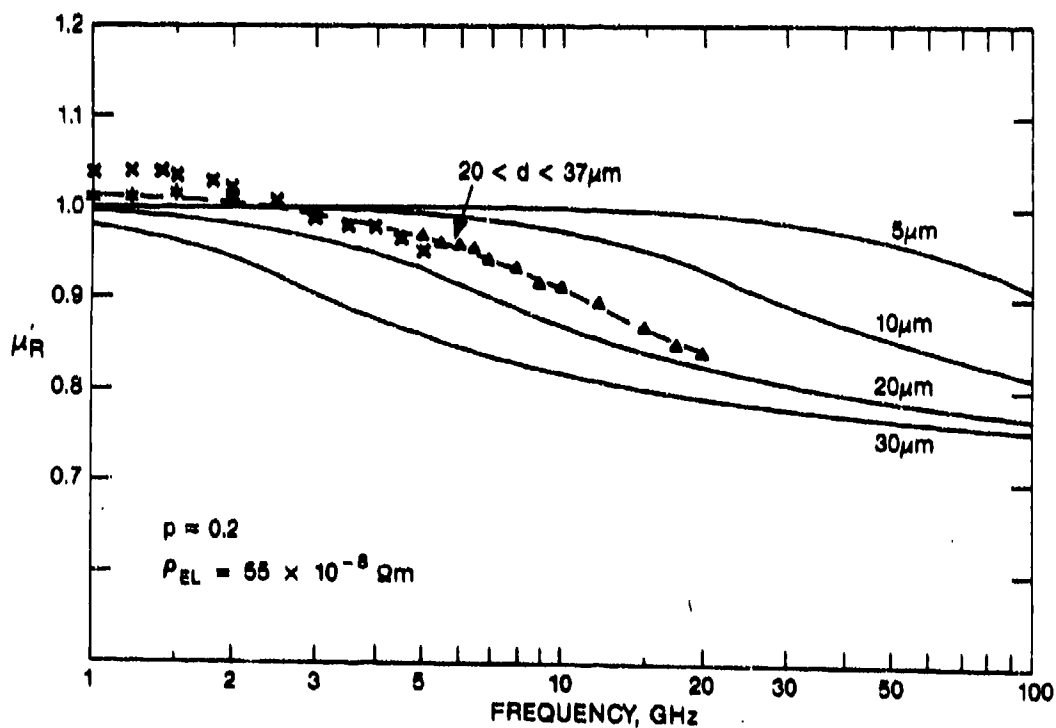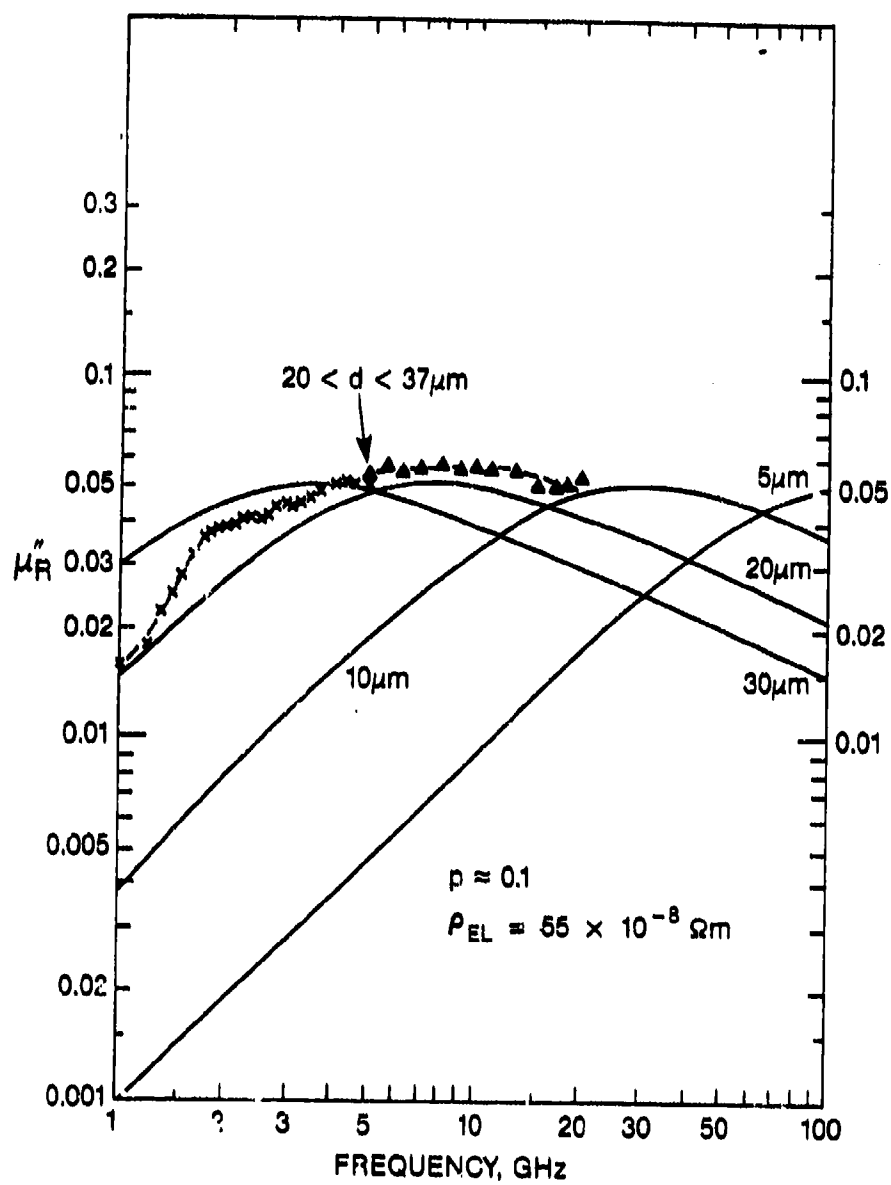
Figure 49. Follow-up measurements on HP 8510B: μ_r'' vs. frequency, superposed on model calculation; composite equivalent to counterpart in Figure 48.
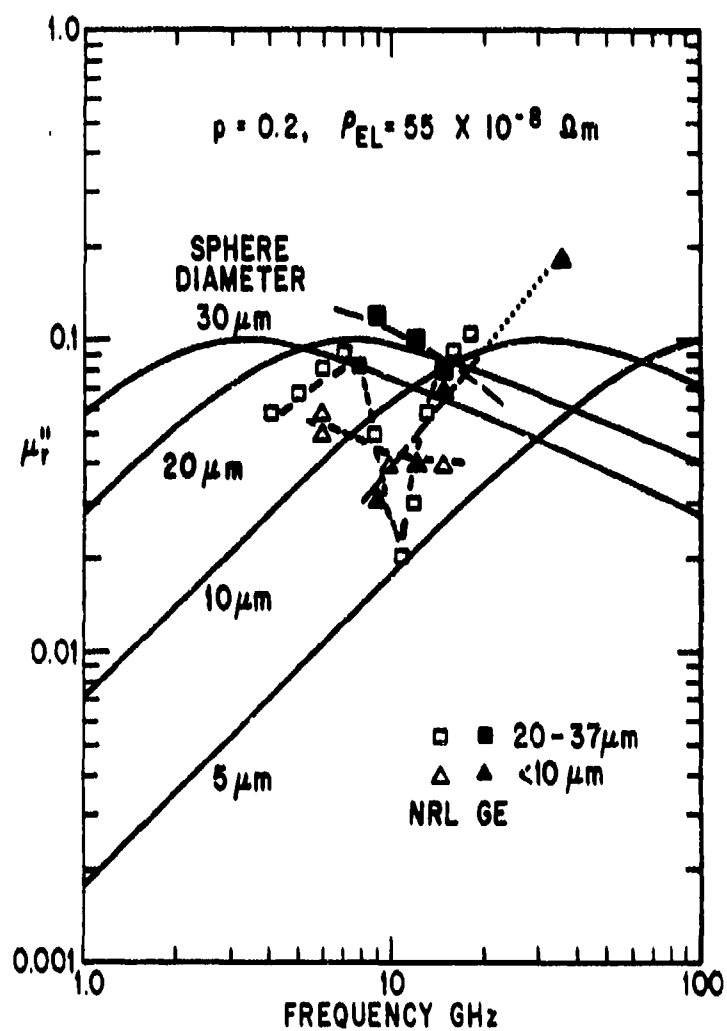
Figure 50. Comparison of experiment and model calculations: μ_r'' vs. frequency, $p = 0.2$; material system of Figure 40. Measurements at GE and NRL.
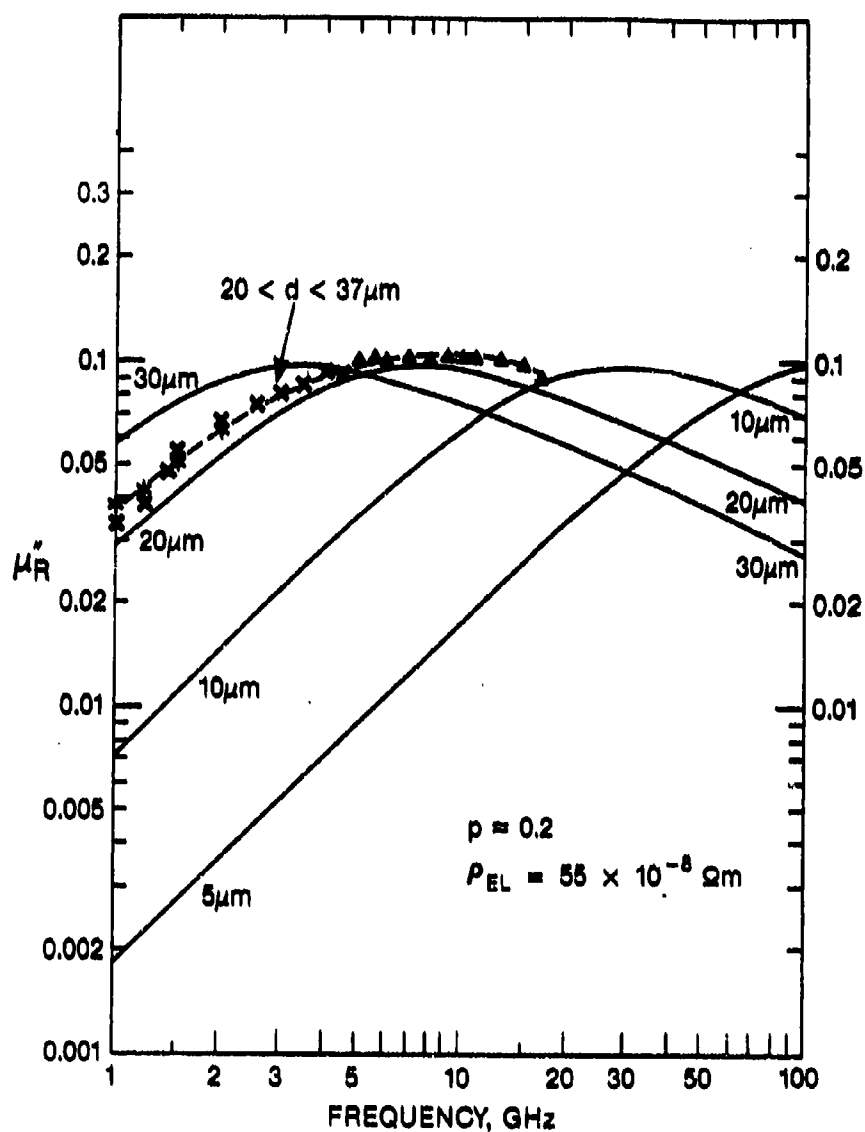
Figure 51. Follow-up measurements on HP 8510B: μ_r'' vs. frequency, superposed on model calculation; composite equivalent to counterpart in Figure 50.
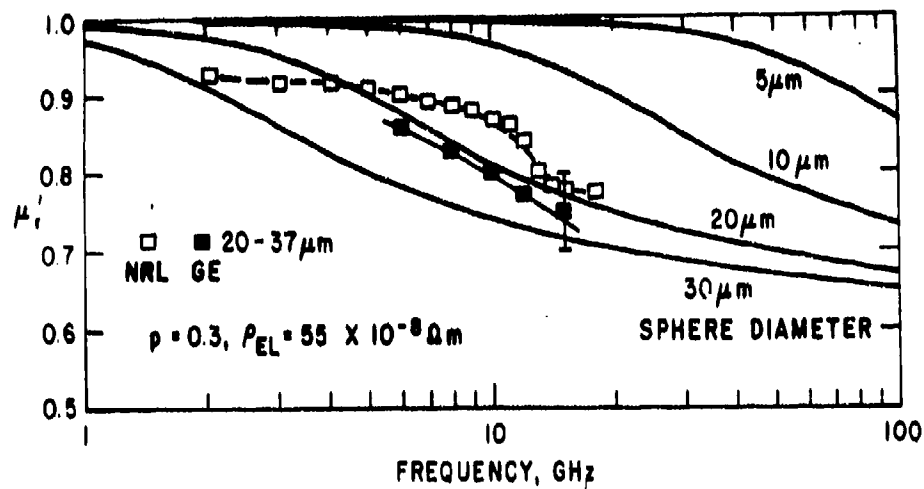
97
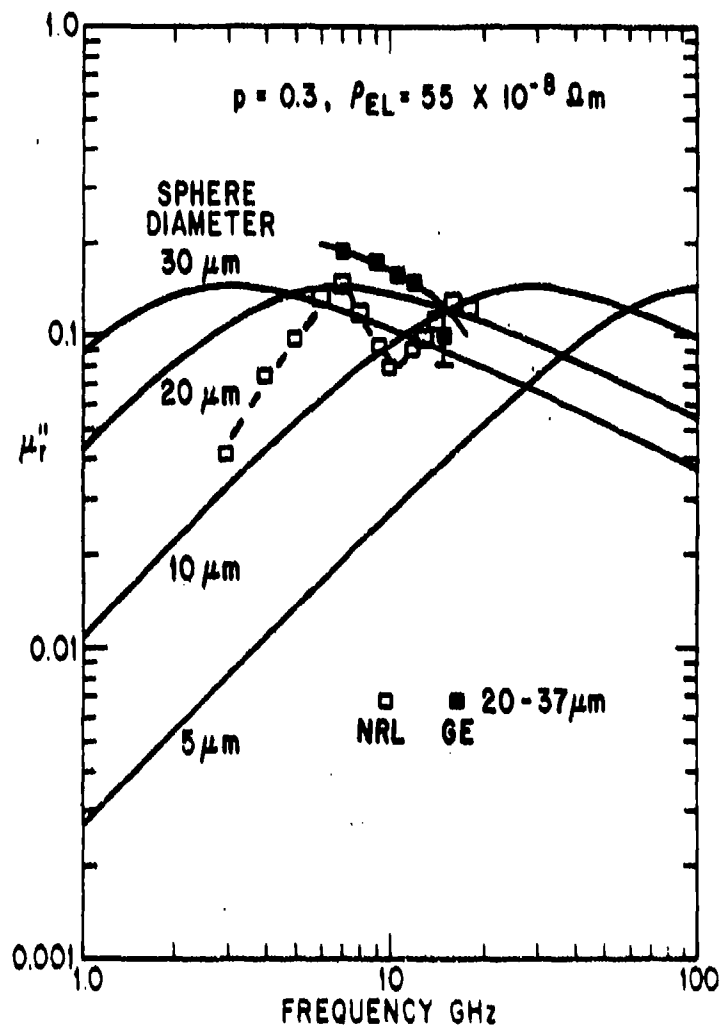
Figure 52. Comparison of experiment and model calculations: μ_r'' vs. frequency, $p = 0.3$; material system of Figure 40. Measurements at GE and NRL.
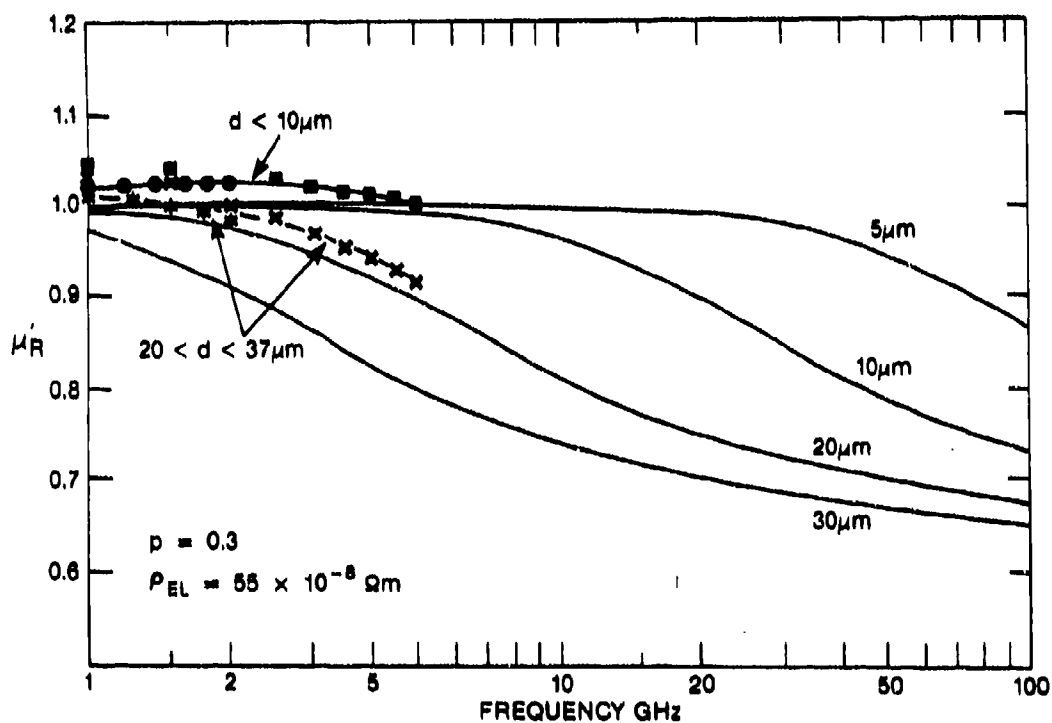
Figure 53. Follow-up measurements on HP 8510B: μ_r'' vs. frequency, superposed on model calculation; composite equivalent to counterpart in Figure 52.

Figure 54. Comparison of experiment and model calculations: μ_r'' vs. frequency, $p = 0.4$; material system of Figure 40. Measurements at GE and NRL.

Figure 55. Follow-up measurements on HP 8510B: μ_r'' vs. frequency, superposed on model calculation; composite equivalent to counterpart in Figure 54.
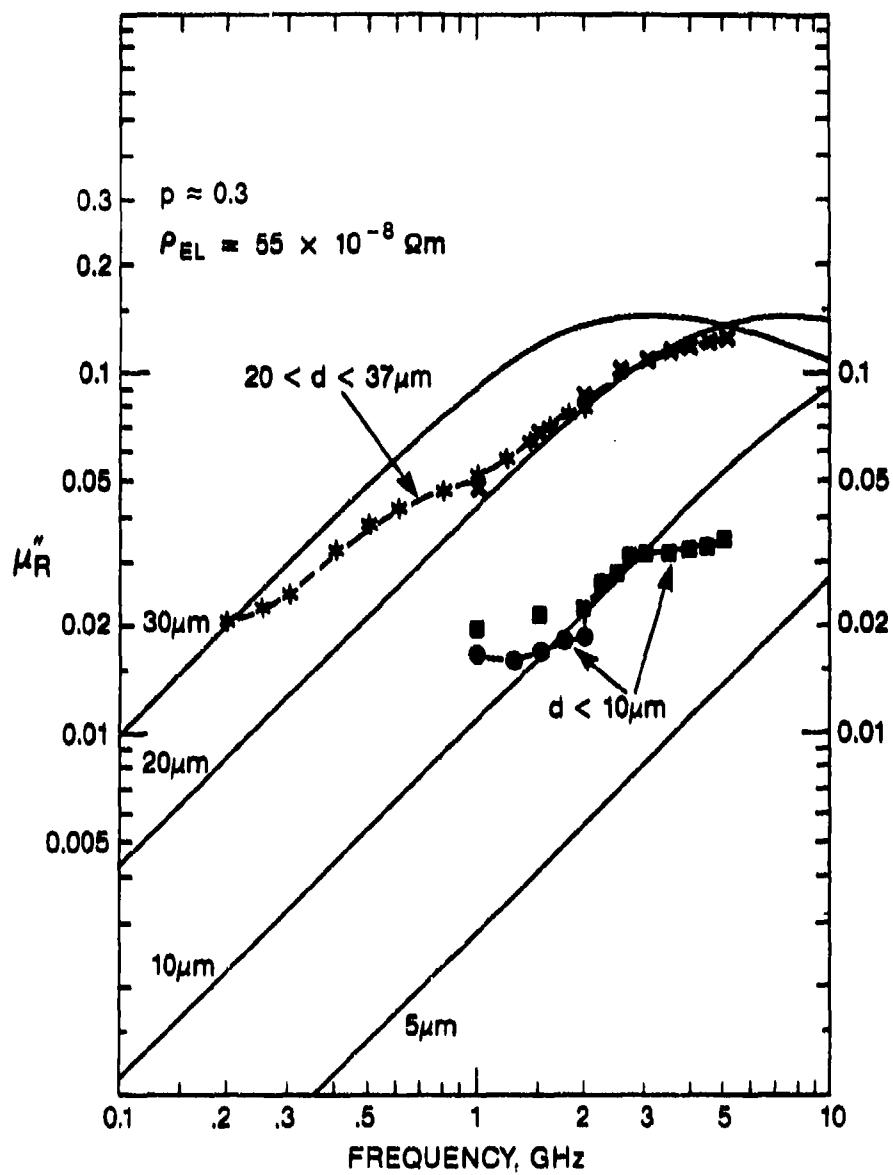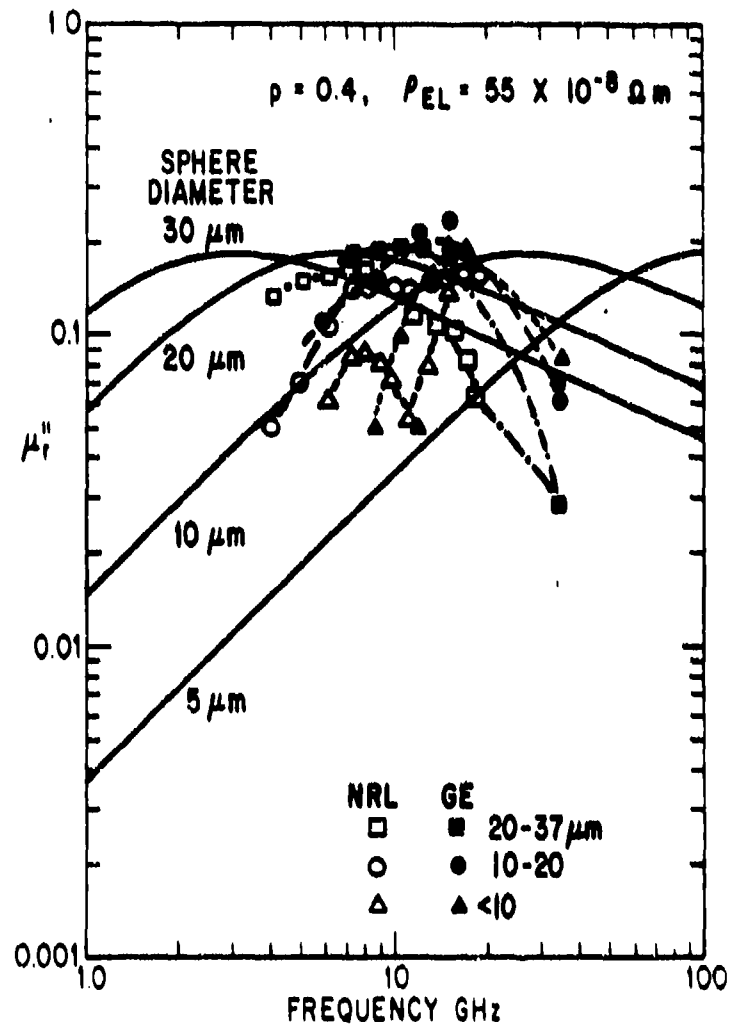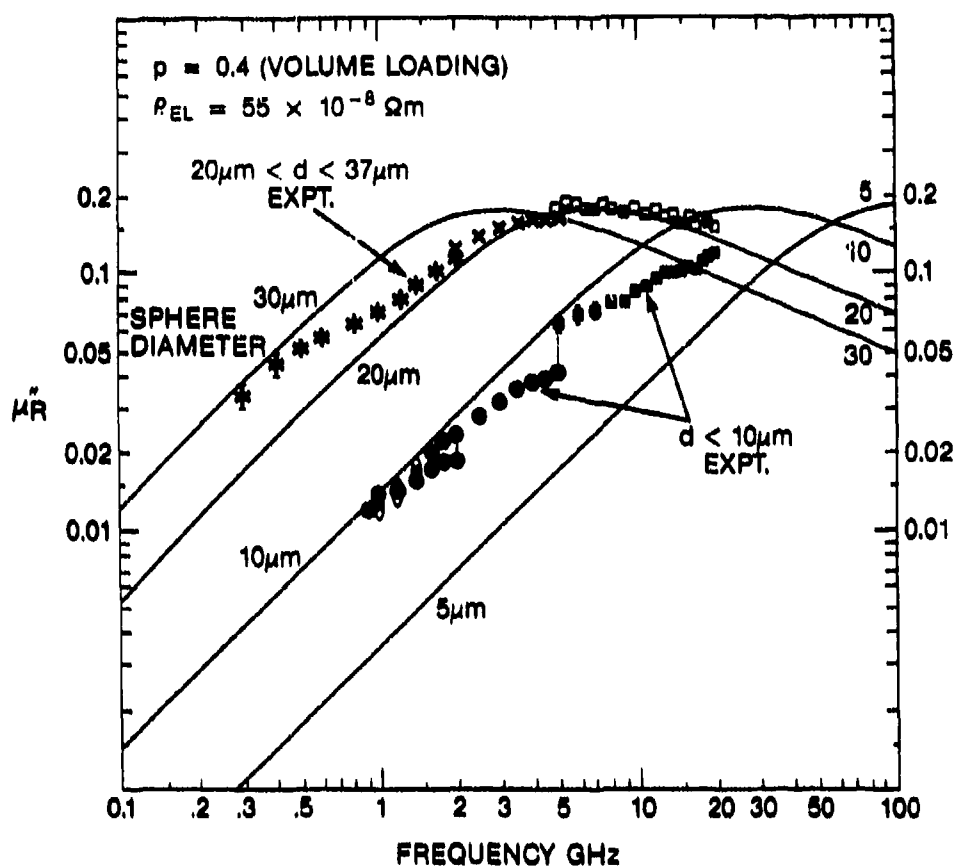
capability when extra care is exercised. In these graphs we have "pushed" to extract lower frequency results as μ_r'' decreases to rather small values. The manufacturer's discussion of instrumentation errors [49] warns the user to expect gradual loss of accuracy as the loss tangent (μ''/μ' or $\varepsilon''/\varepsilon'$) goes below 0.1. In these loss measurements, most results fall into this cautionary region. For this reason we are reluctant to attach significance to the modest inflections displayed in many of these μ_r'' vs. f curves. Indeed, we can probably attribute the tendency toward flattening at a low plateau in the range of μ_r'' equal to 0.02 or 0.03 to these instrumentation errors inherent in the method of measurement. Another factor of possible relevance is the role of deviations from particle sphericity, a point to which we return in the succeeding sections.

Overall, with the ensemble of data from up to six different measurement experiments covering from about 1 GHz to about 100 GHz, we feel very secure with the agreement between the induced complex permeability model and experiment.

V.2.2 High-Frequency Permittivity Results

Our early measurements of the constitutive parameters in the 6-12 GHz range on the outdated HP8410 system yielded reasonable complex permeability values but some rather poor results for permittivity. The uphill struggle in this search is somewhat painfully documented in the series of three annual technical reports under this contract [52-54].

By fortunate contrast, the slotted-line, single frequency measurements at 35 GHz produced results that generally conformed to more reasonable behavior. Even here, some data sets were unacceptable when physically meaningless negative values (of non-negligible magnitude) turned up in computing complex μ and ε. Values of ε'' are expected to be negligibly small in this system, while values of μ'' may be small, although perhaps not very small. Thus the larger, real quantities may be nearly correct, even when the imaginary components are less reliable but not outlandishly so.

A word here about the dielectric behavior of a metal. Following appropriate models [24, 25, 30], the frequency region for a significant electric loss is governed by the intrinsic electron plasma frequency of the metal and the electron relaxation time. These correspond to frequencies in the ultraviolet and visible ranges, respectively, clearly far away from the microwave and millimeter frequency ranges of present interest.

102

For ε' , repeated measurements at 35 GHz provided from two to six closely grouped values for each of the seven composite samples of the series. When we combine these GE-RSD results with the NRL-HP8510A results at the selected frequency of 10 GHz, we obtain the curve of Figure 56. The agreement between the two sets is generally quite good, reinforcing the conclusions of rather small frequency dependence and independence of particle size. The former conclusion is also rather well supported from Figure 37 over the near-decade of frequencies, 2 to 18 GHz. In this same connection, there is also a good accord with results on highly loaded samples obtained at NRL at the higher frequencies (K_a and W bands) described in Section V.1.2 and Figures 38 and 39. It is also worth noting in Figure 56 that there is a smooth departure from the binder-only value with increasing p.

We also see in Figure 56 a marked upward deviation of the data curve from the Maxwell-Mitoff approximation. We have come to expect this from earlier work (Figures 26 and 27) and will examine it more closely in the following section.

V.3 Results – Polymeric Binder Composites with Another Alloy Powder

In this section we present a few results from another study, an IR&D investigation carried out at GE-CRD at the behest of GE-AE (Aircraft Engine) in Evendale, OH. It involves a composite system of coated magnetic alloy particles in the same polyurethane binder as employed for the Ni-Cr alloy powder, and strongly resembles the B-series discussed in Section IV.2.4 herein (from ref. 1). We call this set the C-series, and we discuss its permittivity behavior in relation both to the improved permittivity modeling (Section IV.3) and the results obtained for Ni-Cr alloy powder composites (Section 2.2). The comparison is quite useful for the goals of the present study.

V. 3.1 High Frequency Permittivity Results and Comparisons

The alloy powder of the C-series was prepared at an outside vendor by gas-atomization (cf. Section II.4). Subsequently it was divided by air-classification at GE-AE into a number of close-lying size groups. The sizes were evaluated by three particle size counters, Vortec, Coulter, and Microtrac, as well as by scanning electron micrographs (SEM). We focus here on data from a group of five size fractions called 30R, 35R, 40R, 45R, and 50R. Their average sizes (averaged
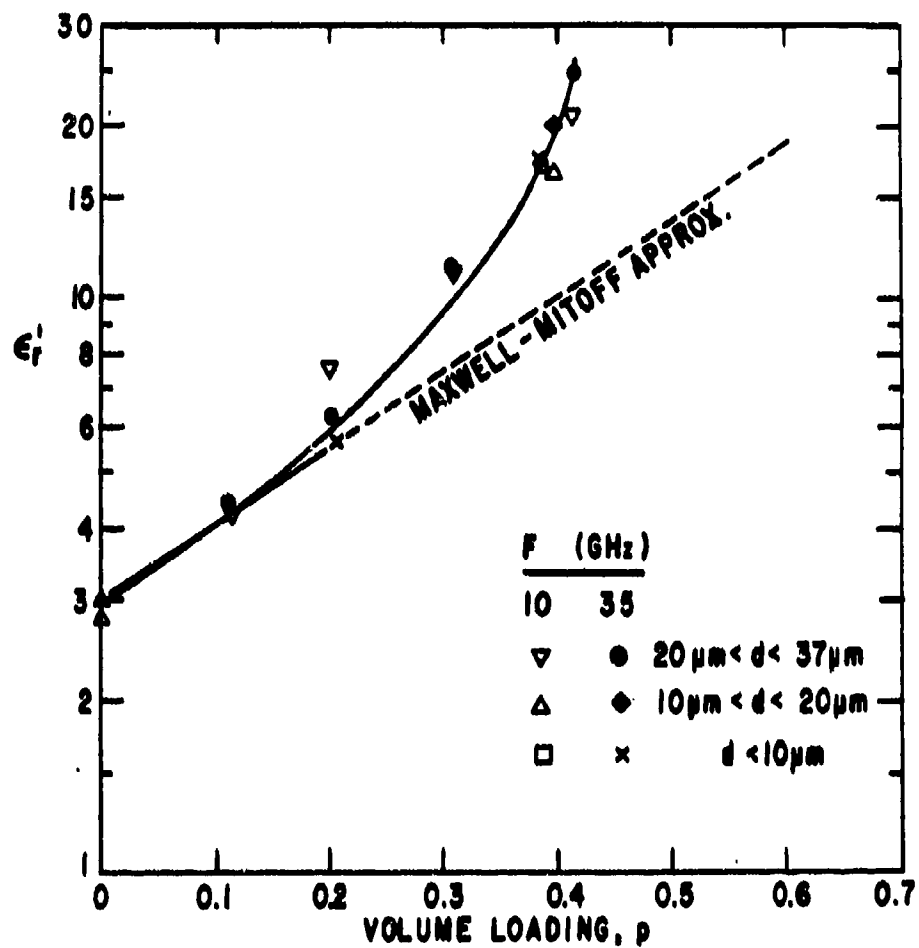
Figure 56. Relative permittivity, ε'_r, vs. volume loading, p, for $Ni_{92}Cr_8$ alloy at various particle sizes in polyurethane composites. Data at 10 GHz from NRL and at 35 GHz from GE-RSD.

104

group of five size fractions called 30R, 35R, 40R, 45R, and 50R. Their average sizes (averaged from the three counters noted) range from 11.0 mm to 14.6 mm. Figure 57 shows SEM photos of the powder fraction designed 35R, average diameter 11.8 mm. The sizing appears to be rather narrow and the particles are quite spherical.

In most cases, the various sized powders were prepared in composites with about seven different loadings. Thus this group of five sizes represents about 35 samples. The permittivity results, at 10 GHz, as measured on the HP8510B at GE-CRD, are shown in Figure 58, as a function of volume loading, p. It might seem that the solid line on the graph is drawn to fit the ensemble of data. In actual fact this predrawn line is the Guillien-Turner Empirical Curve, rescaled to $\varepsilon_b = 2.8$, i.e., a line through the data points of the ideal experiments of References 44 and 46, shown on a reduced basis in Figure 32. The agreement is remarkably good, meaning that we have three widely different experimental families that follow this same behavior. Data that fall below the line are often correlated with samples showing significant porosity. We do not have a glib explanation for the few data values above the line, but can remark that in re-examination of some such cases, a density calculation error, or a sample heterogeneity was found.

We conclude that the Guillien-Turner Empirical Curve is both a reliable guide for judging good quality in systems which confirm to its basic assumptions (i.e., spherical, non-contacting metallic particles) and a usable guide for estimating volume loading from permittivity data in conforming systems. We also note that the fairly close proximity of the Guillien-Turner data and these C-series data to the Doyle Pair-Interaction model line, shown in Figure 32, reinforces the qualitative significance of the model line.

Now we can return to the Ni-Cr alloy composites in order to compare their ε' vs. p data with these other criteria. In Figure 59 we present the ensemble of these data (from Figure 56) in comparison with the Guillien-Turner empirical curve (which is equivalent to the C-series data curve). There remains a marked upward deviation of the Ni-Cr data above about $p = 0.2$, although the initial slope behavior (p near zero) conforms with both the Guillien-Turner curve and the Maxwell/Clausius-Mossotti model. We are led back to the SEM views in Figure 8 of the Ni-Cr alloy powder which showed that non-spherical deviations were fairly common. Their effect on the polarizability, as for the pairs of Figure 29, will be still another enhancement factor.

Finally, the apparent reliability of the ε' vs. p curve for approximating the loading value, given a measured ε'_b, in the reasonably ideal case, suggests that one can extend the procedure even

105

35-R
1100X

35-R
2200X

Figure 57. SEM photo of the alloy powder fraction designated 35R.

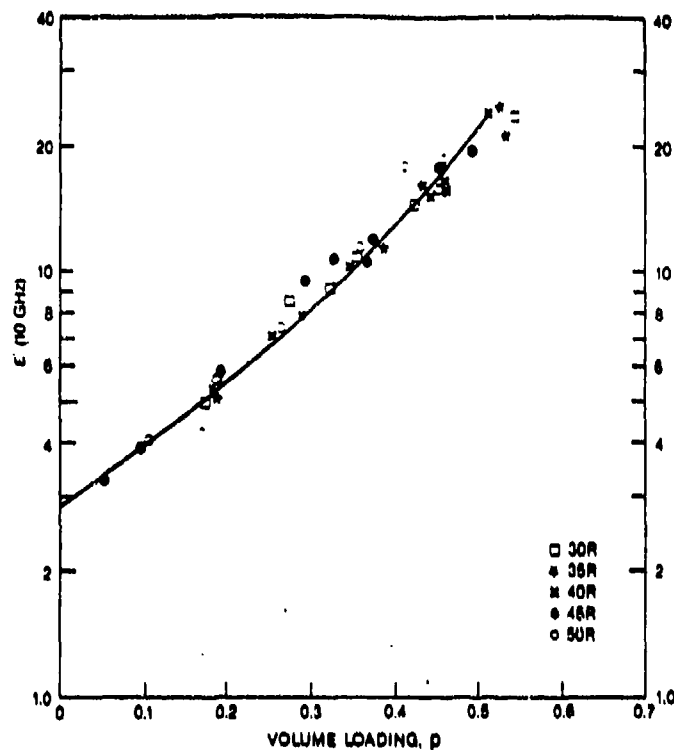Figure 58. Permittivity data at 10 GHz vs. volume loading, p, for composites from the C-alloy powder groups 30R, 35R, 40R, 45R and 50R, compared to the Guillien-Turner Empirical curve
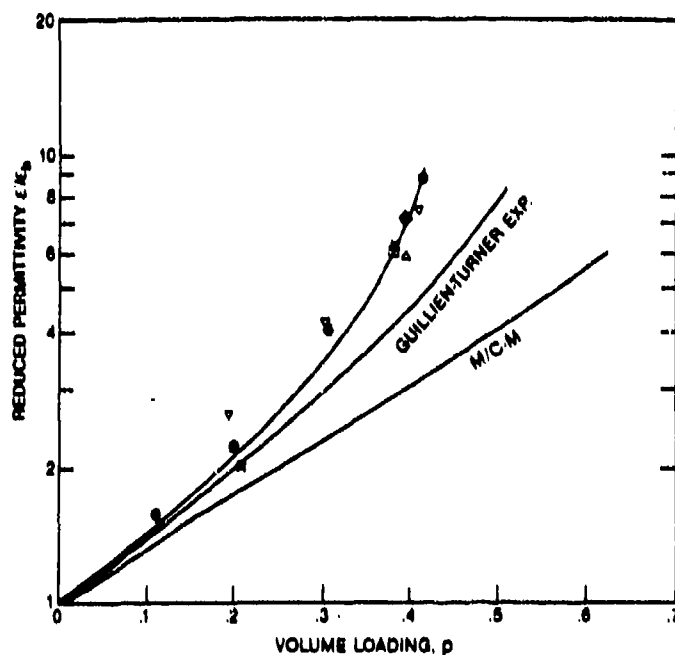

Figure 59. Reduced permittivity $\varepsilon' / \varepsilon_b'$ vs. volume loading ($\varepsilon_b' = 2.8$) for Ni-Cr alloy powder composites, compared with the Guillien-Turner Empirical Curve and the Maxwell/Clausius-Mossotti Model Curve

to non-ideal cases. This is indeed what was done in Section V.2.1 with the follow-on set of Ni-Cr composites which were prepared in order to refine the permeability behavior using the newest equipment.

From these data comparisons, despite the deficiencies of the Ni-Cr powder, we find that the agreement of the permittivity behavior of the related (but more nearly ideal) C-series of alloy powders signals a satisfying level of understanding as regards the permittivity of random metal-particle, non-percolating, artificial dielectrics.

V.4   Results – Ni-Cr Powder Composites with Alternative Inorganic Binder

The background for this part of the study, that of demonstrating the role of binder permittivity on composite properties, was introduced in Section III. It was followed by a description of the search for a suitable material and processing technique to use with our Ni-Cr alloy powder. We settled on a low-melting lead-solder glass, from Owens-Illinois, designated SG-7. After various failed attempts to machine satisfactory toroids for coaxial line microwave characterization, we decided to confine our tests to the simpler solid disks needed for the slotted-line technique used at the single frequency, 35 GHz, by our colleague, J. Hanson, at GE-RSD (Philadelphia).

A new series of samples was fabricated for these measurements. Their initial characterization parameters are shown in Table 9. Although the least aggressive fabrication procedure of the prior work was that of sintering the Ni_{92} Cr_8 alloy powder with the low melting glass, the resulting composites did not have a high density and were still rather weak for subsequent machining. Therefore, a mild hot pressing at relatively low temperature was used for most of the new samples. Based on the early work, this would likely produce slight deformation of the alloy powder, which could influence the electromagnetic results.

V.4.1   High-Frequency Permittivity Measurements

Measurements on solid disks were made at 35 GHz for these samples and for the binder glass. The latter exhibited a dielectric constant, ε_r', of 8.2, almost three times that of the organic polymer polyurethane. Thus a clear binder permittivity effect should be seen. In Figure 60 we

Table 9

THERMOMAGNETIC EVALUATION PARAMETERS OF INORGANIC COMPOSITES USED FOR ELECTROMAGNETIC STUDY

Material: SG-7 Lead-Solder Glass with RS-67 Run of $Ni_{92}Cr_8$, $10 < d < 20\ \mu m$

Sample Identity	Nominal Alloy v/o	Curie Temp K	Sat-Mag σ_{∞} (6 K) emu/g	Specific Grav.	Measured Vol. Load p
SG-7-1A (hp)	10%	151 ± 24	3.47	4.50	.115
SG-7-1B (hp)	10%	149 ± 24	3.22	4.47	.106
SG-7-2A (s)	20%	141 ± 23	5.48	4.67	.196
SG-7-3B (hp)	30%	151 ± 28	7.70	5.28	.298

Notes:

hp = processing by hot pressing around 600 °C and 300 psi.

s = processing by sintering only at 535 °C for 20 min.

Sample 2B broke during machining.
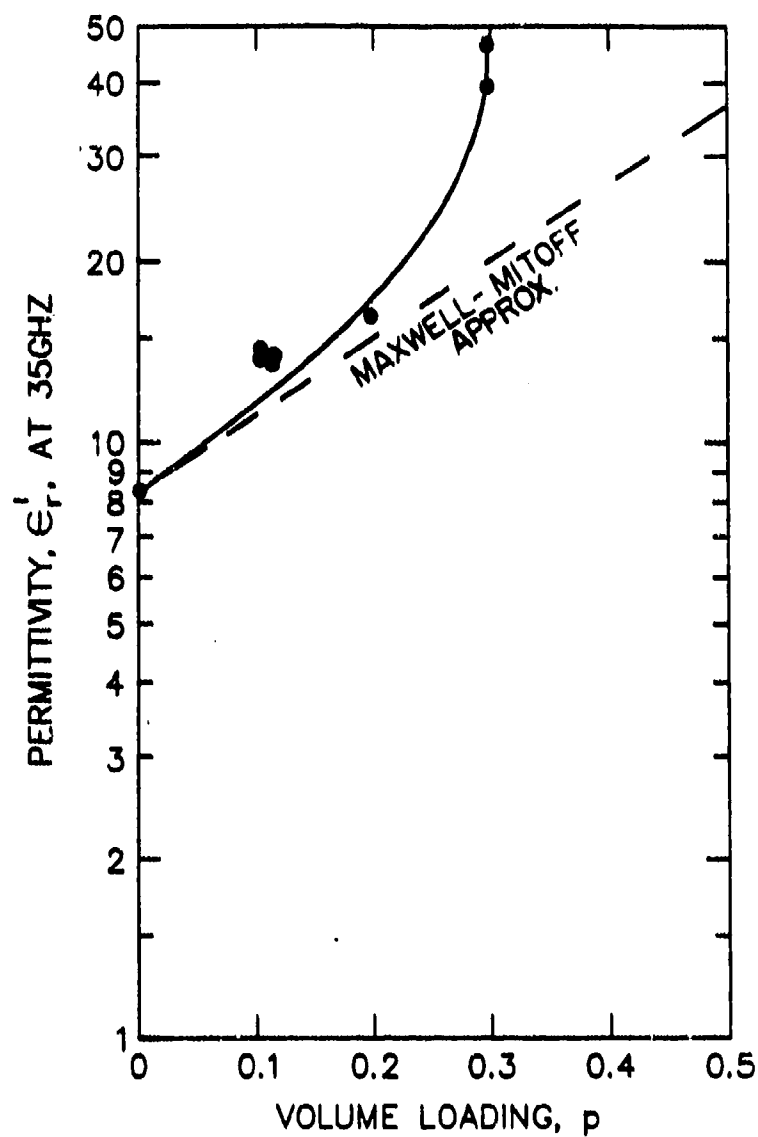
Sample 3A exhibited gross conductivity.

Figure 60. Relative permittivity, ε_r', vs. volume loading, p, for NiCr alloy, 10 μm < d < 20 μm, in lead-solder glass binder, measured at 35 GHz.

show the results for permittivity versus volume loading, ε'_c vs. p, for this series. It should be compared with Figure 56, and the qualitative similarity is obvious.

Next we consider the comparison on a quantitative level, presented in Figure 61. This graph takes $\varepsilon'_c / \varepsilon'_b$ for each binder where ε'_b is 2.8 for the polymer and 8.2 for the glass. At low loadings, up to 20% by volume, the scaled agreement is excellent. There is appreciable deviation at higher p-values.

A possible reason for the deviation is the enhanced polarizability of non-spherical particles such as might have occurred during the hot-pressing preparation. It should also be recalled that the powder preparation run RS-67 already yielded a modest share of non-spherical "pickle-like" particles, as was shown in Figure 8. A comparative scaled plot of polymer composites of this alloy with the Guillien-Turner Empirical curve (which matches the quite spherical C-series alloy powder composite permittivity) was shown in Figure 59. The Ni-Cr alloy series (from RS-67) permittivity data had a considerable upward deviation from the behavior of the C-series, even without any possible deformation of the particles in composite preparation. In hindsight, we now attribute that deviation between the two experimental systems to the non-spherical nature of some of the Ni-Cr alloy RS-67 particles. (We note in passing that Figure 61 also includes 35 GHz data from the K_α-band sweeps at NRL on the two polymeric composites described earlier.)

To sum up this section, the data of Figure 61 do confirm the role of binder permittivity as a scaling parameter in the dielectric behavior of artificial dielectric composites. We remarked earlier that this has an impact on application design. It also could be relevant for quality control in composites. If there were significant porosity in a particular composite preparation, it could be treated according to mixing rules as a diluent to the binder [21, 52], which in turn could lower the final composite permittivity.

V.4.2 High-Frequency Permeability Measurements

These inorganic composite samples measured at 35 GHz also displayed relevant permeability results, along the lines previously modelled for the polymeric binder composites. Inasmuch as both binders are non-conducting and non-magnetic ($\mu'_b = 1, \mu''_b = 0$), there are no changes introduced in the expected permeability behavior by changing binder. Since a single particle size group was used for this series, $10\ \mu m < d < 20\ \mu m$, we make our comparison

111
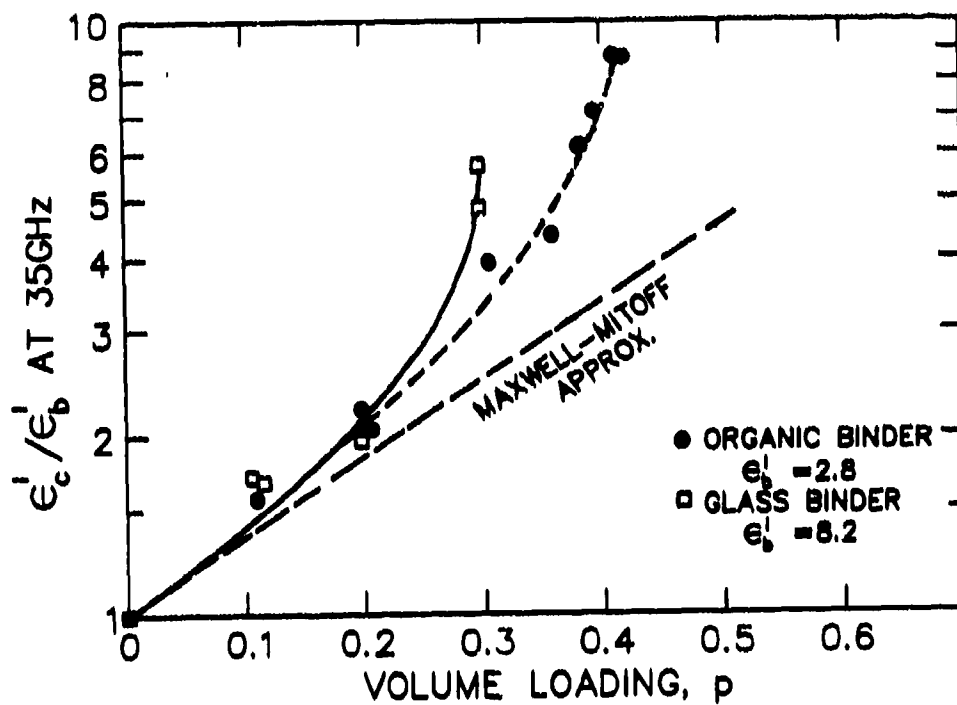
Figure 61. Scaled comparison of permittivity behavior, $\epsilon'_c / \epsilon'_b$, at 35 GHz, for artificial dielectrics with two different binders. Ni-Cr particles in polyurethane [$\epsilon'_b = 2.8$] and in lead-solder glass [$\epsilon'_b = 8.2$].

between experiment and calculation with the expected behavior for $d = 20 \, \mu$m. The comparison is shown in Figure 62 for both real and imaginary parts of the permeability. The bars on the experimental represent the full spread of several data points obtained from various disks of the same nominal (or identical) loadings. The agreement is fully satisfactory, a tribute to the quality of the measurement method and to the adequacy of the model.
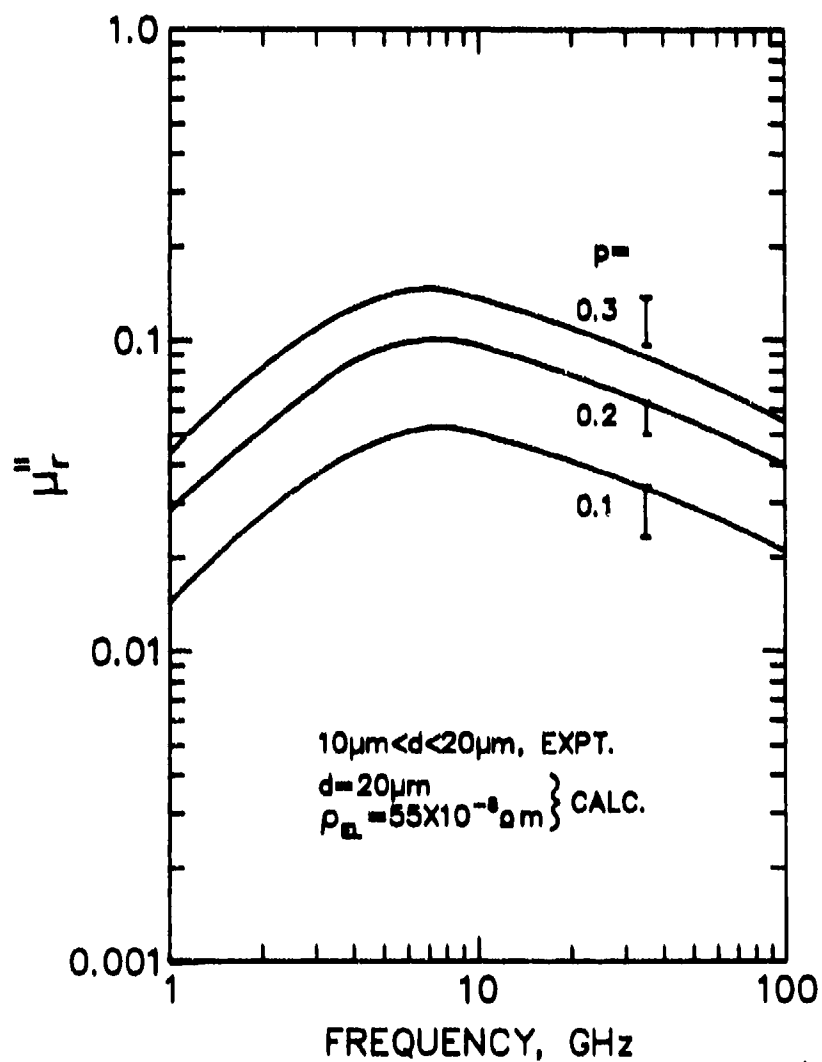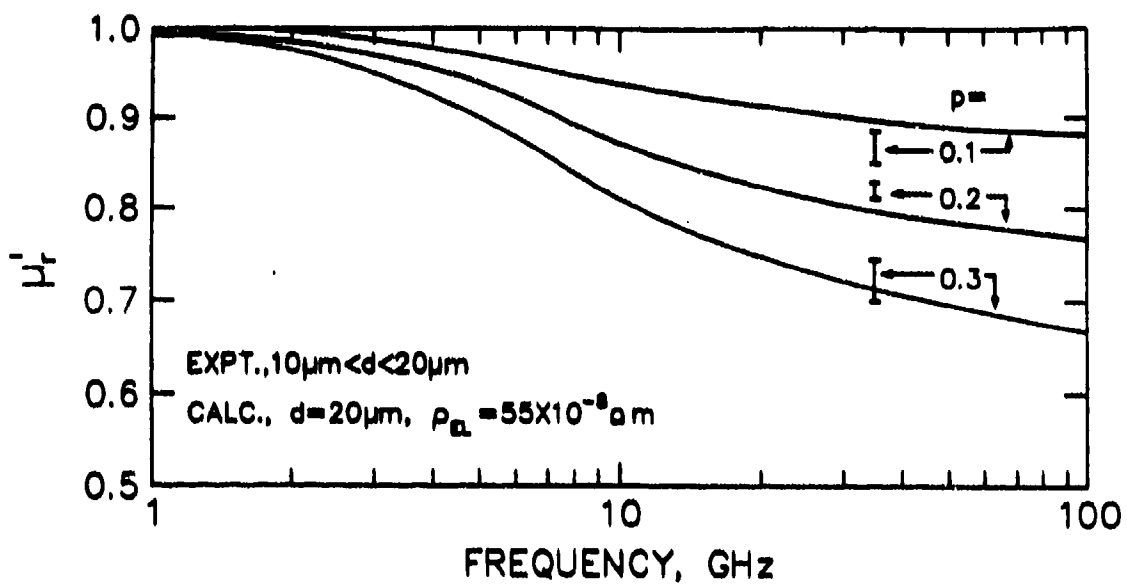
Figure 62. Comparison of experiment and model calculations: μ_r' and μ_r'' vs. frequency, various loadings; for NiCr alloy powder, 10 μm < d < 20 μm, in lead-solder glass. Data at 35 GHz only, from GE-RSD.

114

VI. CONCLUSIONS

This research has been concerned with the development of an interesting class of artificial dielectrics and a deeper understanding of its high-frequency electromagnetic properties. This Final Technical Report – Part A deals with essentially non-magnetic composite dielectrics. Part B, which contains classified material, treats magneto-dielectric composites.

The key ingredient of the artificial dielectric was a powder of spherical Ni-Cr alloy particles of ultimate composition $Ni_{92} Cr_8$ prepared by gas atomization with liquid substrate quenching. The latter step of the preparation produced an insulating oxide coating on each particle. The composites fabricated with this metal powder and polyurethane binder (or with an alternative inorganic, glassy binder) were ferromagnetic only below room temperature $T_c = 160K$ This feature allowed for easy determination of volume loading, using low temperature saturation magnetization measurements. Before mixing with the binder, the alloy particles were classified by size at <10 mm, +10-20 μ m, and +20-37 μ m.

While the original focus was intended to be on permittivity behavior, the realization that induced magnetic dipole (eddy current) effects would be equally important led to the decision to pay close attention to powder size. Calculations of complex magnetic permeability, adapted from the literature, showed that the dominant parameter is the ratio of particle radius to skin depth. The sizes chosen and frequencies of study (centimeter to millimeter wavelength ranges) covered the most interesting behavior anticipated.

An exploration of theoretical developments and history in the dielectric behavior of heterogeneous media successfully addressed one of our original questions, i.e., why our prior (and present) material systems appeared to follow the simple Maxwell (Maxwell-Garnett, Clausius and Mossotti) theoretical model. The inherently isolated metallic particles represent a correlated system even when loaded randomly in a binder, in contrast to the percolation-prone Bruggeman model exemplified in many experimental metal-insulator composites. Modern theories which incorporate higher order electric multipole effects and geometrical packing limits have been validated previously only (to our knowledge) by ordered lattice-like arrays of spherical particles. Our random composites exhibited similar properties, albeit with deviations probably reflecting on their microstructure.

The present study was successful in improving the modeling of permittivity behavior of randomly packed artificial dielectrics. This was a twin success, i.e., on the empirical and on the

"theoretical" fronts. The empirical success rests on the discovery in the literature of several rather different sets of results from ideal experiments involving truly spherical particles, well randomized and non-percolating. Some of our own data sets strongly resemble this ideal behavior. On the theoretical side, we developed, through the work of our consultant, W.T. Doyle, a rather simple pair-interaction model which is a naive oversimplification. However, it shows the importance of local clustering and higher-order multipole effects. This pair interaction description comes closer to describing the experimental results than any other model known to us. This convergence, even if not taken seriously, gives one a feeling of confidence and predictive control in considering the dielectric behavior.

Measurements of the electromagnetic constitutive parameters (permittivity and permeability) for Ni-Cr alloy powder/binder composites were carried out in three laboratories. Centimeter wavelength (2-20 GHz) results were obtained at GE-CRD and at the Naval Research Laboratory. Higher frequency experiments were carried out at GE Re-Entry Systems Department (Philadelphia) at 35 GHz, and at NRL for K_a-band (26-40 GHz) and W-band (75-110 GHz). Also included in our experimental analysis were data obtained in another study under internal sponsorship using a different alloy powder (C-series data). Its particles have a higher quality morphology; i.e., there were fewer deviations from sphericity than for the Ni-Cr alloy.

From the hierarchy of steadily improving experimental results, the induced permeability data are in good quantitative agreement with the calculated model over the parameter ranges examined, i.e., diameters from about 5 μm to 35 μm and frequencies from about 1 GHz to 100 GHz.

The permittivity data are independent of particle size, and change but little over the frequency range covered. The latter small effect is probably due to properties of the binder. The main interests in the permittivity focused primarily on its dependence on volume loading, and secondarily on the scaling properties with change of binder. The C-series permittivity data are in remarkably good agreement with the empirical curve obtained from ideal experiments in the literature, our so-called Guillien-Turner Empirical Curve. The experimental curve has values only slightly higher than those predicted by the oversimplified pair-interaction model of Doyle. As for the Ni-Cr powder composite permittivity, a residual upward deviation of ε' vs. p is attributed to non-spherical departures in particle morphology. These are visible in scanning electron micrographs.

From the experiments with an alternative inorganic, glassy binder, we confirm the scaling normalization law that $\varepsilon_c' / \varepsilon_b'$ (c = composite, b = binder) puts different systems on an equivalent footing. Indeed this was built-in to early theory and had been confirmed many times before.

This research has demonstrated that the microwave electromagnetic behavior of non-percolating, artificial dielectric composites is well understood. Random arrays have their own unique properties, as distinct from ordered arrays. Whereas several reports in the late 1970's and early 1980's [24,25] had pointed to giant deviations from electromagnetic predictions for far-infrared absorption of submicron metal particles, more recent studies [18] showed qualitatively that inadequate inter-particle dispersion was the problem. Our work puts this explanation on a quantitative basis, albeit at modestly lower frequency and larger particle size. The present study also provides a firm foundation for examining the more difficult metallic magneto-dielectric composites discussed in Part B of this Final Report.

REFERENCES

[1] I.S. Jacobs, H. Kirtchik, J.M. McGrath, and R.N. Silz, "Magnetic RAM Technology –
     Phase II (U)," AFWAL-TR-82-1040, Final Technical Report for Contract F33615-80-C-
     1040, General Electric Company, Sept. 1982, SECRET.

[2] R. Landauer, "Electrical Conductivity in Inhomogeneous Media," in *Electrical Transport and
     Optical Properties of Inhomogeneous Media*, ed. by J.C. Garland and D.B. Tanner, AIP
     Conf. Proc. No. 40 (1978), pp. 2-45.

[3] K.D. Cummings, J.C. Garland, and D.B. Turner, "Electromagnetic Propagation in Random
     Composite Materials," in *Physics and Chemistry of Porous Media*, ed. by D.L. Johnson and
     P.N. Sen, AIP Conf. Proc. No. 107 (1984), pp. 38-51.

[4] S.A. Miller, "Amorphous Metal Powder, Production and Consolidation," in *Amorphous
     Metallic Alloys*, ed. by F.E. Luborsky (Butterworth, London, 1983), pp. 506-519; S.A.
     Miller and R.J. Murphy, "A Gas-Water Atomization Process for Producing Amorphous
     Powders," Scripta Met. 13, 673 (1979).

[5] (Ni-Cr): R.M. Bozorth, *Ferromagnetism* (D. Van Nostrand, New York, 1951), pp. 307-8;
     M. Hansen, *Constitution of Binary Alloys* (McGraw-Hill, New York, 1958), pp. 541-6; K.
     Hoselitz, *Ferromagnetic Properties of Metals and Alloys* (Oxford University Press, London,
     1952), p. 302.

[6] (Gd-Y): W.C. Thoburn, S. Legvold, and F.H. Spedding, "Magnetic Properties of the Gd-
     La and Gd-Y Alloys," *Phys. Rev.* 110, 1298-1301 (1958).

[7] I. Cosma, I. Lupsa, O. Pop, and M. Vancea, "Paramagnetic Properties of Ni-Cu-Al Alloys,"
     Physics Lett. 49A, 87-88 (1974); W. Köster, U. Zwicker and K. Moeller, "Mikroskopische
     und röntgenographische Untersuchungen zur Kenntnis des Systems Kupfer-Nickel-
     Aluminium," *Zeits. Metallkunde* 39, 225-231 (1948).

[8] V. Marian, "Les points de Curie ferromagnétiques et la saturation absolue de quelques
     alliages de nickel," *Annales de Physique*, Ser. II, 7, 459-527 (1937).

[9]   C. Sadron, "Sur le ferromagnétisme des alliages de nickel et de chrome," *Compt. rend. Acad. Sci.* 190, 1339-40 (1030).

[10] J. Šafránek, "Aimantation des alliages nickel-chrome au-dessus du point de Curie," *Revue de Métallurgie (Memoires)* 21, 86-111 (1924).

[11] H.C. Van Elst, B. Lubach, and G.J. Van den Berg, "The Magnetization of Some Nickel Alloys in Magnetic Fields up to 15 KOe between 0K and 300K." *Physica* 28, 1297-1317 (1962).

[12] M.J. Besnus, Y. Gottehrer and G. Munschy, "Magnetic Properties of Ni-Cr Alloys," *Phys. Stat. Sol.* (b) 49, 5997-607 (1972).

[13] H. Tange, T. Yonei and M. Goto, "Forced Volume Magnetostriction of Ni-Cr Alloys," *J. Phys. Soc. Japan* 50, 454-460 (1981).

[14] M.A. Simpson and T.F. Smith, "Thermodynamic Studies and Magnetic Ordering of Ni-Cr Alloys Close to the Critical Composition," *Aust. J. Phys.* 35, 307-19 (1982).

[15] K. Hauffe, *Oxidation of Metals* (Plenum Press, New York, 1965), p. 184, Fig. 73.

[16] Y. Saito, T. Inoue, T. Maruyama, and T. Amano, "Effect of Oxygen Pressure on the High Temperature Oxidation of Ni-Cr Alloys" in Proceedings of the Third JIM International Symposium, *High Temperature Corrosion of Metals and Alloys,* Transactions of the Japan Institute of Metals, Supplement, pp. 191-198 (1983).

[17] H. Ottavi, J. Clerc, G. Giraud, J. Roussenq, E. Guyon, and C.D. Mitescu, "Electrical Conductivity of a Mixture of Conducting and Insulating Spheres: an Application of Some Percolation Concepts," *J. Phys. C: Solid State,* 11, 1311-28 (1978).

[18] R.P. Devaty and A.J. Sievers, "Far-Infrared Absorption by Small Metal Particles," *Phys. Rev. Lett.* 52, 1344-47 (1984).

[19] P. Chylek, D. Boice and R.G. Pinnick, "Far-Infrared Absorption of Small-Palladium-Particle Composites," *Phys. Rev. B* 27, 5107-9 (1983).

[20] See, for example, A.R. von Hippel, *Dielectrics and Waves* (John Wiley, New York, 1954) p. 71.

[21] S.P. Mitoff, "Properties Calculations for Heterogeneous Systems" in *Advances in Materials Research,* H. Herman, ed. (Interscience, John Wiley, New York, 1968) vol. 3, pp. 305-329.

[22] A large number of articles and references may be found in *Electrical Transport and Optical Properties of Inhomogeneous Media,* edited by J.C. Garland and D.B. Tanner, AIP Conference Proceedings, No. 40 (American Institute of Physics, New York, 1978).

[23] *Physics and Chemistry of Porous Media,* edited by D.L. Johnson and P.N. Sen, AIP Conference Proceedings, No. 107 (American Institute of Physics, New York, 1984).

[24] D.B. Tanner, A.J. Sievers, and R.A. Buhrman, "Far-infrared Absorption in Small Metallic Particles" *Phys. Rev. B* 11,1330-1341 (1975).

[25] N.E. Russell, J.C. Garland and D.B. Tanner, "Absorption of Far-infrared Radiation by Random Metal Composites," *Phys. Rev. B* 23, 632-9 (1981).

[26] L.D. Landau and E.M. Lifshitz, *Electrodynamics of Continuous Media* (Addison-Wesley, Reading, Mass.; Pergamon Press, New York, 1960), pp. 192-4.

[27] H. Thomas, "Über Widerstandslegierungen," *Zeits. Physik* 129, 219-232 (1951).

[28] W. Heister, "Untersuchung der Frequenz-abhängigkeit der Stoffwerte ferromagnetischer Mischkörper bis zu sehr hohen Frequenzen," *Archiv. f. Elektrotechnik* 41, 142-160 (1953).

[29] D.A.G. Bruggeman, "Berechnung verschiedener physikalische Konstanten von heterogenen Substanzen, I., Dielektrizitätskonstanten und Leitfähigkeiten der Mischkörper aus isotropen Substanzen," *Ann. Phys.* (Leipzig) [5], 24, 636-679 (1935).

[30] M.M. Kharadly and W. Jackson, "The Properties of Artificial Dielectrics Comprising Arrays of Conducting Elements," *Proc. Inst. Elec. Eng.* 100, part 3, 199-212 (1953).

[31] W.T. Doyle, "The Clausius-Mossotti Problem for Cubic Arrays of Spheres," *J. Appl. Phys.* 49, 795-797 (1978).

[32] R.C. McPhedran and D.R. McKenzie, "The Conductivity of Lattices of Spheres. I. The Simple Cubic Lattice," *Proc. Roy Soc. Lond. A* 359, 45-63 (1978).

[33] D.R. McKenzie, R.C. McPhedran and G.H. Derrick, "The Conductivity of Lattices of Spheres. II The Body Centred and Face Centred Cubic Lattices," *Proc. Roy Soc. Lond. A* 362, 211-232 (1978).

[34] K. Lichtenecker, "Die Dielektrizitäts-konstante natürlicher und kunstlicher Mischkörper," *Physik. Zeits.* 27, 115-158 (1926).

[35] The standard reference at this point is H.C. van de Hulst, *Light Scattering by Small Particle* (John Wiley, New York, 1975), but it is not easy to find the equation of interest. Therefore see W. Lamb, D.M. Wood, and N.W. Ashcroft, "Optical Properties and Small Particle Composites: Theories and Applications" in *Electrical Transport and Optical Properties of Inhomogeneous Media,* ed. by J.C. Garland and D.B. Tanner, AIP Conference Proceedings No. 40 (1978), pp. 240-254, esp. eqs. 16,17.

[36] D.M. Grannan, J.C. Garland, and D.B. Tanner, "Critical Behavior of the Dielectric Constant of a Random Composite near the Percolation Threshold," *Phys. Rev. Lett.* 46, 375-378 (1981).

[37] W.E. Kock, "Metallic Delay Lenses," *Bell System Technical Journal* 27, 58-82 (1948).

[38] R.E. Collin, *Field Theory of Guided Waves,* (McGraw-Hill, New York, 1960), Ch. 12 "Artificial Dielectrics," pp. 509-551.

[39] W.T. Doyle, "The Permittivity of Cubic Arrays of Spheres" in *Electrical Transport and Optical Properties of Inhomogeneous Media,* ed. by J.C. Garland and D.B. Tanner, AIP Conference Proceedings No. 40 (1978), pp. 300-304.

[40] R.C. McPhedran and D.R. McKenzie, "Exact Solutions for Transport Properties of Arrays of Spheres," ibid. pp. 294-299.

[41] R.C. McPhedran, personal communication (1986).

[42] H.B. Levine and D.A. McQuarrie, "Dielectric Constant of Simple Gases," *J. Chem. Phys.* 49, 4181-4187 (1968).

[43] G.P. deLoor, "Dielectric Properties of Heterogeneous Mixtures," Thesis, University of Leiden, 1956.

[44] R. Guillien, "Variation de la Polarisation Diélectrique avec la Densité," *Ann. Physique* (Paris), Ser. 11, 16, 205-252 (1941).

[45] F. Lado and S. Torquato, "Effective properties of two-phase disordered composite media. I. Simplification of bounds on the conductivity and bulk modulus of dispersions of impenetrable spheres," *Phys. Rev. B* 33, 3370-3378 (1986); S. Torquato and F. Lado, "Effective properties of two-phased disordered composite media: II. Evaluation of bounds on the conductivity and bulk modulus of dispersions of impenetrable spheres," *Phys. Rev. B* 33, 6428-6435 (1986).

[46] J.C.R. Turner, "Two Phase Conductivity: The Electrical Conductance of Liquid-Fluidized Beds of Spheres," *Chem. Engineering Science.* 31, 487-492, (1976); "Electrical Conductivity of Liquid-Fluidized Beds," *AIChE Symposium Series*, 69, No. 128, pp. 115-122 (1973).

[47] W.T. Doyle and I.S. Jacobs, "Pair Interactions in Artificial Dielectric Media," *Bull. Am. Phys. Soc.* 32, 830 (1987).

[48] I.S. Jacobs, S.A. Miller, H.J. Patchen, J.O. Hanson, F.J. Rachford and S. Browning, "Electromagnetic Properties of Non-Percolating Random Metal-Particle," *Bull. Am. Phys. Soc.* 31, 667 (1986).

[49] "Measuring Dielectric Constant with the HP8510 Network Analyzer," Product Note No. 8510-3, Hewlett-Packard Co., Aug. 1985.

[50] A.M. Nicholson and G.F. Ross, "Measurement of the Intrinsic Properties of Materials by Time-Domain Techniques," *IEEE Trans. Instrum. Meas.* IM-19, 377-383 (1970).

[51] A. von Hippel, *Dielectrics and Waves*, (John Wiley and Sons, New York, 1954) Pt. I, Secs. 14 to 24; W.B. Westphal in *Dielectric Materials and Applications*, A.R. von Hippel, ed. (John Wiley and Sons, New York, 1954), Ch. II. A.2., p. 63.

[52] I.S. Jacobs, "Advanced Artificial Dielectric Materials for Millimeter Wavelength Applications," Annual Technical Report for Contract No. N00014-83-C-0447, Period 1 Aug. 83 to 30 Sept. 1984, General Electric CRD, Oct. 1984.

[53] I.S. Jacobs, "Advanced Artificial Dielectric Materials for Millimeter Wavelength Applications," Annual Technical Report, Part A, for Contract No. N00014-83-C-0447, Period 1 Oct. 1984 to 30 Sept. 1985, General Electric CRD, Dec. 1985 (85-SRD-030).

[54] I.S. Jacobs, "Advanced Artificial Dielectric Materials for Millimeter Wavelength Applications," Annual Technical Report, Part A, for Contract No.00014-83-C-0447, Period 1 Oct. 1985 - 30 June 1987, General Electric CRD, April 1988, (88-SRD-007).